Armed Forces
Radiobiology Research Institute

AFRRI Reports

First - Second Quarters
1997

CONTENTS

Scientific Reports

SR97-1: Kalinich JF, Ramakrishnan N, McClain DE. The antioxidant trolox enhances the oxidation of $1',7'$-dichlorofluorescin to $2',7'$-dichlorofluorescein.

SR97-2: Kandasamy SB. Effect of ondansetron and ICS 205-930 on radiation-induced hypothermia in rats.

SR97-3: Keyser DO, Pellmar TC. Regional differences in glial cell modulation of synaptic transmission.

SR97-4: Landauer MR, McChesney DG, Ledney GD. Synthetic trehalose dicorynomycolate (S-TDCM): Behavioral effects and radioprotection.

SR97-5: Prasanna PGS, Kolanko CJ, Gerstenberg HM, Blakely WF. Premature chromosome condensation assay for biodosimetry: Studies with fission-neutrons.

SR97-6: Savoye C, Swenberg C, Hugot S, Sy D, Sabattier R, Charlier M, Spotheim-Maurizot M. Thiol WR-1065 and disulphide WR-33278, two metabolites of the drug Ethyol (WR-2721), protect DNA against fast neutron-induced strand breakage.

SR97-7: Swenberg CE, Landauer MR, Weiss JF. Radiomodification by caffeine alone and in combination with phosphorothioates: *In vivo* and cell-free studies.

SR97-8: Weaver JL, McKinney L, Schoenlein PV, Goldenberg S, Gottesman MM, Aszalos A. MDR1/P-glycoprotein function. I. Effect of hypotonicity and inhibitors on rhodamine 123 exclusion.

SR97-9: Weaver JL, Aszalos A, McKinney L. MDR1/P-glycoprotein function. II. Effect of hypotonicity and inhibitors on Cl^- efflux and volume regulation.

SR97-10: Vaishnav YN, Swenberg CE. Effects of nitrogen mustard alone and in combination with ionizing radiation on guanine.

The Antioxidant Trolox Enhances the Oxidation of 2',7'-Dichlorofluorescin to 2',7'-Dichlorofluorescein

JOHN F. KALINICH,* NARAYANI RAMAKRISHNAN and DAVID E. MCCLAIN

Applied Cellular Radiobiology Department, Armed Forces Radiobiology Research Institute, Bethesda, MD 20889-5603, USA

The use of antioxidants to prevent intracellular free radical damage is an area currently attracting considerable research interest. The compound 2',7'-dichlorofluorescin diacetate (DCFH-DA) is a probe for intracellular peroxide formation commonly used in such studies. During our studies we unexpectedly found that incubation of Trolox, a water soluble vitamin E analog, with DCFH-DA in cell-free physiological buffers resulted in the deacetylation and oxidation of DCFH-DA to form the fluorescent compound, 2',7'-dichlorofluororescein (DCF). The reaction was time-, temperature-, and pH-dependent. Fluorescence intensity increased with an increase in either Trolox or DCFH-DA concentration. These results indicate that even at physiological pH, DCFH-DA can be deacetylated to form 2',7'-dichlorofluorescin (DCFH). DCFH can then be oxidized to DCF by abstraction of a hydrogen atom by the phenoxyl radical of Trolox. Exposure of the reaction mixture to 10 Gy of ^{60}Co gamma radiation greatly increased production of DCF. Antioxidant compounds reported to "repair" the Trolox phenoxyl radical (e.g., ascorbic acid, salicylate) can also prevent the Trolox-induced DCFH-DA fluorescence. However, compounds that cannot repair the Trolox phenoxyl radical (e.g., catechin) or can themselves form a radical (e.g., uric acid, TEMPOL) either have no effect or can increase levels of DCF. These results demonstrate that experimental design must be carefully considered when using DCFH-DA to measure peroxide formation in combination with certain antioxidants.

INTRODUCTION

Measurements of intracellular oxidation levels and attenuation of these levels with antioxidants are key components in the study of free radical damage to cells. One procedure to assay intracellular peroxide formation utilizes 2',7'-dichlorofluorescin diacetate (DCFH-DA).[1–6] This compound is readily transported across the plasma membrane to the interior of the cell. There, intracellular esterases convert the DCFH-DA to 2',7'-dichlorofluorescin (DCFH) by the removal of the acetate groups.[5] This reaction "locks" the DCFH inside the cell where it can react with intracellular peroxides to form the fluorescent compound 2',7'-dichlorofluorescein (DCF). The formation of DCF can be followed spectrofluorometrically.

Trolox [6-hydroxy-2,5,7,8-tetramethylchroman-2-carboxylic acid], a water soluble vitamin E analog, is a free radical scavenger and inhibitor

---

*Corresponding author. Phone: 301-295-9242. Fax: 301-295-6503. Email: kalinich@vax.afrri.usuhs.mil.

of lipid peroxidation.[7-9] The Trolox phenoxyl radical, resulting from the donation of a hydrogen from Trolox to a free radical, is a relatively stable species that can be "repaired" by ascorbic acid.[10] During our studies of radiation-induced intra-cellular peroxide production, we observed that incubation of DCFH-DA with Trolox in cell-free physiological buffers resulted in increased fluorescence. This finding has led us to investigate the effect of Trolox, alone and in combination with other antioxidants, on the conversion of the non-fluorescent DCFH-DA to the fluorescent DCF. Our results presented here clearly demonstrate that care must be taken when designing and interpreting experiments involving the use of DCFH-DA in conjunction with other antioxidant compounds.

MATERIALS AND METHODS

Materials

2′,7′-Dichlorofluorescin diacetate (Molecular Probes, Eugene, OR) was prepared as a 50 mM stock solution in DMSO and stored in 50 μl aliquots in the dark at –20°C. A fresh stock tube of DCFH-DA was used for each experiment. Stock tubes were used once and were not refrozen. Trolox (Aldrich Chemical Co., Milwaukee, WI) was prepared fresh daily as a 300 mM solution in 1 M NaHCO$_3$ and the pH adjusted to pH 7.0.[11] All other materials were purchased from the Sigma Chemical Co. (St. Louis, MO) with the exception of TEMPOL, which was obtained from the Aldrich Chemical Co. All antioxidants were prepared just prior to use.

Experimental Conditions

A typical reaction contained 25 μM DCFH-DA and 10 μM Trolox in HMCK buffer (50 mM HEPES pH 7.4; 5 mM MgCl$_2$; 3 mM CaCl$_2$; 25 mM KCl) and was incubated at 37°C in the dark for 24 h. Fluorescence was measured with an SLM 8000 spectrofluorometer (SLM/Aminco Instruments,

Urbana, IL) in a stirred cuvette with excitation and emission wavelengths at 485 and 530 nm (4 nm band width), respectively. Any additions to the reaction mixture or changes in the reaction conditions are as noted in the figure legends.

The following protocol was used for experiments testing the effect of various antioxidants on Trolox-induced DCFH fluorescence. Reaction mixtures contained 25 μM DCFH-DA in HMCK buffer and 10 μM or 10 mM of the antioxidant, alone or in the presence of 10 μM Trolox. The samples were incubated in the dark at 37°C for 24 h and the fluorescence intensity determined spectrophotometrically using the parameters described above. For samples containing no Trolox, the fluorescence intensity values (machine values) obtained for each antioxidant-containing sample was normalized to the values obtained for samples containing no antioxidant (control). In this case, the data are expressed as "% of Control". For reactions run in the presence of Trolox, the fluorescence intensity values obtained for the antioxidant-containing samples in the presence of 10 μM Trolox were normalized to the values obtained for samples containing Trolox alone (no other antioxidant present). In this case, the data are expressed as "% of Trolox".

Irradiation Conditions

Irradiations were performed with the Armed Forces Radiobiology Research Institute's ^{60}Co gamma radiation source at room temperature using bilateral exposures at a dose rate of 0.5 Gy/min for a total dose of 10.0 Gy.

RESULTS

As shown in Figure 1, incubation of Trolox with DCFH-DA in HMCK buffer at 37°C resulted in a time-dependent increase in the fluorescence of DCF. Initially there was a lag in the Trolox-induced DCF fluorescence, however, between 2 and 4 h the fluorescence intensity of the Trolox-
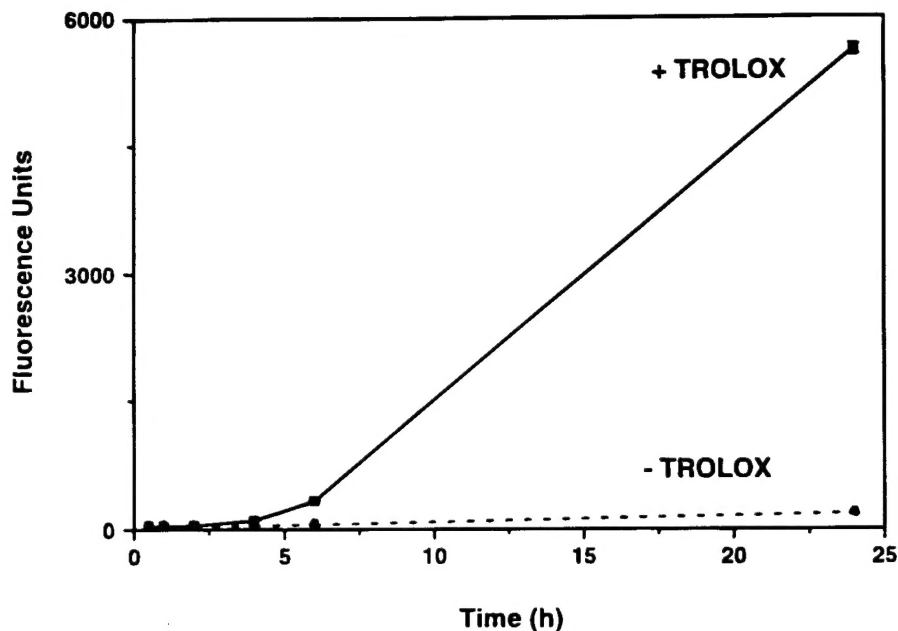
FIGURE 1   Effect of Trolox on oxidation of DCFH-DA.
Reactions contained 25 µM DCFH-DA in HMCK buffer and were incubated in the dark at 37°C for indicated times in presence (■----■) or absence (●----●) of 10 mM Trolox. Oxidation of DCFH-DA to DCF was determined spectrofluorometrically. Data represents the mean (± s.e.m.) of 6 independent determinations. Error bars smaller than symbols are not visible on the graph.

containing samples more than doubled. After a 24 h incubation the fluorescence intensity of the Trolox-containing samples was over 30-fold greater than the samples without Trolox. The UV spectra of the reaction mixtures demonstrated an increase in absorption at 503 nm that correlated with the increased DCF fluorescence. This is in agreement with previously published work that showed DCF has a λ_{max} of 503 nm.[2,5]

There is a significant temperature effect on the Trolox-induced oxidation of DCFH-DA (Fig. 2). Virtually no change in DCF fluorescence was observed in the presence or absence of Trolox at 4, 15, or 23°C. However, at incubation temperatures of 37 and 42°C there was a substantial increase in the level of fluorescence associated with the Trolox-containing samples. The pH of the reaction mixture also plays a significant role in Trolox-induced DCF oxidation (Fig. 3). Below pH 7.0 there was very little fluorescence of DCF as a result of the presence of Trolox; however, the Trolox-induced DCF fluorescence increased

greatly at pHs greater than 7.0. Buffer composition does not affect Trolox-induced DCF fluorescence. Different buffers (e.g., Tris, HEPES, PIPES, phosphate) at the same pH and concentration did not affect the level of DCF fluorescence observed in the presence or absence of Trolox. In addition, common buffer components ($MgCl_2$, $CaCl_2$, KCl) also had no effect. Therefore, for our studies, we utilized the same buffer used previously for our cellular studies (HMCK buffer).

The extent of DCF fluorescence resulting from the presence of Trolox in the reaction mixture depends on both DCFH-DA and Trolox concentration. As shown in Figure 4A, as the concentration of Trolox in the reaction mixture was increased from 10 µM to 10 mM, the DCF-associated fluorescence also increased. Increasing the DCFH-DA concentration (5 to 100 µM) in the presence of a fixed concentration of Trolox also resulted in increased DCF fluorescence (Fig. 4B), but not to the extent seen by increasing the Trolox concentration.
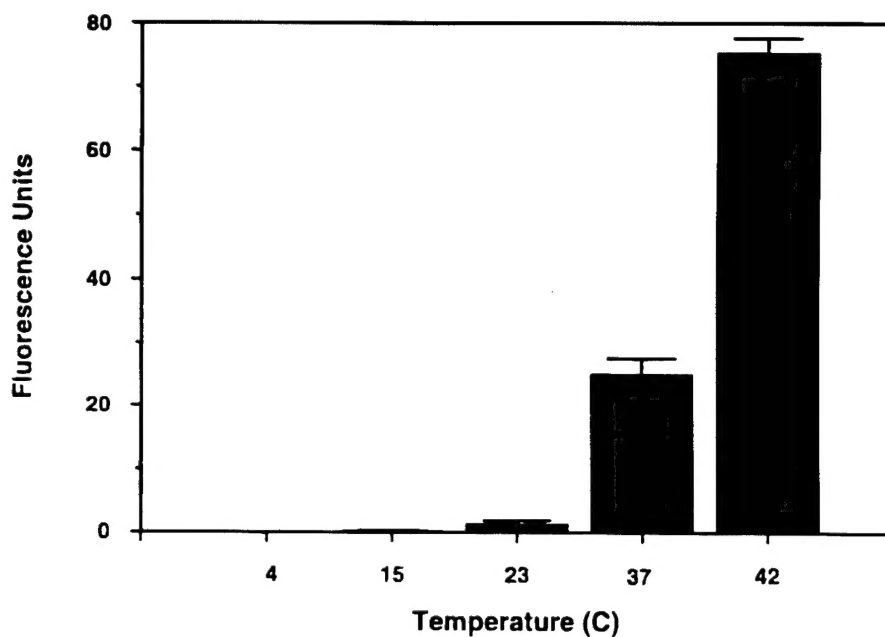
FIGURE 2   Effect of temperature on Trolox-induced DCFH-DA oxidation.
   Reaction mixtures containing 25 μM DCFH-DA in HMCK buffer were incubated in the dark for 24 h at indicated temperatures. Fluorescence values of samples incubated without Trolox were subtracted from those containing Trolox (10 μM). Data represent the mean (± s.e.m.) of 3 independent experiments.
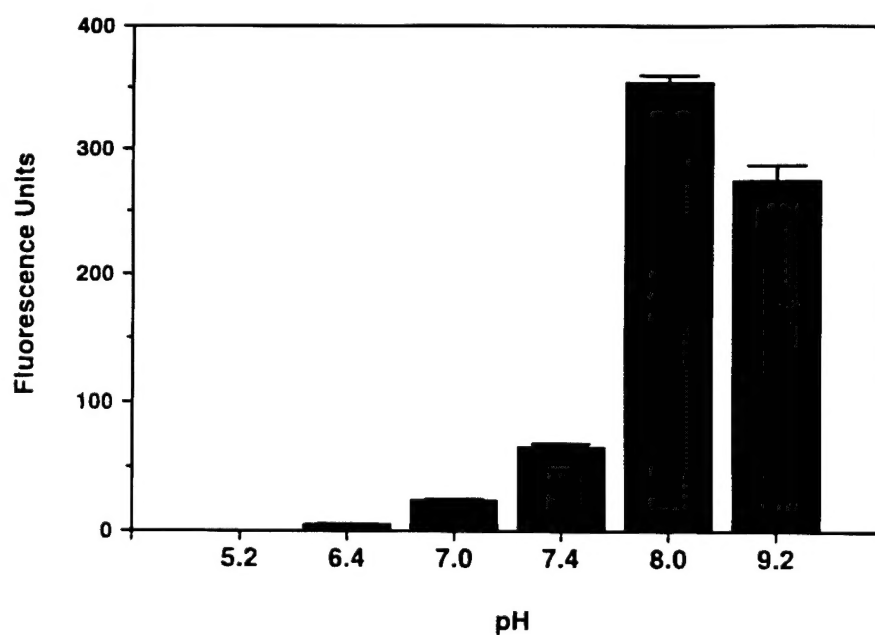
FIGURE 3   Effect of pH on Trolox-induced DCFH-DA oxidation.
   Reaction mixtures, containing 25 μM DCFH-DA in presence and absence of 10 mM Trolox, were incubated in the dark at 37°C for 2 h in 50 mM of the following buffers: acetate pH 5.2, PIPES pH 6.4, phosphate pH 7.0, HEPES pH 7.4, and Tris pH 8.0 and 9.2. Fluorescence intensity was determined and values obtained for control reactions (no Trolox) subtracted from values obtained for the samples containing Trolox. Data represent the mean (± s.e.m.) of 3 independent experiments.
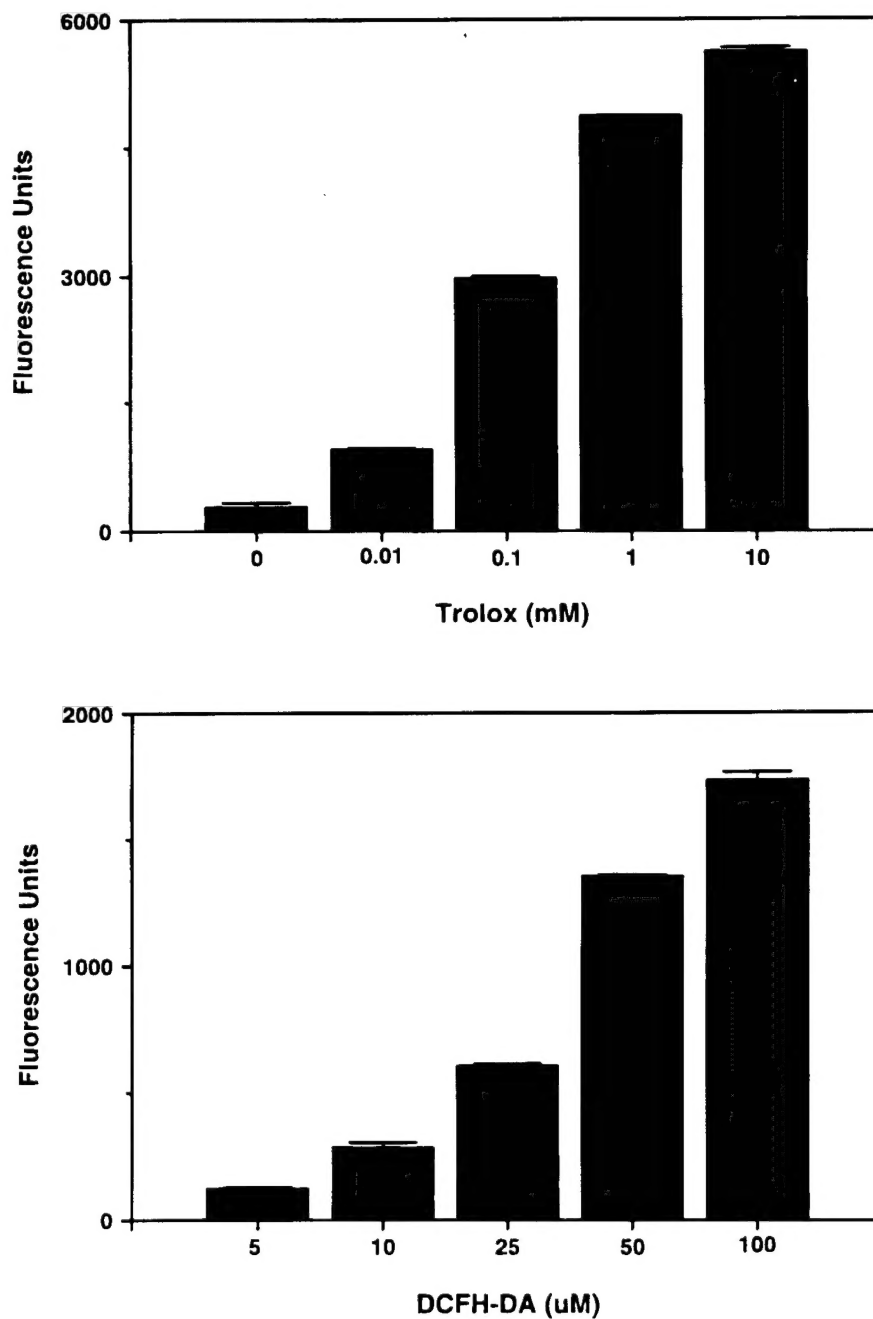
FIGURE 4   Effect of increasing concentrations of Trolox (Panel A) and DCFH-DA (Panel B) on Trolox-induced DCFH-DA oxidation. Reaction mixtures contained 25 μM DCFH-DA in HMCK buffer with increasing concentrations of Trolox (0 to 10 mM, Panel A) or 10 μM Trolox in HMCK buffer with increasing concentrations of DCFH-DA (5 to 25 μM, Panel B). Samples were incubated in the dark at 37°C for 24 h before fluorescence intensity was measured. Data represent mean (± s.e.m.) of 6 independent experiments.

After observing the initial lag in Trolox-induced DCF fluorescence, we attempted to determine if a prior incubation of either Trolox or DCFH-DA in buffer, followed by addition of the missing component affected the level of DCF fluorescence. Figure 5 shows the results of these preincubation experiments. Preincubation of DCFH-DA (25 μM) in HMCK buffer for 24 h at 37°C prior to the addition of Trolox (10 mM) resulted in substantially greater DCF fluorescence over the sampling period than that obtained with either control or Trolox preincubation reactions. This increase in fluorescence intensity occurred almost immediately following the addition of Trolox to the preincubated DCFH-DA. On the other hand, the control and Trolox preincubation reactions continued to show a lag period of approximately 2 h before fluorescence intensity increased, with the Trolox preincubation exhibiting somewhat greater fluorescence intensity than did the controls.

Since a major focus of our research is the role of radiation-induced free radicals in the cell, we investigated the effect of ^{60}Co gamma radiation exposure on Trolox-induced DCFH-DA oxidation. As shown in Figure 6 the fluorescence intensity of both the control (0 Gy) and irradiated (10 Gy) samples exhibited a lag or plateau period lasting approximately 2 h post-irradiation, although the 10 Gy samples had a 2- to 3-fold greater fluorescence intensity during this period. After 2 h the fluorescence intensity of the irradiated samples increased at a much greater rate than the unirradiated samples, and, by 6 h post-irradiation, the irradiated samples showed a 7-fold higher fluorescence intensity than unirradiated controls. Lower radiation doses (2.5 and 5.0 Gy) had no effect on Trolox-induced DCFH-DA oxidation (data not shown). In
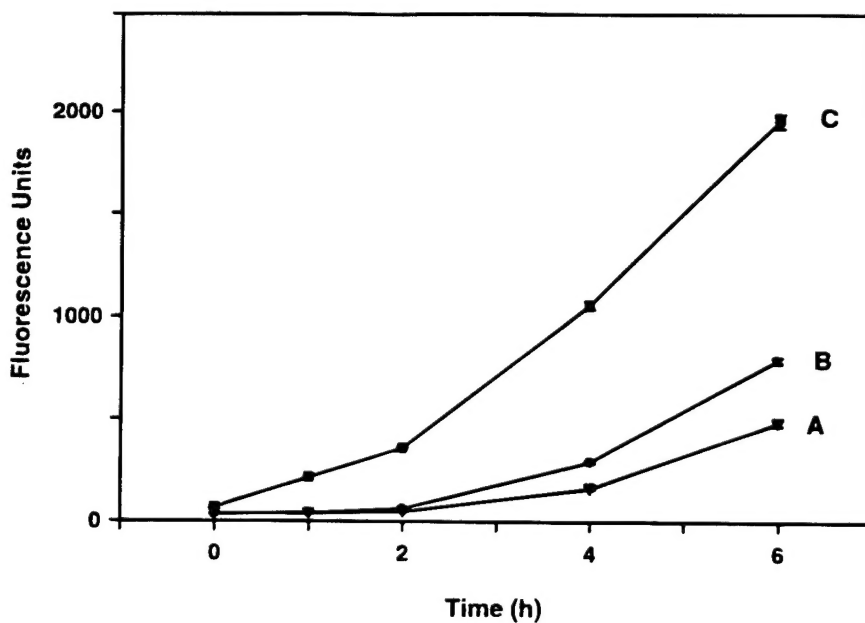
FIGURE 5   Effect of "preincubation" on Trolox-induced DCFH-DA oxidation.

Curve A (buffer preincubation): HMCK buffer was incubated in the dark at 37°C for 24 h after which DCFH-DA and Trolox were added and incubation continued for an additional 6 h. Curve B (Trolox preincubation): HMCK buffer and Trolox were incubated in the dark at 37°C for 24 h after which DCFH-DA was added and incubation continued for an additional 6 h. Curve C (DCFH-DA preincubation): HMCK buffer and DCFH-DA were incubated in the dark at 37°C for 24 h after which Trolox was added and incubation continued for an additional 6 h. Fluorescence intensity was measured immediately following (within 2 min) addition of the missing reaction component(s) and then at 1, 2, 4, and 6 h post-addition. In all cases final DCFH-DA concentration was 25 μM and final Trolox concentration was 10 mM. Data represent mean (± s.e.m.) of 6 independent determinations.

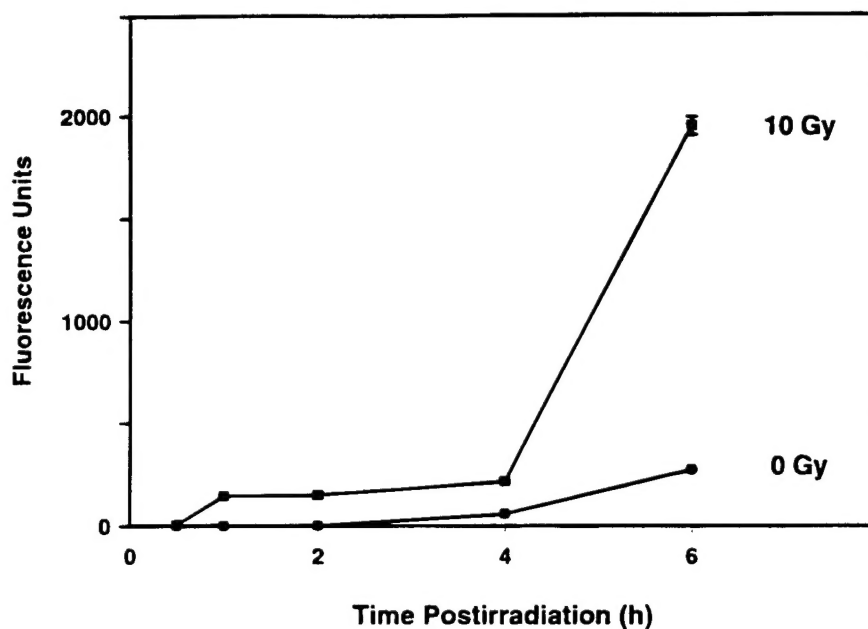FIGURE 6   Effect of 10 Gy ^{60}Co gamma radiation on Trolox-induced DCFH-DA oxidation.

Reaction mixtures contained 25 μM DCFH-DA in HMCK buffer with or without 10 mM Trolox. Samples received either 0 Gy (unirradiated control) or 10 Gy of ^{60}Co gamma radiation (dose rate 0.5 Gy/min) and were incubated at 37°C in the dark. Fluorescence intensity was measured at 0.5, 1, 2, 4, and 6 h post-irradiation and values obtained for samples containing no Trolox were subtracted from appropriate Trolox-containing sample values. Data represent the mean (± s.e.m.) of 3 independent experiments.

addition, radiation exposure had no effect on the oxidation of DCFH-DA in the absence of Trolox (data not shown).

To determine if the capacity to induce the oxidation of DCFH-DA was unique to Trolox we tested whether a variety of other antioxidants, alone or in combination with Trolox, can oxidize DCFH-DA. As shown in Table I, compounds such as ascorbic acid and glutathione, which can repair the phenoxyl radical of Trolox,[10] could also prevent the Trolox-induced oxidation of DCFH-DA. However, glutathione alone also oxidized DCFH-DA, although to a much lesser extent than Trolox. Compounds that are free radicals (e.g., TEMPOL) or can form stable radicals (catechin, uric acid, n-propyl gallate) appear to be able to oxidize DCFH-DA and, in some cases, also enhance the Trolox-induced oxidation of DCFH-DA. Quercetin, although structurally similar to catechin, behaved differently. The presence of quercetin in the reaction mixture

not only eliminated the Trolox-induced oxidation of DCFH-DA but also inhibited the endogenous oxidation of DCFH-DA to much the same extent as ascorbic acid. Antioxidants such as superoxide dismutase, catalase, ethylene glycol, ethanol, vitamin E, butylated hydroxytoluene, and dihydrolipoic acid, alone, did not enhance the oxidation of DCFH-DA, nor did they have any effect on the Trolox-induced oxidation of DCFH-DA (data not shown).

DISCUSSION

The compound 2′,7′-dichlorofluorescin diacetate (DCFH-DA) is an important and widely-used tool with which to study intracellular peroxide formation. In the diacetate form the compound readily crosses the plasma membrane. Once inside, the diacetate groups are removed by cellular esterases to yield 2′,7′-

TABLE I

Compound	Concentration	% of Control	% of Trolox
Trolox	10 µM	949	—
	10 mM	5617	—
Ascorbic Acid	10 µM	76	68
	10 mM	28	4
Glutathione	10 µM	364	76
	10 mM	381	22
Salicylate	10 µM	116	154
	10 mM	93	75
Catechin	10 µM	149	164
	10 mM	882	99
TEMPOL	10 µM	394	172
	10 mM	4386	404
Uric Acid	10 µM	342	242
	10 mM	6174	474
Quercetin	10 µM	60	91
	10 mM	26	4
n-Propyl Gallate	10 µM	58	19
	10 mM	2190	259

Experimental details are given in the text. Values listed in "% of Control" give an indication of the ability of that particular antioxidant to oxidize DCFH-DA. Values listed in "% of Trolox" give an indication of the ability of that particular antioxidant to inhibit or enhance the Trolox-induced oxidation of DCFH-DA. Data are the average of three independent determinations.

dichlorofluorescin (DCFH). Neither DCFH-DA nor DCFH is fluorescent, but abstraction of a hydrogen atom from DCFH results in the formation of 2′,7′-dichlorofluorescein (DCF), which is fluorescent. These reactions have been used to quantitate intracellular peroxides by us[12] and others.[5,13–15]

As a part of our earlier work with DCFH-DA, we made several puzzling observations. As expected, DCFH-DA incubated with buffer alone produced low levels of fluorescence. However, when the antioxidant drug Trolox, a water-soluble analog of vitamin E, was included in the buffer with DCFH-DA, we observed a substantial increase in fluorescence intensity. Because of the possibility that factors such as this might influence the interpretation of our experiments assessing the antioxidant effect of Trolox, we sought to investigate the role Trolox and other antioxidants might play in promoting the conversion of DCFH-DA to the fluorescent DCF.

A plausible mechanism of action was not immediately clear, because neither the structure of Trolox nor the species involved in the DCFH-DA conversion suggested any obvious reaction between them that would tend to enhance the production of DCF. Our experiments indicate that the keys to understanding the Trolox effect are (1) the fact that the antioxidant Trolox, when oxidized, can serve as an effective reducing agent and (2) the oxidized Trolox potentiates the conversion of DCFH, the intermediate produced as a result of the deesterification of DCFH-DA, to the fluorescent DCF. While no reports have emerged on the Trolox-induced oxidation of DCFH, the prooxidant properties of Trolox have been studied in several experimental systems investigating oxidative damage to DNA,[16] lipids,[17] and proteins.[18] The ability to bind and reduce metabolically important metals such as iron[16,17] and copper[18] appears to be the key step in Trolox's prooxidant behavior in these systems.

It is known that Trolox exerts its antioxidant effect through its capacity to scavenge free radicals. Trolox in solution reacts with free radicals—

spontaneously or experimentally induced—to produce the relatively stable phenoxyl radical (see Fig. 7). One normally considers the activity of antioxidants in terms of their capacity to reduce oxidized species. During this process, some antioxidants are themselves oxidized. The phenoxyl (oxidized) form of Trolox is such an example. Trolox is an effective antioxidant because the more stable phenoxyl radical is far less reactive than the species it reduced. This does not mean the phenoxyl radical is unreactive, however. The phe-

noxyl form has the capacity to oxidize other species, regenerating the native form of Trolox in the process.

We believe the DCFH intermediate is such a substrate for the Trolox phenoxyl radical, a reaction whose products would be Trolox and fluorescent DCF. One conceptual problem with this hypothesis is that deesterification of DCFH-DA was previously thought to occur only at high pH[2] or as a result of esterase activity.[5] Our experiments have shown, however,
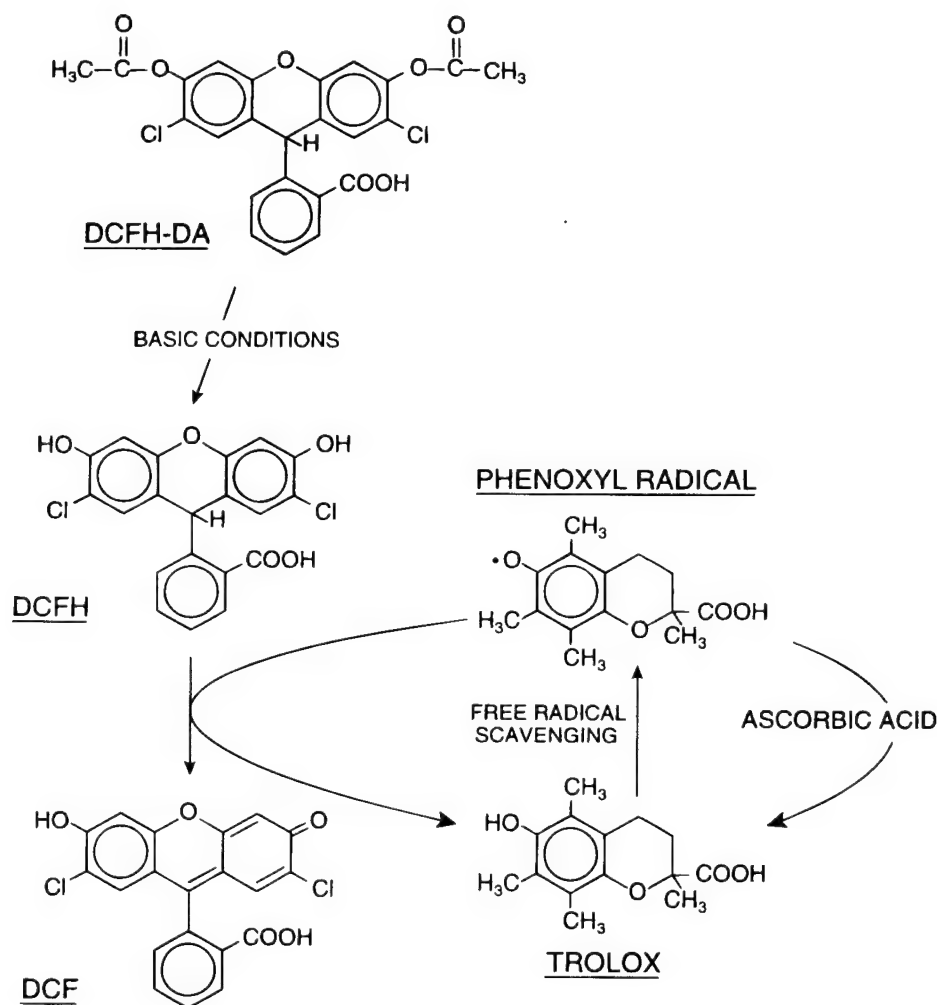

FIGURE 7 Possible mechanism of Trolox-induced DCFH-DA oxidation.
Schematic showing the activation of DCFH-DA to DCFH and the role of Trolox in the oxidation of DCFH to the fluorescent DCF. Details are given in the text.

that deacetylation can also occur at physiological pH in the absence of esterases (Fig. 3). Incubation of DCFH-DA in even the slightly alkaline (pH 7.4) HMCK buffer used in our experiments is sufficient to induce deacetylation. It should be stated that we did not measure the production of DCFH in our experiments directly because it is very unstable and, as a result, difficult to measure. However, its existence has been demonstrated by others.[2] Even in the absence of any other evidence, based on the chemistry of the overall reaction, one could also correctly infer its role as an obligatory intermediate in the conversion to DCF.

In the absence of any potentiating conditions, the abstraction of hydrogen from DCFH to form DCF does not occur readily. When DCFH-DA was incubated with buffer (pH 7.4) at 37°C for periods up to 24 h, virtually no change in fluorescence occurred. However, when Trolox (10 mM) was added to the incubation mixture, there was a slow but steady increase in fluorescence intensity that was 30 times greater than controls by 24 h (Fig. 1). Formation of DCF in such experiments was temperature-dependent (Fig. 2) and was most effective around pH 8 (Fig. 3). Preincubating DCFH-DA overnight before adding Trolox enhanced the production of DCF (Fig. 5), presumably because there was a greater quantity of DCFH present in the reaction mixture at that time to react with the Trolox phenoxyl radical. An overnight incubation of buffer containing Trolox, followed by the addition of DCFH-DA produced somewhat higher levels of fluorescence than controls (buffer preincubated alone, followed by addition of DCFH-DA and Trolox), but much less fluorescence than that obtained by preincubating DCFH-DA. The low levels of free radicals that would presumably be spontaneously present in such an incubation could convert small amounts of Trolox to the phenoxyl radical form that would facilitate the oxidation of any DCFH produced after the addition and deesterification of DCFH-DA. Exposing solutions containing DCFH-DA and Trolox to 10 Gy gamma radiation greatly enhanced the production of fluorescence, probably by increasing the number of free radicals available to react with Trolox to produce the phenoxyl radical form. Irradiation of solutions containing DCFH-DA without Trolox failed to produce a significant increase in fluorescence, which shows that free radicals produced by the radiation do not directly oxidize the intermediate DCFH to DCF.

Further support for the role of the Trolox phenoxyl radical is provided by the observation that compounds having the capacity to form stable, oxidizing radicals also promote the production of the fluorescent DCF (Table I). Many are more effective than Trolox. If the formation of the Trolox phenoxyl radical is important in this process, one would expect that reactions that suppress the levels of the phenoxyl radical in solution would also inhibit the conversion to DCF. This was the case. For example, ascorbic acid (10 mM), which has been shown to reduce the Trolox phenoxyl radical to its native form,[10] almost completely eliminated the Trolox-mediated oxidation of DCFH-DA.

To summarize, we have shown that the incubation of DCFH-DA with Trolox and other antioxidants can promote the production of significant levels of the fluorescent DCF in the absence of peroxides. Trolox, when oxidized by free radicals generated spontaneously or as a result of irradiation, forms the Trolox phenoxyl radical that oxidizes the intermediate DCFH to produce DCF. We have also shown that the deesterification of DCFH-DA to produce the DCFH intermediate occurs in even slightly alkaline physiological buffers in the absence of esterases. The results presented here demonstrate that caution must be taken when designing and interpreting any experiments using DCFH-DA in the presence of certain antioxidant compounds.

References

[1] A. S. Keston and R. Brandt (1965) The fluorometric analysis of ultramicro quantities of hydrogen peroxide. *Analytical Biochemistry*, **11**, 1–5.

[2] R. Brandt and A. S. Keston (1965) Synthesis of diacetyl-dichlorofluorescin: a stable reagent for fluorometric analysis. *Analytical Biochemistry*, **11**, 6–9.

[3] M. J. Black and R. B. Brandt (1974) Spectrofluorometric analysis of hydrogen peroxide. *Analytical Biochemistry*, **58**, 246–254.

[4] R. Cathcart, E. Schwiers and B. Ames (1983) Detection of picomole levels of hydroperoxides using a fluorescent dichlorofluorescein assay. *Analytical Biochemistry*, **134**, 111–116.

[5] D. A. Bass, J. W. Parce, L. R. Dechatelet, P. Szejda, M. C. Seeds and M. Thomas (1983) Flow cytometric studies of oxidative product formation by neutrophils: a graded response to membrane stimulation. *Journal of Immunology*, **130**, 1910–1917.

[6] G. Melino, I. Savini, P. Guerrieri and A. Finazzi-Agro (1990) Redox buffering ability of lymphoid cells evaluated by the oxidation of 2′,7′-dichlorofluorescin. *Free Radical Research Communications*, **11**, 213–221.

[7] J. W. Scott, W. M. Cort, H. Harley, D. R. Parrish and G. Saucy (1974) 6-Hydroxychroman-2-carboxylic acids: novel antioxidants. *Journal of the American Oil Chemists Society*, **51**, 200–203.

[8] W. M. Cort, J. W. Scott, M. Araujo, W. J. Mergens, M. A. Cannalonga, M. Osadca, H. Harley, D. R. Parrish and W. R. Pool (1975) Antioxidant activity and stability of 6-hydroxy-2,5,7,8-tetramethylchroman-2-carboxylic acid. *Journal of the American Oil Chemists Society*, **52**, 174–178.

[9] W. M. Cort, J. W. Scott and J. H. Harley (1975) Proposed antioxidant exhibits useful properties. *Food Technology*, **29**, 46–50.

[10] M. J. Davies, L. G. Forni and R. L. Willson (1988) Vitamin E analogue Trolox C. E.s.r. and pulse-radiolysis studies of free-radical reactions. *Biochemical Journal*, **255**, 513–522.

[11] D. E. McClain, J. F. Kalinich and N. Ramakrishnan (1995) Trolox inhibits apoptosis in irradiated MOLT-4 lymphocytes. *FASEB Journal*, **9**, 1345–1354.

[12] N. Ramakrishnan, J. F. Kalinich and D. E. McClain (1996) Ebselen inhibition of apoptosis by reduction of peroxides. *Biochemical Pharmacology*, **51**, 1443–1451.

[13] K. Frenkel and C. Gleichauf (1991) Hydrogen peroxide formation by cells treated with a tumor promoter. *Free Radical Research Communications*, **12–13**, 783–794.

[14] T. Paraidathathu, H. de Groot and J. P. Kehrer (1992) Production of reactive oxygen by mitochondria from normoxic and hypoxic rat heart tissue. *Free Radicals in Biology and Medicine*, **13**, 289–297.

[15] W. O. Carter, P. K. Narayanan and J. P. Robinson (1994) Intracellular hydrogen peroxide and superoxide anion detection in endothelial cells. *Journal of Leukocyte Biology*, **55**, 253–258.

[16] O. I. Aruoma, P. J. Evans, H. Kaur, L. Sutcliffe and B. Halliwell (1990) An evaluation of the antioxidant and potential pro-oxidant properties of food additives and of Trolox C, vitamin E and probucol. *Free Radical Research Communications*, **10**, 143–157.

[17] K. M. Ko, P. K. Yick, M. K. Poon and S. P. Ip (1994) Prooxidant and antioxidant effects of Trolox on ferric ion-induced oxidation of erythrocyte membrane lipids. *Molecular and Cellular Biochemistry*, **141**, 65–70.

[18] M. J. Burkitt and L. Milne (1996) Hydroxyl radical formation from Cu(II)-Trolox mixtures: insights into the pro-oxidant properties of alpha-tocopherol. *FEBS Letters*, **379**, 51–54.

Effect of Ondansetron and ICS 205-930 on Radiation-Induced Hypothermia in Rats

S. B. Kandasamy

Radiation Pathophysiology and Toxicology Department, Armed Forces Radiobiology Research Institute, Bethesda, Maryland 20889-5603

Kandasamy, S. B. Effect of Ondansetron and ICS 205-930 on Radiation-Induced Hypothermia in Rats. Radiat. Res. 147, 741–746 (1997).

This study determined the effects of the 5-hydroxytryptamine (5-HT) serotonin antagonists ondansetron and [3α-tropanyl]-1H-indole-3-carboxylic acid ester HCl (ICS 205-930) on hypothermia induced in rats by irradiation and by administration of a 5-HT3 receptor agonist, 2-methyl-5-hydroxytryptamine (2-Me-5-HT). Intraperitoneal (i.p.) administration of 50–200 µg/kg of ondansetron and intraventricular administration of 5–20 µg of ondansetron attenuated hypothermia induced by 20 Gy γ rays. However, the same doses of ondansetron administered i.p. or intraventricularly did not antagonize the hypothermia induced by 10 µg 2-Me-5-HT. In contrast, i.p. administration of 50–200 µg/kg of ICS 205-930 and intraventricular administration of 5–20 µg of ICS 205-930 attenuated hypothermia induced by radiation and 2-Me-5-HT. These results indicate that ICS 205-930 attenuates hypothermia induced by radiation and 2-Me-5-HT. However, the doses of ondansetron that attenuated radiation-induced hypothermia did not attenuate hypothermia induced by 2-Me-5-HT. © 1997 by Radiation Research Society

INTRODUCTION

Exposure to ionizing radiation causes changes in body temperature. The nature and magnitude of the effect depend partly on the species, with hyperthermia occurring in cats, rabbits and humans (*1, 2*), hypothermia in guinea pigs (*3*) and a biphasic response (i.e. a fall in temperature followed by a rise) in monkeys.[1] In rats, the direction of the change in temperature is dependent on dose: Hyperthermia occurs when the dose is less than 15 Gy, while hypothermia occurs when the dose is greater than 20 Gy. In rats, the change in temperature appears to be centrally mediated because irradiation of the head alone causes these effects, while irradiation of the trunk only does not (*5*). Radiation-

induced hyperthermia is mediated by prostaglandin E2, and radiation-induced hypothermia is mediated by histamines (*4, 5*). The central mediation of the hypothermia response is not unique to rats; it is also seen in guinea pigs (*3*).

5-Hydroxytryptamine (5-HT) is involved in thermoregulation (*6*). Administration of 5-HT or 5-HT agonists has produced marked changes in the body temperature of rats (*7*). The existence of three major subtypes of 5-HT receptors—5-HT1, 5-HT2 and 5-HT3—in the central nervous system has been reported (*8*), and 5-HT3 receptor binding sites have been identified in both the central and peripheral nervous system (*9, 10*). The 5-HT1 and 5-HT2 classes of receptors are both G protein-coupled receptors (*11*). The 5-HT3 receptor is unique, being the only monoamine neurotransmitter receptor that is known to function as a ligand-operated ion channel (*11*). Stimulation of 5-HT3 receptors enhances Na^+, K^+ and Ca^{2+} currents (*11–13*). Richardson and Engel (*14*) divided the 5-HT3 receptor group into three subtypes, 5-HT3a, 5-HT3b and 5-HT3c, based primarily on the different affinities of specific 5-HT3 receptor antagonists for different peripheral tissues. However, recent evidence suggests that the differences in the properties of the 5-HT3 responses may be due to species differences rather than tissue differences (*15, 16*). The 5-HT3 receptors have facilitated the release of 5-HT from rat hypothalamus slices. This effect was mimicked by 2-methyl-5-hydroxytryptamine (2-Me-5-HT), a selective 5-HT3 receptor agonist, and antagonized by ondansetron and ICS 205-930 ([3α-tropanyl]-1H-indole-3-carboxylic acid ester HCl), selective antagonists of 5-HT3 receptors (*18*).

Evidence is accumulating in support of the potential therapeutic importance of 5-HT3 receptor antagonists, for example, in the inhibition of emesis induced by radiation exposure and cytotoxic agents used to treat neoplastic disease (*18, 19*). Since 5-HT3 receptors have multiple effects on the functioning of the central nervous system (CNS), it is obviously desirable to study the actions of 5-HT3 receptor antagonists on physiological changes, such as temperature regulation in experimental animals, so that unforeseen effects may be identified.

The purpose of the present study was to determine the effects of ondansetron and ICS 205-930 on hypothermia induced by radiation or by administration of 2-Me-5-HT.

---

[1] W. L. McFarland and J. A. Willis, Cerebral temperature changes in the monkey (*Macaca mulatta*) after 2500 rads of ionizing radiation, Scientific Report SR 74-7, Armed Forces Radiobiology Research Institute, Bethesda, MD, 1974.

Preliminary findings on the effect of ondansetron on radiation-induced hypothermia have been reported.[2]

MATERIALS AND METHODS

Drugs. The drugs used were ondansetron (Glaxo Pharmaceuticals, Herts, England), ICS 205-930 (Sandoz, Sommerville, NJ), 2-Me-5-HT (Research Biochemicals International, Natick, MA), ketamine (Parke-Davis, Detroit, MI), xylazine (Hayer Lockhart, Shawnee, KS) and acepromazine (Ayerst Laboratories Inc., New York).

Animals. Male Sprague-Dawley rats [Crl:CD(SD)BRD; Charles River Breeding Laboratories, Kingston, NY] weighing 250–300 g were used in these experiments. Rats were quarantined upon arrival and screened for evidence of disease by serology and histopathology before being released from quarantine. Rats were housed individually in polycarbonate isolator cages (Lab Products, Maywood, NJ) on autoclaved hardwood contact bedding (Beta Chip, Northern Products Corp., Warrensburg, NY) and were provided commercial rodent chow (Wayne Rodent Blok, Continental Grain Co., Chicago, IL) and acidified water (pH 2.5 using HCl) *ad libitum.* Animal holding rooms were kept at 21 ± 1°C with 50% ± 10% relative humidity on a 12-h light:dark cycle with no twilight.

Radiation exposure. Rats were placed in well-ventilated clear plastic containers for approximately 5 min before irradiation or sham exposure. The animals were exposed bilaterally to γ rays using a ^{60}Co source at a rate of 10 Gy/min with a total dose of 20 Gy. Prior to irradiation, the dose rate at the midline of an acrylic rat phantom was measured using a 0.05-ml tissue-equivalent chamber manufactured by Exradin, Inc. The dose rate at the same location with the phantom removed was measured using a 50-ml ionization chamber fabricated at AFRRI. The ratio of these two dose rates, the tissue–air ratio, was 0.93. All ionization chambers that were used have calibration factors traceable to the National Institute of Standards and Technology. Dosimetry measurements were performed following the AAPM Task Group 21 protocol for determining the absorbed dose from high-energy photon and electron beams (*20*).

Central administration of drugs. Rats were anesthetized with 1 ml/kg of a mixture of ketamine (50 mg/kg), xylazine (5 mg/kg) and acepromazine (1 mg/kg) given intramuscularly and were placed in a rat stereotaxic apparatus (David Kopf Instruments, No. 320). A single cannula was inserted into the lateral ventricle according to coordinates derived from the atlas of Pelligrino *et al.* (*21*): 0.8 mm posterior to bregma (the point on the surface of the skull at the junction of the coronal and sagittal sutures), 2.5 mm lateral. Administration by this route will be referred to as intraventricular. The cannula was inserted until cerebrospinal fluid rose in the cannula. Dental acrylic was used to secure the cannula. At least 1 week was allowed for recovery before animals were used for experiments. In the meantime they were inspected daily for infection, and none was detected. At the end of an experiment, injection sites were verified histologically. The volume of injection was always 10 μl. Injections/irradiations were performed at the same time of day (0900) to avoid diurnal variations in temperature. The antagonists (ondansetron or ICS 205-930) were given 30 min before irradiation or administration of 2-Me-5-HT.

Measurement of body temperature. All experiments were performed at an environmental temperature of 22 ± 1°C. The measurement of body temperature was performed as described previously (*4, 5*). Briefly, the animals were placed in restraining cages 1 h before the beginning of the experiments, and body temperatures were measured every 15 min for 2 h with thermistor probes inserted approximately 6 cm into the rectum and connected to dataloggers (Minitrend 205). The probes were removed from the animals just prior to irradiation or sham irradiation. After exposure, the probes were reinserted, and body temperatures were measured
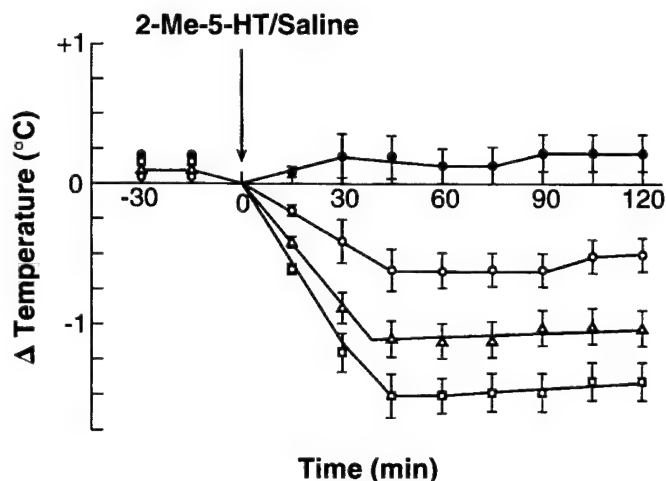
---

[2]S. B. Kandasamy, T. Mott and A. H. Harris, Effect of ondansetron on radiation-induced hypothermia in rats. Presented at the meeting of the American Society for Clinical Pharmacology and Therapeutics, 1993.

FIG. 1. Effect of intraventricular administration of 2-methyl-5-hydroxytryptamine (2-Me-5-HT) on body temperature. Controls given (●) saline or (○) 5, (△) 10 or (□) 20 μg 2-Me-5-HT. Each point represents the mean effect ± SE in five animals. Zero on the ordinate represents the temperature at the time of injection of 2-Me-5-HT.

again. Immediately after each experiment, all animals were euthanized via inhalation with an overdose of carbon dioxide.

Statistics. Statistical evaluations of the data were performed using analysis of variance. Post hoc comparisons between groups were performed using Tukey's *t* test.

RESULTS

Intraventricular administration of 5, 10 or 20 μg of 2-Me-5-HT induced significant dose-dependent hypothermia compared to saline-treated controls (Fig. 1). Rats treated with 5, 10 and 20 μg of 2-Me-5-HT showed significant reductions in body temperature ($P < 0.01$). In contrast, intraperitoneal (i.p.) administration of 1000–5000 μg/kg of 2-Me-5-HT did not induce significant hypothermia ($P > 0.05$); data are not shown.

Administration of ondansetron (50–300 μg/kg i.p. or 5–20 μg intraventricularly) did not induce changes in temperature in sham-irradiated animals (Figs. 2A1 and 2B1). However, it attenuated hypothermia induced by 20 Gy γ rays (Figs. 2A2 and 2B2; Table I), but did not attenuate hypothermia induced by 10 μg 2-Me-5-HT administered intraventricularly (Figs. 2A3 and 2B3; Table I). In contrast to the response of irradiated rats given only saline, both i.p. (Fig. 2A2; Table I) and intraventricularly (Fig. 2B2; Table I) administration of ondansetron were effective in attenuating hypothermia. The response was dependent on the dose of the drug, and the intraventricular route required substantially less drug to produce the same effect as the i.p. route.

Doses of 50–300 μg/kg i.p. or intraventricular administration of 5–20 μg of ICS 205-930 did not induce temperature changes in sham-irradiated animals (Figs. 3A1 and 3B1); however, they attenuated hypothermia induced by both radiation and 2-Me-5-HT (Figs. 3A2–3 and 3B2–3). Compared to irradiated rats given saline only, i.p. administration
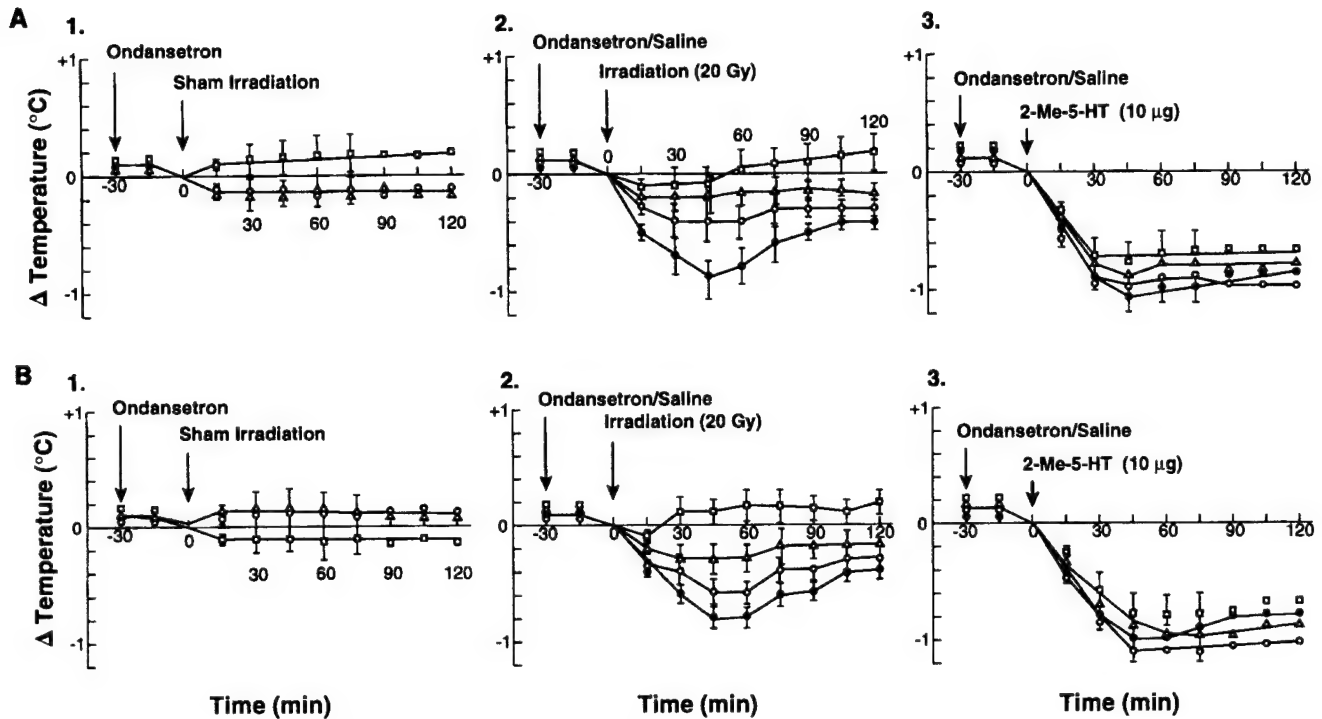
FIG. 2. Effect of i.p. (panel A) or intraventricular (panel B) administration of ondansetron on radiation-induced and 2-Me-5-HT-induced hypothermia. Panel A1: Sham irradiation preceded by i.p. treatment with (○) 50, (△) 100 or (□) 300 μg/kg ondansetron; panel B1: sham irradiation preceded by intraventricular treatment with (○) 5, (△) 10 or (□) 20 μg 2-Me-5-HT ondansetron; panel A2: 20 Gy irradiation (●) alone or in the presence of (○) 50, (△) 100 or (□) 300 μg/kg ondansetron; panel B2: 20 Gy irradiation (●) alone or in the presence of (○) 5, (△) 10 or (□) 20 μg ondansetron; panel A3: 10 μg of 2-Me-5-HT (●) alone or in the presence of (○) 50, (△) 100 or (□) 300 μg/kg ondansetron; panel B3: 10 μg of 2-Me-5-HT (●) alone or in the presence of (○) 5, (△) 10 or (□) 20 μg ondansetron. Each point represents the mean effect ± SE in five animals. Zero on the ordinate represents the temperature at the time of (1) sham irradiation, (2) irradiation and (3) 2-Me-5-HT administration.

of ICS 205-930 produced a significant attenuation of the hypothermia induced by exposure to 20 Gy γ rays that was dependent on the dose of the drug (Fig. 3A2; Table II). Compared to the rats treated with 2-Me-5-HT and given saline only, i.p. administration of ICS 205-930 produced a significant attenuation of the hypothermia induced by the intraventricular administration of 10 μg of 2-Me-5-HT that was dependent on the dose of the drug (Fig. 3A3; Table II). Compared to irradiated rats given saline only, intraventricular administration of ICS 205-930 produced a significant

attenuation of the hypothermia induced by exposure to 20 Gy γ rays (Fig. 3B2; Table II). Compared to the rats treated with 2-Me-5-HT that were given saline only, intraventricular administration of ICS 205-930 produced a significant attenuation of the hypothermia induced by the intraventricular administration of 10 μg of 2-Me-5-HT that was dependent on the dose of the drug (Fig. 3B3; Table II).

Higher doses of ondansetron or ICS 205-930 administered i.p. were not tested for their effect on radiation-induced hypothermia because they induced hypothermia in

TABLE I
Effects of Ondansetron on Radiation-Induced or 2-Me-5-HT-Induced Hypothermia

Pretreatment	Radiation-induced hypothermia	Level of significance of antagonism	2-Me-5-HT-induced hypothermia
50 μg/kg i.p.	Antagonism	$P < 0.05$	No antagonism
100 μg/kg i.p.	Antagonism	$P < 0.01$	No antagonism
300 μg/kg i.p.[a]	Antagonism	$P < 0.01$	No antagonism
5 μg intraventricularly	Antagonism	$P < 0.01$	No antagonism
10 μg intraventricularly	Antagonism	$P < 0.01$	No antagonism
20 μg intraventricularly[b]	Antagonism	$P < 0.01$	No antagonism

[a] 300 μg/kg i.p. of ondansetron produced greater attenuation of radiation-induced hypothermia than did 50 or 100 μg/kg ($P < 0.01$).
[b] 20 μg intraventricularly of ondansetron produced greater attenuation of radiation-induced hypothermia than did 5 or 10 μg ($P < 0.01$).
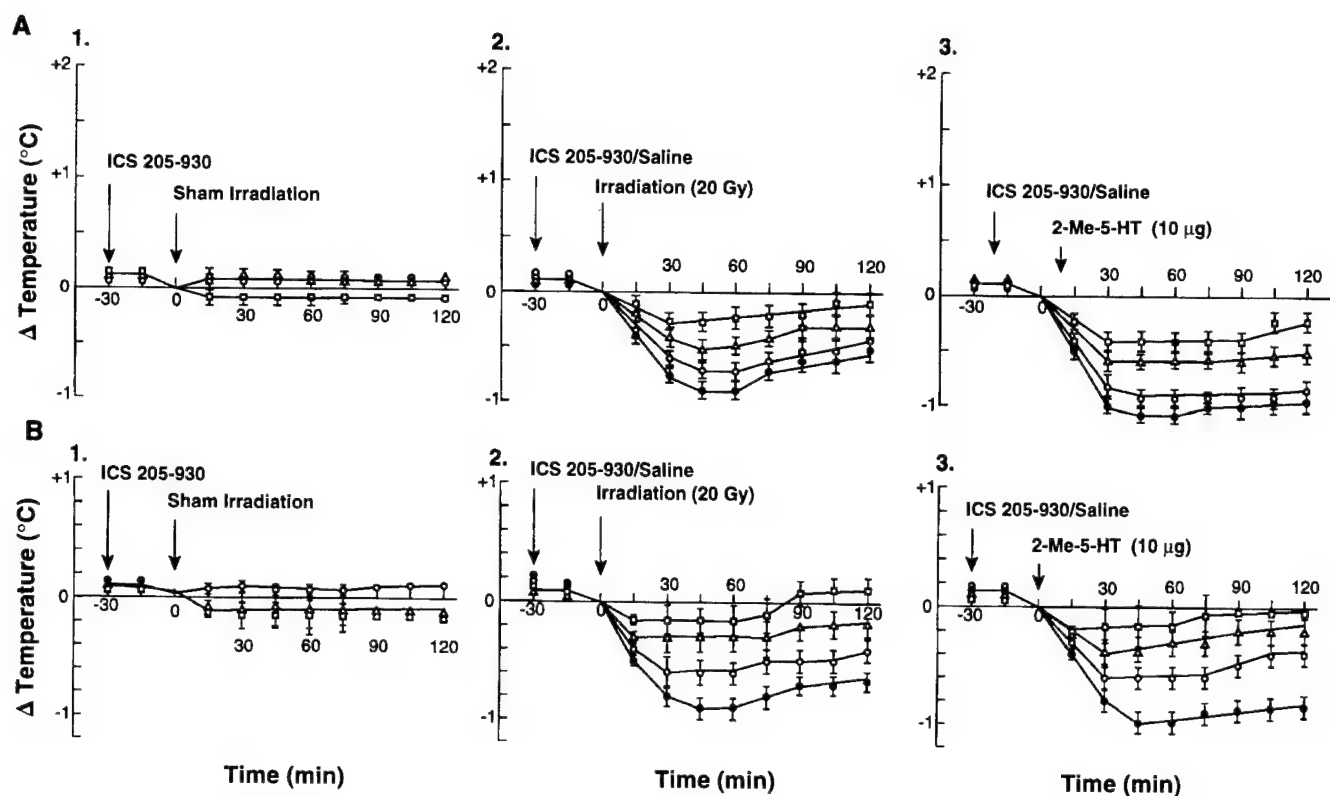
FIG. 3. Effect of ICS 205-930 given i.p. (panel A) or intraventricularly (panel B) on radiation-induced and 2-Me-5-HT-induced hypothermia. Panel A1: Sham irradiation preceded by i.p. treatment with (○) 50, (△) 100 or (□) 300 µg/kg ICS 205-930; panel B1: sham irradiation preceded by intraventricular treatment with (○) 5, (△) 10 or (□) 20 µg ICS 205-930; panel A2: 20 Gy irradiation (●) alone or in the presence of (○) 50, (△) 100 or (□) 300 µg/kg ICS 205-930; panel B2: 20 Gy irradiation (●) alone or in the presence of (○) 5, (△) 10 or (□) 20 µg ICS 205-930; panel A3: 10 µg of 2-Me-5-HT (●) alone or in the presence of (○) 50, (△) 100 or (□) 300 µg/kg ICS 205-930; panel B3: 10 µg of 2-Me-5-HT (●) alone or in the presence of (○) 5, (△) 10 or (□) 20 µg ICS 205-930. Each point represents the mean effect ± SE in five animals. Zero on the ordinate represents the temperature at the time of (1) sham irradiation, (2) irradiation and (3) 2-Me-5-HT administration.

control animals. For example, 0.5 mg/kg and 1 mg/kg of ondansetron induced 0.4 ± 0.10°C and 0.7 ± 0.15°C reductions in temperature, respectively (six animals). A similar induction of hypothermia in control animals was observed after 0.5 mg/kg and 1 mg/kg of ICS 205-930.

DISCUSSION

The hypothalamus is the most important central site for temperature regulation. The perfusion of the anterior hypothalamus with an artificial cerebrospinal fluid containing an excessive amount of calcium induces hypothermia (22). In our study, when 2-Me-5-HT was administered into the lateral ventricle of the brain, it induced hypothermia; when it was administered peripherally, it did not change body temperature. At this time, it is not known how centrally injected 2-Me-5-HT induces hypothermia and why peripherally injected 2-Me-5-HT does not induce changes in temperature except to suggest that an effective concentration of 2-Me-5-HT is not achieved in the brain because of the blood–brain barrier. In addition, it has been suggested that an increase in the intracellular concentration of calcium from the extracel-

lular environments might be responsible for the induction of hypothermia since an increase in intracellular calcium has been demonstrated in a hybrid (mouse neuroblastoma × rat glioma: NG 108-15) cell line (12, 13) by 5-HT3 receptor stimulation. It is not uncommon for 2-Me-5-HT to induce different responses when it is administered centrally and peripherally. For example, injection of 2-Me-5-HT directly into the area postrema of ferrets evoked only signs of nausea (23). By contrast, oral administration of 2-Me-5-HT evoked emesis in ferrets (24). Intravenous injection of 2-Me-5-HT did not evoke emesis in ferrets or dogs (25, 26).

Ionizing radiation causes tissue damage predominantly through generation of free radicals (27). A variety of free radical species are likely to be generated. Free radicals such as superoxide $O_2^{\bullet-}$, the hydroxyl radical ($^\bullet$OH) and hydrogen peroxide are typically generated by the exposure of living tissue to ionizing radiation (27). Membrane damage caused by these reactive oxygen species may allow the entry of excess calcium into cells with subsequent cellular dysfunction and death (28, 29). Calcium channel blockers have a radioprotective effect when used alone or with other types of radioprotectors (30). As men-

TABLE II
Effects of ICS 205-930 on Radiation-Induced or 2-Me-5-HT-Induced Hypothermia

Pretreatment	Radiation-induced hypothermia	Level of significance of antagonism	2-Me-5-HT-induced hypothermia	Level of significance of antagonism
50 µg/kg i.p.	Antagonism	$P < 0.01$	Antagonism	$P < 0.05$
100 µg/kg i.p.	Antagonism	$P < 0.01$	Antagonism	$P < 0.01$
300 µg/kg i.p.[a]	Antagonism	$P < 0.01$	Antagonism	$P < 0.01$
5 µg intraventricularly	Antagonism	$P < 0.01$	Antagonism	$P < 0.01$
10 µg intraventricularly	Antagonism	$P < 0.01$	Antagonism	$P < 0.01$
20 µg intraventricularly[b]	Antagonism	$P < 0.01$	Antagonism	$P < 0.01$

[a] 300 µg/kg i.p. of ICS 205-930 produced greater attenuation of radiation-induced or 2-Me-5-HT-induced hypothermia than did 50 or 100 µg/kg ($P < 0.01$).

[b] 20 µg intraventricularly of ICS 205-930 produced greater attenuation of radiation-induced or 2-Me-5-HT-induced hypothermia than did 5 or 10 µg ($P < 0.01$).

tioned earlier, perfusion of the anterior hypothalamus with an artificial cerebrospinal fluid containing an excessive amount of calcium induces hypothermia (*22*). Increased intracelluar calcium might be responsible for the abnormal electrochemical changes in the heart induced by hypothermia. Treatment with calcium channel blockers such as nisoldipine prevented an increase in intracellular calcium and greatly reduced arhythmias induced by hypothermia (*31*). It has been reported that hypothermia induced by ionizing radiation is mediated by histamine H1 and H2 receptors (*3–5*). Although the mechanism involved in radiation-induced hypothermia is unknown at this time, it has been suggested that free radicals induced the increase in intracellular calcium and histamine may also have played an important role. To date, there are no reports on the effects of calcium channel blockers on radiation-induced hypothermia.

The doses of ondansetron and ICS 205-930 used in this study were chosen from pilot studies that were based on previous studies reporting effectively attenuated radiation- and chemotherapy-induced emesis (*16, 17*). Although ondansetron and ICS 205-930, which are 5-HT3 antagonists and antiemetics, did attenuate radiation-induced hypothermia, only ICS 205-930 attenuated 2-Me-5-HT-induced hypothermia. At this time there is no explanation to offer for the difference except to suggest that, although the subtypes of 5-HT3 receptors are not fully established, the hypothermia induced by 2-Me-5-HT is due to some known or unknown subtypes of 5-HT3 receptors that are sensitive to ICS 205-930 and insensitive to ondansetron. In addition, it is possible that hypothermia is like emesis, in which some emetic stimuli are inhibited by 5-HT3 antagonists (cytotoxic therapy, migraine, ipecac, emetine, oral 2-Me-5-HT and phenylbiguanide) while some emetic stimuli are unaffected by 5-HT3 receptor antagonism (motion sickness, apomorphine, morphine, erythromycin, histamine, pilocarpine, protoveratrine, copper sulfate and urethane) (*32*).

Antioxidant enzymes such as superoxide dismutase (SOD), glutathione peroxidase and catalase offer protection against ionizing radiation-induced oxidants (*33*).

Although there are no reports on the effects of antioxidant enzymes on radiation-induced hypothermia, treatment with SOD and glutathione peroxidase prevented radiation-induced hyperthermia in rats (*34*). It has been suggested that ondansetron and ICS 205-930 might act as histamine antagonists (*4, 5*) or calcium antagonists (*30*) to attenuate radiation-induced hypothermia by inhibiting radiation-induced calcium overloading inside the cell (*28, 29*). In addition, ondansetron and ICS 205-930 might have antioxidative effects that scavenge free radicals generated by radiation. Further work is required to verify whether or not ondansetron and ICS 205-930 have histamine antagonist, calcium antagonist and free radical scavenging properties.

This study demonstrates the effects of 5-HT3 receptor antagonists ondansetron and ICS 205-930 on hypothermia induced by radiation and by administration of the 5-HT3 receptor agonist 2-Me-5-HT. Ondansetron and ICS 205-930 attenuate radiation-induced hypothermia. However, in contrast to ICS 205-930, which attenuates 2-Me-5-HT-induced hypothermia, ondansetron does not attenuate the hypothermia induced by 2-Me-5-HT.

ACKNOWLEDGMENT

REFERENCES

1. T. S. Veninga, Implications of bioamines in the X-ray temperature response of cats and rabbits. *Radiat. Res.* **48**, 358–367 (1971).

2. H. Fanger and C. C. Lushbaugh, Radiation death from cardiovascular shock following a criticality accident. *Arch. Pathol.* **84**, 446–460 (1967).

3. S. B. Kandasamy and W. Hunt, Involvement of histamine H1 and H2 receptors in hypothermia induced by ionizing radiation in guinea pigs. *Life Sci.* **42**, 555–563 (1988).

4. S. B. Kandasamy, W. A. Hunt and G. A. Mickley, Implication of prostaglandins and histamine H1 and H2 receptors in radiation-

induced temperature responses of rats. *Radiat. Res.* **114**, 42–53 (1988).

5. S. B. Kandasamy and W. A. Hunt, Involvement of prostaglandins and histamine in radiation-induced temperature responses in rats. *Radiat. Res.* **121**, 84–90 (1990).

6. W. Feldberg and R. D. Myers, Changes in temperature produced by microinjections of amines into the anterior hypothalamus of cats. *J. Physiol.* **177**, 239–245 (1965).

7. L. I. Crawshaw, Effects of intracerebral 5-hydroxytryptamine injection on thermoregulation in rats. *Physiol. Behav.* **9**, 133–140 (1972).

8. P. B. Bradley, G. Engel, W. Fenuik, J. R. Fozard, P. P. A. Humphrey, D. N. Middlemiss, E. J. Mylecharane, B. P. Richardson and P. R. Saxena, Proposals for the classification and nomenclature of functional receptors for 5-hydroxytryptamine. *Neuropharmacology* **25**, 563–576 (1986).

9. G. J. Kilpatrick, B. J. Jones and M. B. Tyers. Identification and distribution of 5-HT3 receptors in rat brain using radioligand binding. *Nature* **330**, 746–748 (1987).

10. G. J. Kilpatrick, B. J. Jones and M. B. Tyers, Binding of the 5-HT3 ligand [^{3}H]GR65630 to rat area postrema, vagus nerve and the brains of several species. *Eur. J. Pharmacol.* **159**, 157–164 (1989).

11. E. S. Bush and S. E. Mayer, 5-Hydroxytryptamine (serotonin) receptor agonists and antagonists. In *Goodman and Gilman's The Pharmacological Basis of Therapeutics*, 9th ed. (J. G. Hardman, L. E. Limbird, P. B. Molinoff, R. W. Ruddon and A. G. Gilman, Eds.), pp. 249–264. McGraw-Hill, New York, 1996.

12. G. Reiser, Mechanism of stimulation of cyclic GMP level in a neuron cell line mediated by serotonin (5-HT3) receptors. *Eur. J. Biochem.* **189**, 547–552 (1990).

13. G. Reiser, Molecular mechanisms of action induced by 5-HT3 receptors in a neuronal cell line and by 5-HT2 receptors in a glial cell line. In *Molecular Biology, Receptors and Functional Effects* (J. R. Fozard and P. R. Saxena, Eds.), pp. 69–83. Birkhauser, Basel, 1991.

14. B. P. Richardson and G. Engel, The pharmacology and function of 5-HT3 receptors. *Trends Neurosci.* **9**, 424–428 (1986).

15. S. J. Peroutka, Species variations in 5-HT3 recognition sites labeled by ^{3}H-quipazine in the central nervous system. *Naunyn-Schmiedeberg's Arch. Pharmacol.* **338**, 472–475 (1988).

16. N. R. Newberry, S. H. Cheshire and M. J. Gilbert, Evidence that the 5-HT3 receptors of the rat, mouse and guinea-pig superior cervical ganglion may be different. *Br. J. Pharmacol.* **102**, 615–620 (1991).

17. A. M. Galzin and S. Z. Langer, Modulation of 5-HT release by presynaptic inhibitory and facilitatory 5-HT receptors in brain slices. *Adv. Biosci.* **82**, 59–62 (1991).

18. A. J. Freeman, K. T. Cunningham and M. B. Tyers, Selectivity of 5-HT3 receptor antagonists and anti-emetic mechanisms of action. *Anticancer Drugs* **3**, 79–85 (1992).

19. S. M. Grunberg and P. J. Hesketh, Control of chemotherapy-induced emesis. *N. Engl. J. Med.* **329**, 1790–1796 (1993).

20. Task Group 21, Radiation Therapy Committee, AAPM, A protocol for the determination of absorbed dose from high energy photon and electron beams. *Med. Phys.* **10**, 741 (1983).

21. L. S. Pelligrino, A. S. Pelligrino and A. J. Cushman, *A Sterotaxic Atlas of the Rat Brain*. Plenum Press, New York, 1979.

22. R. D. Myers and W. L. Veale, Body temperature: Possible ionic mechanism in the hypothalamus controlling the set point. *Science* **170**, 95–97 (1970).

23. G. A. Higgins, G. J. Kilpatrick, K. T. Bunce, B. J. Jones and M. B. Tyers, 5-HT3 receptor antagonists injected into the area postrema inhibit cisplatin-induced emesis in the ferret. *Br. J. Pharmacol.* **97**, 247–255 (1989).

24. L. F. Sancilio, L. M. Pinkus, C. B. Jackson and H. R. Munson, Studies on the emetic and anti-emetic properties of zacopride and its enantiomer. *Eur. J. Pharmacol.* **192**, 365–369 (1991).

25. I. Monkovic and J. A. Gylys, Developments in the antiemetic area: Chemistry, pharmacology and therapy. *Prog. Med. Chem.* **27**, 297–323 (1990).

26. I. M. Lang and M. Steensrud, The effects of 2-m-5-HT on gastrointestinal motor activity. *Gastroenterology* **100**, A462 (1991). [Abstract]

27. E. J. Hall, The physics and chemistry of radiation absorption. In *Radiobiology for the Radiologist*, 4th ed., pp. 1–13. J. B. Lippincott, Philadelphia, 1994.

28. D. W. Choi, Glutamate neurotoxicity and diseases of the nervous system. *Neuron* **1**, 623–634 (1988).

29. S. M. Rothman and J. W. Olney, Excitotoxicity and the NMDA receptor. *Trends Neurosci.* **10**, 299–302 (1987).

30. G. L. Floersheim, Radioprotective effects of calcium antagonists used alone or with other types of radioprotectors. *Radiat. Res.* **133**, 80–87 (1993).

31. H. Bjornstad, D. A. Lathrop and H. Refsum, Prevention of some hypothermia induced electrochemical changes by calcium channel blockade. *Cardiovasc. Res.* **28**, 55–60 (1994).

32. G. J. Sanger, The involvement of 5-HT3 receptors in visceral function. In *Central and Peripheral 5-HT3 Receptors* (M. Hamon, Ed.), pp. 208–255. Academic Press, San Diego, 1992.

33. E. J. Hall, Radioprotectors. In *Radiobiology for the Radiologist*, 4th ed., pp. 183–190. J. B. Lippincott, Philadelphia, 1994.

34. S. B. Kandasamy, K. S. Kumar and A. H. Harris, Involvement of superoxide dismutase and glutathione peroxidase in attenuation of radiation-induced hyperthermia by interleukin-1α in rats. *Brain Res.* **606**, 106–110 (1993).

Regional Differences in Glial Cell Modulation of Synaptic Transmission

David O. Keyser* and Terry C. Pellmar

Physiology Department, Armed Forces Radiobiology Research Institute, Bethesda, Maryland

ABSTRACT: Metabolic integrity of glial cells in field CA1 of the guinea pig hippocampus is critical to maintenance of synaptic transmission (Keyser and Pellmar [1994] Glia 10:237–243). To determine if this tight glial-neuronal coupling is equally important in other brain regions, we compared the effect of fluoroacetate (FAC), a glial specific metabolic blocker, on synaptic transmission in field CA1 to synaptic transmission in area dentata (DG). FAC was significantly more effective in decreasing synaptic potentials in CA1 than in DG. A similar regional disparity in the FAC-induced decrease in ATP levels was evident. Isocitrate, a glial specific metabolic substrate, prevented the FAC-induced synaptic depression in both CA1 and DG. The results suggest that glia of CA1 and dentate respond differently to metabolic challenge. Modulation of this glial-neuronal coupling could provide a regionally specific mechanism for synaptic plasticity. Additionally, site-specific glial-neuronal interactions can impact on a variety of physiological and pathophysiological conditions. *Hippocampus 7:73–77, 1997.*   © 1997 Wiley-Liss, Inc.[†]

KEY WORDS: hippocampus; dentate gyrus; neuroglia; fluoroacetate; metabolism

INTRODUCTION

Glial-neuronal coupling has long been considered a passive process whereby glial cells ensure proper maintenance of the extracellular milieu without taking an active role in neural transmission. This view has recently been challenged by us and others (Keyser and Pellmar, 1994; Parpura et al., 1994; Nedergaard, 1994; Mennerick and Zorumski, 1994) who have shown that glia can directly influence neuronal activity. Recent evidence suggests that glial cells are integral to the maintenance of synaptic transmission in the hippocampus (Keyser and Pellmar, 1994). Additionally, identification of glial-neuronal gap junctions (Nedergaard, 1994), neurotransmitter receptors on glial cells (Murphy and Pearce, 1987; Hansson, 1989; von Blankenfeld and Kettenmann, 1991) and rapid glial-glial (Cornell-Bell et al., 1990) and glial-neuronal (Mennerick and Zorumski, 1994; Nedergaard, 1994; Parpura et al., 1994) communication further suggests that glial cells not only act to maintain central nervous system (CNS) functions but may serve to modulate these activities.

We previously identified a role for glial cells in the maintenance of excitatory neurotransmission in field CA1 of the guinea pig hippocampal slice preparation (Keyser and Pellmar, 1994). When glial cells are metaboli-cally challenged with the glial specific metabolic blocker fluoroacetate (FAC), excitatory neurotransmission is decreased in a dose- and time-dependent manner. Since mechanisms of synaptic plasticity can vary with brain region, regional differences in this glial phenomenon also might reflect a role in plasticity. In contrast, a support role of glial cells is more likely to be constant across regions.

We now report that glial-neuronal coupling differs in field CA1 and area dentata (DG) of the hippocampus. Electrophysiological and biochemical measurements show that the DG is far less sensitive to glial metabolic challenge than CA1. These data demonstrate that glial-neuronal coupling can be influenced by location and support a role for glial cells in neuronal plasticity.

MATERIALS AND METHODS

Electrophysiological Preparation

All electrophysiological experiments were performed using brains from male Hartley guinea pigs and handled as previously described (Pellmar, 1987). Guinea pigs were anesthetized with isoflurane and euthanized via cervical dislocation according to the guidelines set forth by the American Veterinary Medical Association (American Veterinary Medical Association, 1993). The brain was rapidly removed, hemisected and placed in ice-cold artificial cerebrospinal fluid (ACSF) containing (in mM): 124 NaCl, 3 KCl, 2.4 CaCl$_2$, 1.3 MgSO$_4$, 1.24 KH$_2$PO$_4$, 10 glucose, 26 NaHCO$_3$; pH 7.4. The hippocampus was dissected from cerebral hemispheres, and slices (450 μm) were made using a McIlwain tissue chopper. To allow for metabolic recovery following slice preparation the tissue was incubated in oxygenated ACSF at room temperature for at least 1 h prior to use. Slices for electrophysiology were transferred to a submerged slice recording chamber (Zbicz design) and continuously perfused with oxygenated ACSF maintained at 30 ± 1°C. All drugs used were purchased through Sigma Chemical Company (St. Louis, MO), dissolved in ACSF and perfused at a rate of 1–2 ml/min. FAC was handled

*Correspondence to: David O. Keyser, Diving and Experimental Physiology Department, Naval Medical Research Institute, 8901 Wisconsin Avenue, Bethesda, MD 20889-5607.

cautiously at all times. Gloves and masks were employed to minimize contact with FAC.

The CA1 region of the pyramidal cell layer or the dentate granule cell layer of the DG was visually identified under a dissecting microscope. Extracellular synaptic potentials were recorded with glass microelectrodes filled with 2 M NaCl and positioned in stratum radiatum of CA1 or in the molecular layer of the dentate gyrus. Neurons were impaled with glass microelectrodes (20–40 MΩ) filled with 2 M KCl or 2 M K-Acetate as previously described (Pellmar, 1987). Acceptable CA1 pyramidal cells had resting membrane potentials of −60 mV or greater with input resistances above 30 MΩ. Criteria for dentate granule cells was a resting membrane potential of −75 mV or greater, no "burst" firing and a strong spike adaptation response to depolarizing current injections. Data were collected using a Dagan 8100 under current clamp mode using the switching circuitry.

Postsynaptic potentials (PSPs) were evoked with a concentric bipolar stainless steel stimulating electrode placed in either stratum radiatum, for recording from a CA1 neuron or the outer molecular layer of the DG for recording from a dentate granule cell. Holding current (50–200 pA) was often passed to hyperpolarize CA1 cells (−70 to −80 mV) so that 5–15 mV PSPs could be reliably elicited without evoking action potentials. At these membrane potentials, inhibitory PSPs are very close to their reversal potential and minimally contribute to the PSPs recorded with 2 M potassium acetate-filled electrodes. In experiments using 2 M KCl-filled electrodes, the chloride equilibrium potential (and consequently the inhibitory PSP reversal potential) is shifted and the recorded PSP is a mix of excitatory and inhibitory potentials. Results were similar under both recording conditions.

ATP Measurements

For ATP measurements, hippocampal slices were incubated in 10 ml of oxygenated experimental solution for 30 min at 29°–31°C. Slices were then removed and CA1 and DG regions were rapidly isolated. CA1 and DG regions of the hippocampal slice were identified under a dissecting microscope and isolated by making two vertical cuts to remove the subiculum and CA2/CA3 regions. CA1 and DG were then separated by a medial cut superior to the dentate granule cell layer. Tissue from 3–4 slices was placed in 1 ml of 50 mM HEPES buffer (pH 7.4) and rapidly frozen in liquid nitrogen. ATP was measured using a fluorescence assay. Preparations were rapidly thawed and homogenized. Additions of 10 mM glucose and 50 U hexokinase, to convert ATP and glucose to glucose-6-phosphate, were made and the preparations incubated on a rotator at room temperature. After 45 min 1 mM NADP$^+$ and 10 U glucose-6-phosphate dehydrogenase were added and the preparations incubated on a rotator overnight at room temperature. The accumulated NADPH was then measured using a Cytoflor (Millipore), excitation filter 360 nM, emission filter 460 nM. ATP standards were handled in similar fashion and measured with each experiment. Protein for each group was measured using the Bio-Rad Protein Assay (Bio-Rad, Richmond, CA) and values expressed as nmol ATP/mg protein. For presenta-
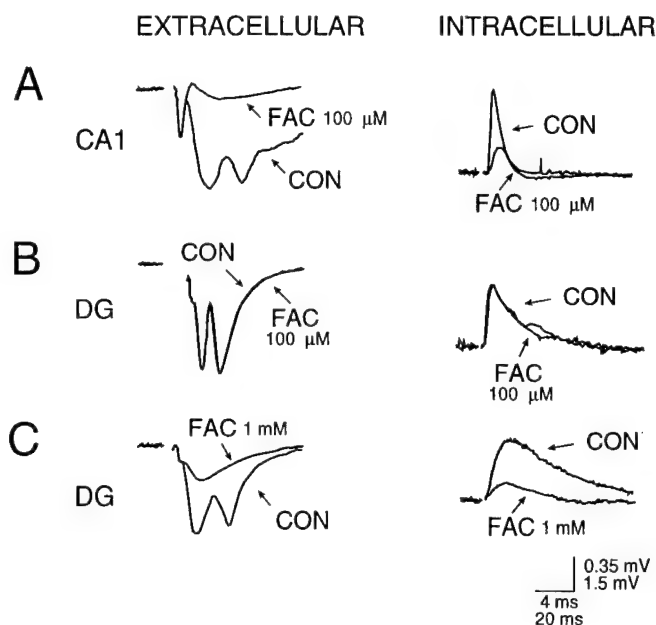
FIGURE 1.   Regional sensitivity to fluoroacetate-induced depression of evoked synaptic transmission. Shown are superimposed voltage traces recorded in control (CON) ACSF and following 30 min application of FAC using either extracellular or intracellular recording paradigms. A: FAC (100 μM) causes a marked depression in field and intracellularly recorded PSPs in CA1 pyramidal neurons. B: 100 μM FAC has no effect on evoked synaptic transmission in the dentate. C: FAC at 1 mM depresses synaptic transmission in dentate granules neurons.

tion data are expressed as the percent change from the paired control.

Quantitation and Analyses

PSP slope depression was calculated for each preparation as the percent change of the initial segment of the slope of the PSP after 30 min in drug compared to control PSP slope measurements. Dose-response curves are best fit to the function $y = a \cdot x/(b + x)$ where a = maximal depression, b = IC$_{50}$, x is the concentration of FAC and y is either the resulting depression in ATP levels or synaptic potentials. The maximal depression and IC$_{50}$ parameters were determined through RS1 (BBN Software, Cambridge, MA).

RESULTS

The glial-specific metabolic inhibitor fluoroacetate (FAC) decreases evoked postsynaptic potentials (PSPs) in CA1 and DG of the guinea pig hippocampal slice preparation. In CA1, exposure to 100 μM FAC for 30 min reduced both intracellularly (68.9 ± 6.6% decrease of PSP slope; N = 8) and extracellularly (68.6 ± 8.8%; N = 4; Fig. 1A) recorded PSPs. In contrast 100 μM FAC had little effect on PSPs recorded from dentate granule neurons (Fig. 1B). Comparable synaptic depression of evoked PSPs (extracellular = 73.2 ± 10.6%, N = 4; intracellular =
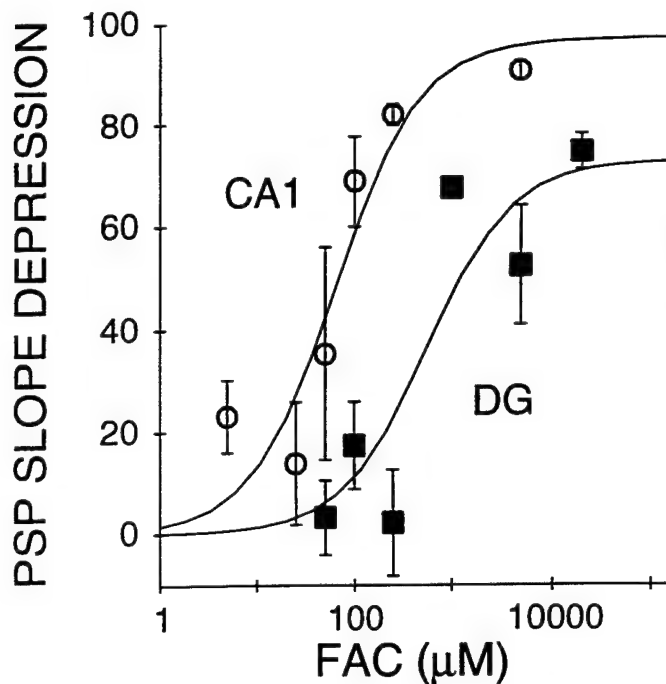
FIGURE 2.   Dentate gyrus is less sensitive to FAC than CA1. Percent PSP slope depression is graphed as a function of FAC concentration for field PSPs recorded in CA1 or DG. There is a strong shift to the right of the dose-response relationship in DG. For CA1 the $IC_{50} = 65$ μM and for DG the $IC_{50} = 554$ μM. Circles represent the mean ± SEM of 3–8 preparations.

$67.2 \pm 1.7\%$, N = 5) in the DG was observed only when the concentration of FAC was increased to 1 mM (Fig. 1C). Membrane potentials for CA1 (CON = -69.3 ± 2.4 mV, FAC (100 μM) = -70.6 ± 3.6 mV, N = 8) and DG (CON = -80.4 ± 2.0 mV, FAC (1 mM) = -78.3 ± 2.6 mV) and input resistances for CA1 (CON = 39.7 ± 4.8 MΩ, FAC (100 μM) = 40.9 ± 6.1 MΩ, N = 8) and DG (CON = 56.3 ± 8.4 MΩ, FAC (1 mM) = 60.7 ± 6.5 MΩ, N = 5) were not significantly affected by FAC.

The dose-response relationship for CA1 shows a maximal effect at concentrations of FAC above 500 μM with an IC_{50} of 65 μM (Fig. 2). In the DG, the dose response relationship shows an IC_{50} of 554 μM, almost an order of magnitude greater (Fig. 2). At concentrations of 1 mM or more, FAC elicits a maximal effect in the DG; at concentrations of 250 μM or less the effect is minimal.

Previous work has shown that FAC-induced synaptic depression in CA1 can be prevented by pretreatment with isocitrate (Fig. 3A). The target enzyme for FAC is the Krebs cycle enzyme aconitase which catalyzes the conversion of citrate to isocitrate. Therefore, isocitrate, which is taken up preferentially by glia, should short circuit the FAC effect on glial metabolism. Isocitrate (3 mM) effectively prevents FAC-induced synaptic depression in DG (Fig. 3B). This is consistent with a glial metabolic mechanism underlying the FAC-induced synaptic depression in both CA1 and DG.

Changes in ATP can also reflect metabolic disruption. Figure 4 illustrates the dose-response relationship for FAC on ATP levels in

CA1 and DG. As with the electrophysiological dose-response, these curves demonstrate that CA1 is much more sensitive to FAC than DG. The IC_{50} for FAC in DG is 4.5 mM, far greater than that observed in CA1 ($IC_{50} = 31$ μM).

DISCUSSION

Using the glial specific metabolic blocker FAC we have now demonstrated that there are regional differences in glial cell influence on synaptic transmission between field CA1 and DG of the guinea pig hippocampus. Synaptic transmission in CA1 is an order of magnitude more sensitive to FAC than is DG.

The protection afforded by the metabolic substrate isocitrate suggests that in both CA1 and DG, FAC disrupts the Krebs cycle. In CA1 the dose-response curves for reduction of the PSP and the decrease in ATP appear closely related with similar IC_{50}s and maximally effective concentrations. Yet in DG, the synaptic potentials are reduced at FAC concentrations that do not alter the ATP levels suggesting that synaptic transmission can be affected without a concurrent decrease in ATP. Similarly others (Hassel et al., 1994; Swanson and Graham, 1994) have reported that in cultured astrocytes fluorocitrate (the active form of fluoroacetate)

ISOCITRATE 1 mM
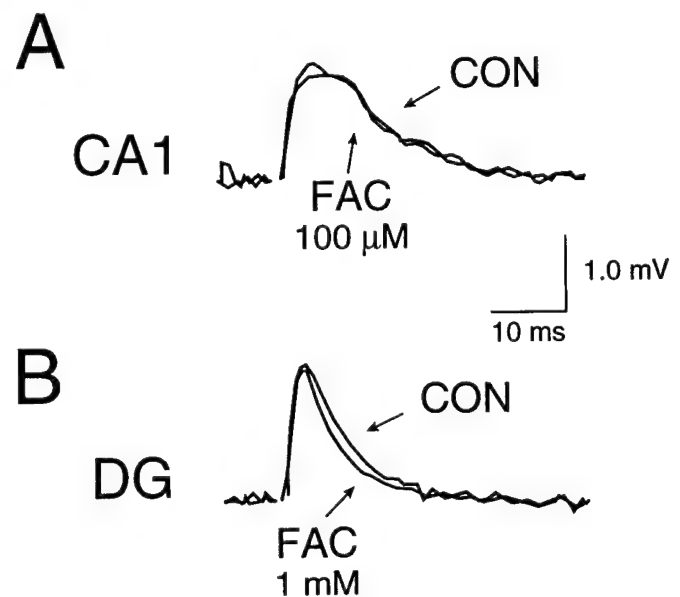
FIGURE 3.   Similar mechanism of FAC-induced synaptic depression in CA1 and dentate gyrus. Superimposed voltage traces of intracellularly recorded PSPs from CA1 (A) and DG (B) neurons in control (CON) ACSF and following 30 min application of FAC (100 μM in CA1; 1 mM in DG) in the presence of isocitrate (ISO, 1 mM). Isocitrate inhibited FAC-induced depression of synaptic transmission in both regions. Isocitrate is taken up specifically by glial cells and acts as a metabolic substrate to prevent the metabolic effect of FAC.
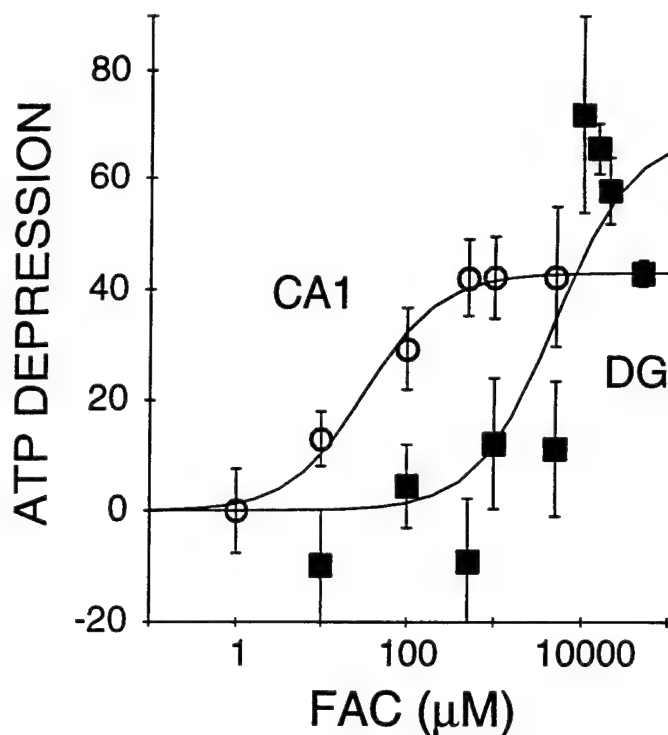
FIGURE 4.   DG is less sensitive than CA1 to FAC-induced metabolic inhibition. Percent depression in ATP levels is illustrated as a function of FAC concentration for CA1 and DG regions. There is a strong shift to the right of the dose-response relationship in DG. For CA1 the IC$_{50}$ = 31 μM and for DG the IC$_{50}$ = 4.5 mM. Circles represent the mean ± SEM of 3–8 preparations. Control ATP measurements: CA1 = 9.36 ± 1.9 nmol ATP/mg protein (N = 12), DG = 12.46 ± 3.6 nmol ATP/mg protein (N = 12). These values agree with previously reported ATP measurements (Erecinska et al., 1991; Kass et al., 1992; Keyser and Pellmar, 1994).

can decrease glutamine levels without changes in ATP. Hassel et al. (1994) suggest that glutamine feeds back into the Krebs cycle as α-ketoglutarate to maintain ATP. The same could be happening in the cells of the DG. Glutamine, normally used as a precursor for glutamate at the synaptic terminal, would be decreased and thus result in impaired synaptic transmission.

Glutamine is synthesized from glutamate in astrocytes through the ATP-dependent enzyme glutamine synthetase (Fonnum, 1993; Yudkoff et al., 1993). This enzyme is regionally distributed within the hippocampus. Both in human (Derouiche and Ohm, 1994) and in rat (Derouiche and Frotscher, 1991) hippocampus the highest levels are in the dentate. With very efficient machinery to produce glutamine in DG it may be possible to maintain glutamate supplies as well as ATP levels against a greater metabolic stress. In contrast in CA1, a lower level of glutamine synthetase could result in limited supplies of glutamine to the presynaptic terminal.

In CA1 this system of modulating presynaptic glutamine may be a basis for glial-mediated synaptic plasticity. In this scheme, modulation of the glutamate/glutamine cycle could alter levels of glutamine precursor and hence the glutamate availability at the presynaptic terminal. We describe a mechanism whereby alter-

ation in glial metabolism is the causative factor in synaptic modulation. In fact, glutamine pretreatment of slices attenuates FAC-induced synaptic inhibition in CA1 (Keyser and Pellmar, 1994). Since glutamine can also enter the TCA cycle and act as a substrate this evidence only partially supports our hypothesis. In contrast, the glutamine synthetase-rich dentate is unlikely to use this as a modulatory mechanism.

Physiologically there are several factors that have effects on the glutamate/glutamine cycle. Metabotropic glutamate receptor activation (Miller et al., 1992), ischemia (Sher and Hu, 1990; Tanaka et al., 1992; Petito et al., 1992), radiation (Dimberg et al., 1992), lead (Sierra and Tiffany-Castiglioni, 1991), hypoxia (Sher and Hu, 1990), glucocorticoids (Zielke et al., 1990; O'Callaghan et al., 1991; Laping et al., 1994) and second messengers (Zielke et al., 1990; Kentroti et al., 1991) have been identified as modulators of glutamine synthetase activity. Additionally, glucocorticoids (Tombaugh and Sapolsky, 1992) and adrenergic neurotransmitters (Hertz, 1992) have also been shown to affect glial metabolism. These factors may act physiologically via actions on the glutamate/glutamine cycle.

We cannot rule out the possibility that other glial factors play a part in the mechanism of FAC-induced inhibition of synaptic transmission. Glial cells are known to be highly regulatory and could influence neurotransmission by release of neuromodulatory factors (e.g. taurine or growth factors), modulation of gap junctions or morphological changes. More studies are needed to identify how other such mechanisms would contribute to regional specificity of glial modulation of synaptic transmission.

Our data show that glial-neuronal coupling differs between hippocampal regions. This finding may be critical to the understanding of information processing and plasticity of synaptic transmission in the hippocampus.

Acknowledgments

REFERENCES

American Veterinary Medical Association (1993) 1993 Report of the AVMA panel on euthanasia. JAVMA 202(2):229–249.

Cornell-Bell AH, Finkbeiner SM, Cooper MS, Smith SJ (1990) Glutamate induces calcium waves in cultured astrocytes: Long-range glial signaling. Science 247:470–473.

Derouiche A, Frotscher M (1991) Astroglial processes around identified glutamatergic synapses contain glutamine synthetase: Evidence for transmitter degradation. Brain Res 552:346–350.

Derouiche A, Ohm TG (1994) Glutamine synthetase immunoreactivity

in the human hippocampus is lamina-specific. Neurosci Lett 165:179–182.

Dimberg Y, Tottmar O, Aspberg A, Ebendal T, Johansson KJ, Walinder G (1992) Effects of low-dose X-irradiation on mouse-brain aggregation cultures. Int J Radiat Biol 61:355–363.

Erecinska M, Dagani F, Nelson D, Deas J, Silver IA (1991) Relations between intracellular ions and energy metabolism: A study with monensin in synaptosomes, neurons, and C6 glioma cells. J Neurosci 11:2410–2421.

Fonnum F (1993) Regulation of the synthesis of the transmitter glutamate pool. Prog Biophys Molec Biol 60:47–57.

Hansson E (1989) Co-existence between receptors, carriers, and second messengers on astrocytes grown in primary cultures. Neurochem Res 14:811–819.

Hassel B, Sonnewald U, Unsgard G, Fonnum F (1994) NMR spectroscopy of cultured astrocytes: Effects of glutamine and the gliotoxin fluorocitrate. J Neurochem 62:2187–2194.

Hertz L (1992) Autonomic control of neuronal-astrocytic interactions, regulating metabolic activities, and ion fluxes in the CNS. Brain Res Bull 29:303–313.

Kass IS, Abramowicz AE, Cottrell JE, Chambers G (1992) The barbiturate thiopental reduces ATP levels during anoxia but improves electrophysiological recovery and ionic homeostasis in the rat hippocampal slice. Neuroscience 49:537–543.

Kentroti S, Baker R, Lee K, Bruce C, Vernadakis A (1991) Platelet-activating factor increases glutamine synthetase activity in early and late passage C-6 glioma cells. J Neurosci Res 28:497–506.

Keyser DO, Pellmar TC (1994) Synaptic transmission in the hippocampus: Critical role for glial cells. Glia 10:237–243.

Laping NJ, Nichols NR, Day JR, Johnson SA, Finch CE (1994) Transcriptional control of glial fibrillary acidic protein and glutamine synthetase in vivo shows opposite responses to corticosterone in the hippocampus. Endocrinology 135(5):1928–1933.

Mennerick S, Zorumski CF (1994) Glial contributions to excitatory neurotransmission in cultured hippocampal cells. Nature 368:59–62.

Miller S, Cotman CW, Bridges RJ (1992) 1-Aminocyclopentane-trans-1,3-dicarboxylic acid induces glutamine synthetase activity in cultured astrocytes. J Neurochem 58:1967–1970.

Murphy S, Pearce B (1987) Functional receptors for neurotransmitters on astroglial cells. Neuroscience 22:381–394.

Nedergaard M (1994) Direct signaling from astrocytes to neurons in cultures of mammalian brain cells. Science 263:1768–1771.

O'Callaghan JP, Brinton RE, Mcewen BS (1991) Glucocorticoids regulate the synthesis of glial fibrillary acidic protein in intact and adrenalectomized rats but do not affect its expression following brain injury. J Neurochem 57:860–869.

Parpura V, Basarsky TA, Liu F, Jeftinija K, Jeftinija S, Haydon PG (1994) Glutamate-mediated astrocyte-neuron signalling. Nature 369:744–747.

Pellmar TC (1987) Peroxide alters neuronal excitability in the CA1 region of guinea-pig hippocampus in vitro. Neuroscience 23(2):447–456.

Petito CK, Chung MC, Verkhovsky LM, Cooper AJL (1992) Brain glutamine synthetase increases following cerebral ischemia in the rat. Brain Res 569:275–280.

Sher PK, Hu S (1990) Increased glutamate uptake and glutamine synthetase activity in neuronal cell cultures surviving chronic hypoxia. Glia 3:350–357.

Sierra EM, Tiffany-Castiglioni E (1991) Reduction of glutamine synthetase activity in astroglia exposed in culture to low levels of inorganic lead. Toxicology 65:295–304.

Swanson RA, Graham SH (1994) Fluorocitrate and fluoroacetate effects on astrocyte metabolism in vitro. Brain Res 664:94–100.

Tanaka H, Araki M, Masuzawa T (1992) Reaction of astrocytes in the gerbil hippocampus following transient ischemia—immunohisto-chemical observations with antibodies against glial fibrillary acidic protein, glutamine synthetase, and S-100 protein. Exp Neurol 116:264–274.

Tombaugh GC, Sapolsky RM (1992) Corticosterone accelerates hypoxia- and cyanide-induced ATP loss in cultured hippocampal astrocytes. Brain Res 588:154–158.

von Blankenfeld G, Kettenmann H (1991) Glutamate and GABA receptors in vertebrate glial cells. Mol Neurobiol 5:31–43.

Yudkoff M, Nissim I, Daikhin Y, Lin ZP, Nelson D, Pleasure D, Erecinska M (1993) Brain glutamate metabolism: Neuronal-astroglial relationships. Dev Neurosci 15:343–350.

Zielke HR, Tildon JT, Landry ME, Max SR (1990) Effect of 8-bromo-cAMP and dexamethasone on glutamate metabolism in rat astrocytes. Neurochem Res 15(11):1115–1122.

Synthetic Trehalose Dicorynomycolate (S-TDCM):
Behavioral Effects and Radioprotection

MICHAEL R. LANDAUER, DANIEL G. MCCHESNEY
AND G. DAVID LEDNEY

Armed Forces Radiobiology Research Institute 8901 Wisconsin Avenue
Bethesda, MD 20889–5603, USA

Radiation protection/Locomotor activity/Food consumption/S-TDCM/Immunomodulator

This study evaluated synthetic trehalose dicorynomycolate (S-TDCM), an immunomodulator, for its survival enhancing capacity and behavioral toxicity in B6D2F1 female mice. In survival experiments, mice were administered S-TDCM (25-400 µg/mouse i.p.) 20-24 hr before 5.6 Gy mixed-field fission-neutron irradiation (n) and γ-photon irradiation. The 30-day survival rates for mice treated with 100-400 µg/mouse S-TDCM were significantly enhanced compared to controls. Toxicity of S-TDCM was measured in nonirradiated mice by locomotor activity, food intake, water consumption, and alterations in body weight. A dose-dependent decrease was noted in all behavioral measures in mice treated with S-TDCM. Doses of 100 and 200 µg/mouse S-TDCM significantly reduced motor activity beginning 12 hr postinjection with recovery by 24 hr. A dose of 400 µg/mouse significantly decreased activity within the first 4 hr after administration and returned to control levels by 32 hr following injection. Food and water intake were significantly depressed at doses of 200 and 400 µg/mouse on the day following drug administration, and were recovered in 24 hr. Body weight was significantly decreased in the 200 µg/mouse group for 2 days and in the 400 µg/mouse group for 4 days following injection. A dose of 100 µg/mouse effectively enhanced survival after fission-neutron irradiation with no adverse effect on food consumption, water intake, or body weight and a minimal, short-term effect on locomotor activity.

Address correspondence to:
Michael R. Landauer, Ph.D.
Armed Forces Radiobiology Research Institute
AFRRI/RPT
8901 Wisconsin Avenue
Bethesda, MD 20889–5603, USA
phone: (301) 295–5606
FAX: (301) 295–6552
E-Mail: landauer@vax.afrri.usuhs.mil

INTRODUCTION

Trehalose dimycolate (TDM), a naturally produced substance also known as cord factor, is a glycolipid secreted on the surface of the cell walls of several strains of bacteria including *Mycobacteria*, *Nocardia* and *Corynebacteria*[1,2]. Bloch[3] observed a rapid weight loss and death in mice injected with TDM; he referred to this substance as a "toxic lipid".

Irradiation compromises nonspecific immune defenses of the hematopoietic and intestinal cell systems, making the host susceptible to bacterial infection. The increasing use of radiotherapy for the treatment of malignant tumors demonstrates the need for effective stimulants of proliferative hematopoietic cells to help reduce aplastic and septic conditions found in irradiated hosts. A number of bacterially and chemically derived agents are able to promote survival after lethal doses of radiation[4,5], but most do so only at behaviorally toxic doses[6,7]. In this study, we examined the use of synthetic trehalose dicorynomycolate (S-TDCM), a biological response modifier known to have beneficial properties in normal and irradiated mice. S-TDCM, for example, enhances survival following pure γ- or mixed fission-neutron and γ-photon irradiation[8-11], enhances resistance to bacterial infection[12] and activates macrophages[13-14] that can produce biological response mediators such as interleukin-6, colony stimulating factor, and interferon[8,15].

The toxicity of native TDM delivered in oil emulsions is well documented. Mycobacterial TDM produces a toxic effect in mice and leads to anorexia, cachexia, and death[3,16]. Bloch[3] originally reported that a single injection of TDM (from *Mycobacterium tuberculosis*) administered i.p. or subcutaneously in paraffin oil was not toxic to Swiss-Webster or DBA mice, but both the CF1 and C57 strains exhibited slight weight loss. Three to seven repeated injections resulted in progressive weight loss and death in all mouse strains tested[3]. With highly purified TDM from *M. tuberculosis* prepared in oil, a single injection (3 or 10 μg) administered to C57BL/6[17] or C57BL/10 mice[18] resulted in interstitial and hemorrhagic pneumonitis with deaths reported for 5% of the animals at 4 weeks postinjection. Multiple injections increased the number of deaths. In addition, Saito et al.[19] found that a single i.p. injection of 10 μg TDM in Drakeol resulted in diarrhea and weight loss in C57 mice. Furthermore, repeated administration of TDM suppressed weight gain. Within 3 days after the fifth injection of TDM, 10% of AKR mice and 70% of C57BL mice died. The toxicity may be directly related to the percent of oil used as the vehicle[1].

Synthetic TDM (S-TDCM) is prepared by the condensation of potassium mycolate containing 32 carbon atoms with 2,3,4,2',3',4'-hexa-O-trimethylsilyl-a,a-trehalose activated at the 6 and 6' positions. S-TDCM has a molecular weight of 1374 daltons, compared with 2860 daltons for naturally occurring TDM isolated from *M. phlei*. The synthetic product retains most of the beneficial effects of the native TDM, is less toxic, and is easier to obtain. S-TDCM can be administered in a nontoxic vehicle, 0.2% Tween 80/saline, instead of the toxic squalene emulsion in which the naturally occurring TDM is often administered[1].

Administration of S-TDCM increased survival in B6D2F1 mice made neutropenic by exposure to ionizing radiation[10]. In addition, mice given a sublethal γ or mixed-field fission-neutron and γ-photon radiation dose and challenged with *Klebsiella pneumoniae* survived when administered S-TDCM 1 hr postirradiation[8,20].

The effectiveness of S-TDCM in increasing survival in irradiated mice[8] has made it an excellent candidate for additional testing. In this study, the survival enhancing properties of S-TDCM administered prior to mixed-field fission-neutron and γ-photon irradiation were further delineated. In addition, general toxicity, reflected by food intake, water consumption, body weight, and locomotor activity was examined. These parameters are useful in evaluating the toxic effects of radiation or putative radioprotective

compounds[6,21–23].

MATERIALS AND METHODS

Subjects

Female B6D2F1 mice (15-18 weeks of age; 24-29 g) were obtained from Jackson Laboratories (Bar Harbor, ME). They were quarantined on arrival for 2 weeks, and representative mice were examined by microbiology, serology, and histopathology to assure the absence of specific bacteria, particularly *Pseudomonas aeruginosa*, and common murine diseases. Mice were housed in plastic Micro-Isolator cages on hardwood chip contact bedding in a facility accredited by the American Association for the Accreditation of Laboratory Animal Care. Rooms were maintained at 21°C +/– 1°C with 50% relative humidity on a 12 hr light-dark cycle. Commercial rodent chow (Wayne Rodent Blox) and acidified water (pH = 2.5) to minimize *Pseudomonas* colonization were freely available[24]. All research was conducted in accordance with National Institutes of Health guidelines and was approved by the AFRRI Institutional Animal Care and Use Committee.

Immunomodulator

S-TDCM was produced by Ribi ImmunoChem Research, Inc. (Hamilton, MT) and was prepared in depyrogentated glassware as an aqueous suspension in a 0.2% Tween 80/saline vehicle[20].

Radiation

The techniques and dosimetry of exposing mice to radiation fields containing both fission-neutrons and γ-photons produced by the AFRRI Training, Research, Isotope, General Atomic (TRIGA) reactor were previously described[25]. Mice were administered a midline tissue (MLT) dose of 5.6 Gy (1 Gy = 100 rad) at 0.4 Gy/min with a neutron dose to total dose ratio [n/ (n + γ)] of 0.67 (+/–10%). This ratio was achieved by using a 15.2-cm lead shield in front of the reactor wall. The MLT dose was measured by paired ionization chambers[26]. Chamber calibrations for mixed fields were traceable to standards maintained by the National Institute of Standards and Technology. Mice were individually irradiated in well-ventilated aluminum restraining tubes that rotated at 1.5 revolutions/min.

Survival

To evaluate the protective efficacy of S-TDCM, we selected a radiation dose of 5.6 Gy at which approximately 80% of saline-treated mice of this strain die within 30 days ($LD_{80/30}$). Mice were each administered either a single i.p. injection of 0.5 ml of saline vehicle, or 25, 50, 100, 200, or 400 µg/mouse S-TDCM (N = 20/group), 20-24 hr before irradiation.

Locomotor Activity Measurement

A computerized Digiscan Animal Activity Monitor (Omnitech Electronics, Columbus, OH) was used to quantitate locomotor behavior. The apparatus consisted of a 20.3-cm × 20.3-cm acrylic arena with an array of infrared photodetectors spaced 2.5 cm apart to detect locomotor activity, which was expressed as the total distance traveled. Nonirradiated mice each received a single i.p. injection either of the vehicle or 100, 200, or 400 µg/mouse S-TDCM (N = 10-11/ group). Immediately after injection the mice were each

placed into the activity monitor where ambulation was recorded at 2-hr intervals for the first 6 hr and again at 24 and 48 hr. All testing began at the onset of the dark portion of the light-dark cycle.

Food and Water Consumption, Body Weight

A separate group of nonirradiated mice treated similarly to those in the locomotor study were used to measure food and water intake and body weight. Three days before the drugs were administered, the mice were each weighed and placed into individual cages. Body weight was balanced across groups at the beginning of the experiment so that the mean weights of the groups were within 1 g. One day before the experiment, baseline values for food and water intake and body weight were determined and then measured for 8 consecutive days following injection. The amount consumed was determined by daily weighing of the food hoppers and water bottles. Mice were each injected i.p. (day 0) either with the vehicle (0.2% Tween 80/saline), or with 50, 100, 200, or 400 µg/mouse of S-TDCM. We previously determined that there was no difference in body weight or consummatory behavior following injections of saline or the vehicle.

Statistical Analysis

Locomotor activity as well as daily food, water, and body weight data were analyzed by one-way ANOVA. Posthoc comparisons were made with Dunnett's test. Survival data were analyzed with the Fisher exact test[27].

RESULTS

Survival

As illustrated in Fig 1, administration of 25, 50, 100, 200, or 400 µg/mouse S-TDCM 20-24 hr before 5.6-Gy mixed-field neutron irradiation resulted in 30-day survival rates of 35%, 45%, 80%, 80%, and 95%, respectively. The survival rate for saline-treated mice was 15% which was not statistically different from the 30% rate observed for subjects administered the vehicle, Tween-80/saline. Compared to the vehicle control group, significantly ($p < .001$) greater survival was observed for mice treated with 100, 200, and 400 µg S-TDCM.

Locomotor Activity

Fig. 2 illustrates the locomotor activity of mice over a 3-day period after receiving S-TDCM. The mice were on a 12-hr light/dark cycle and testing began at the onset of the dark period (indicated by the solid bar). The activity rhythm, plotted in 4 hr intervals, of these nocturnal rodents is clear. Locomotor activity of control animals was maximal during the first time interval of the dark period and gradually decreased during the remainder of each 24-hr period. Locomotor activity in the 100 and 200 µg/mouse groups was significantly ($p< 0.01$) depressed beginning 12 hr after injection and recovered by 24 hr. Mice treated with 400 µg/mouse exhibited significantly ($p< 0.01$) reduced locomotor activity that commenced earlier (4 hr), was sustained longer (up to 28 hr), and was of a greater magnitude than the lower dosed groups.
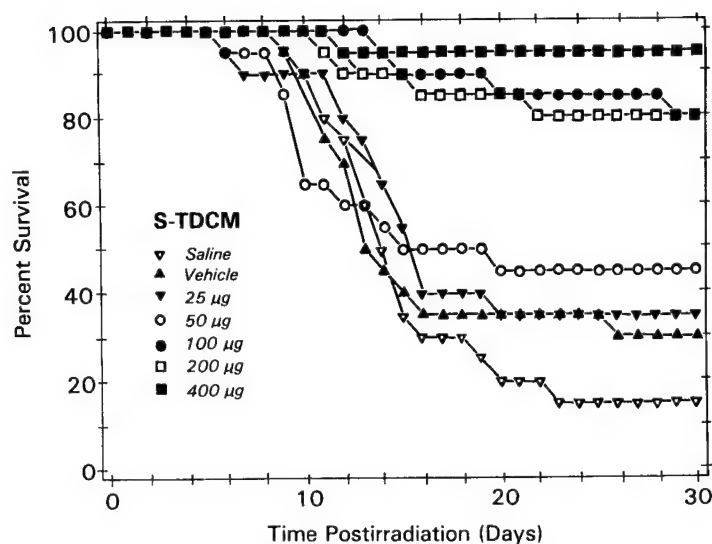
Fig. 1. Thirty-day survival curves for mice administered synthetic trehalose dicorynomycolate (S-TDCM) 20-24 hr before 5.6-Gy mixed-field fission-neutron and γ-photon irradiation (N = 20/group).
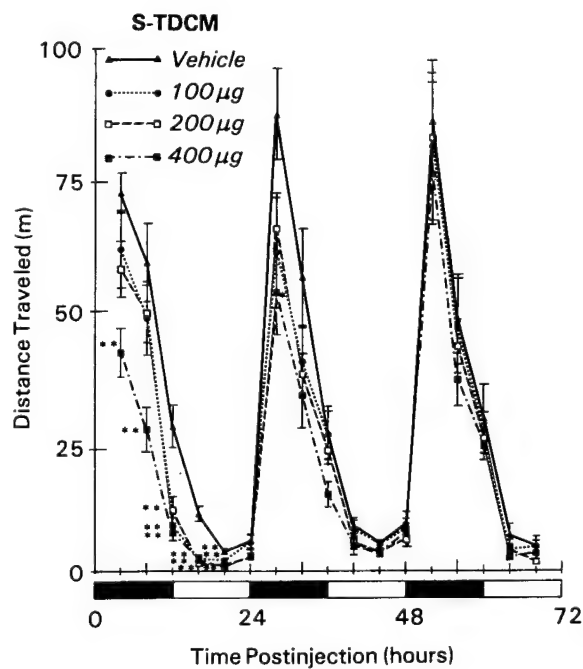

Fig. 2. Circadian rhythm in locomotor behavior of control and S-TDCM treated mice over a 3-day period. Locomotor activity is expressed as the total distance traveled (meters) in 4-hr intervals. The solid bar along the abscissa represents the dark period of the light-dark cycle. Mice each received a single i.p. injection of vehicle or S-TDCM at the beginning of the dark period on the first day. Vertical lines represent the SEM. (N = 10-11/group) * $p < 0.05$, ** $p < 0.01$ from vehicle control group.

Food and water consumption, body weight

Food (Fig. 3) and water (Fig. 4) consumption was significantly ($p < 0.01$) decreased within 24 hr (day 1) following administration of doses of 200 and 400 µg/mouse of S-TDCM. A dose of 100 µg/mouse did not significantly decrease either food consumption or water intake. Food and water consumption in all groups returned to control levels by the second day after drug administration.

Body weight (Fig. 5) was not affected by a dose of 100 µg/mouse S-TDCM. Doses of 200 µg/mouse or greater significantly depressed body weights ($p < 0.01$) beginning 24 hr after injection. Mice administered 200 and 400 µg/mouse S-TDCM had significantly lower weights than control animals for 2 ($p < 0.01$) and 4 ($p < 0.05$) days, respectively.

DISCUSSION

In this study, the lowest dose at which S-TDCM exhibited a beneficial radioprotective effect (100 µg), had no significant effect on food and water consumption, or body weight, and had a minimal, reversible effect on locomotor activity. A dose of 200 µg significantly reduced all parameters evaluated, with complete recovery within 24 hr of administration. A dose of 400 µg significantly decreased locomotor activity for 28 hr, consummatory behaviors for 48 hr, and body weight for 96 hr. After these time periods, all parameters returned to control levels. Thus, S-TDCM at the most radioprotective doses, offered short-term, adverse behavioral effects that were completely reversible.
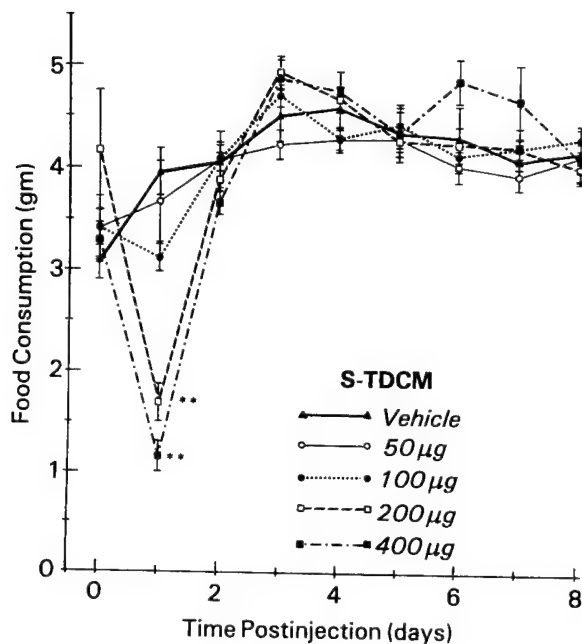
Fig. 3. Food consumption after treatment with S-TDCM. Food intake was measured daily for 8 days following a single i.p. injection of S-TDCM. Day 0 refers to the day of injection. Vertical lines represent the SEM. (N = 12/group) ** $p < 0.01$ from vehicle control group.
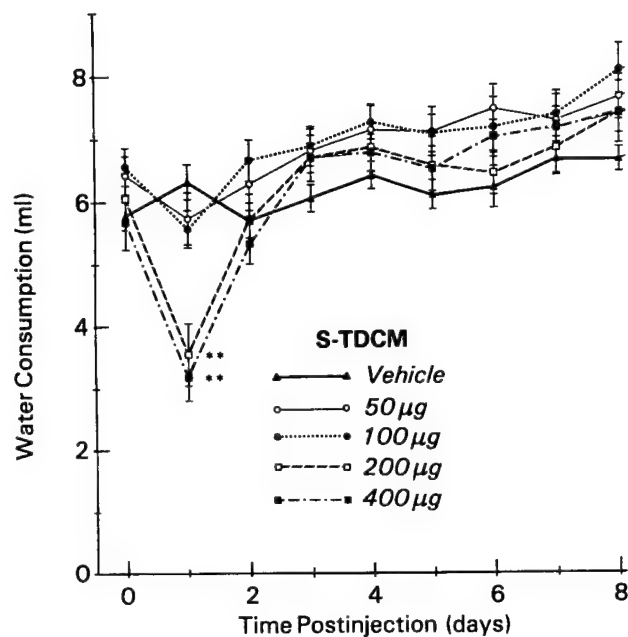
Fig. 4. Water consumption after S-TDCM treatment. Water intake was measured daily for 8 days after a single i.p. injection of S-TDCM. Day 0 is the day of injection. Vertical lines represent the SEM. (N = 12/group) ** $p < 0.01$ from vehicle control group.
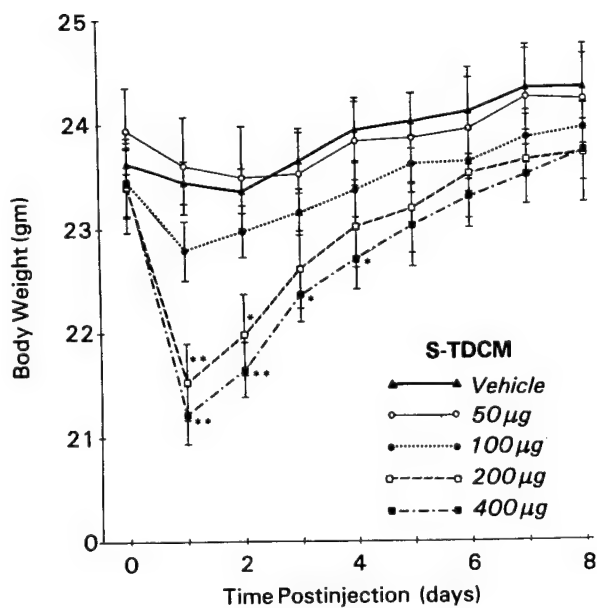
Fig. 5. Body weight after S-TDCM treatment. Body weight was measured daily for 8 days following a single i.p. injection of S-TDCM. Day 0 equals the day of injection. Vertical lines represent the SEM. (N = 12/group) * $p < 0.05$, ** $p < 0.01$ from vehicle control group.

The onset of behavioral decrements observed in this study at approximately 4 hr postinjection (400 µg group) corresponded to some of the toxic manifestations previously reported for native TDM in a hexadecane vehicle. Seggev and colleagues[17] found that 25% of mice showed mild mononuclear cell infiltrations within 6 hr postinjection and Silva et al.[28] reported that mice injected i.p. with TDM in mineral oil exhibited a decrease in body weight and were reluctant to move after a single injection.

The locomotor decrement as well as reductions in food, water, and body weight observed in our study may have resulted directly from the direct action of S-TDCM on the gastrointestinal tract or indirectly through a metabolite, a change in hormone concentration, or the production of cytokines. With reference to cytokines, Silva et al.[28] detected tumor necrosis factor (TNF) in the plasma of animals injected with TDM. In other studies, S-TDCM increased the splenic gene expression for interleukin-1 (IL-1) beta, IL-3, IL-6, and granulocyte colony stimulating factor (G-CSF)[15]. Moreover, decreases in food intake and investigatory or motor behavior were observed in rodents after administration of IL-1 beta, or correlated with a rise in endogenous IL-1 beta[29-31], IL-3[32], IL-6[29] or TNF[29,33]. In addition, evidence from our laboratory indicated that 400 µg/mouse S-TDCM resulted in a 2 to 4°C rise in mouse basal body temperature within 3 hr of administration. The onset of this temperature increase may also be related to the onset of the locomotor activity decrement observed in the present experiment.

This is the first comprehensive paper evaluating the effects of an acute administration of S-TDCM on consummatory and locomotor behavior. However, the toxic effects of naturally occurring TDM has been well documented especially in instances in which the compound was dissolved in an oil and water emulsion and repeated injections were administered. The toxicity (lung granuloma, weight loss, and death) depended on the percent of oil used in the injection and on the size of the oil droplets[1]. After i.p. administration of TDM, interstitial and hemorrhagic pneumonitis was likely to occur[17,18]. Unpublished work from our laboratory indicated that the squalene vehicle used to emulsify TDM was behaviorally toxic as shown by significant decreases in locomotor behavior. Squalene at doses of 0.5%, 1%, and 2% produced locomotor deficits in mice, while a dose of 0.1% did not. However, we found that S-TDCM in a 0.2% Tween-80/saline vehicle did not differ from that in saline-treated animals with respect to locomotor activity[34].

TDM in saline is not toxic to mice but also does not offer as much protection from γ rays as does TDM in oil[20]. In nonirradiated mice injected i.p. with doses of 50-1000 µg TDM/saline, body weight was comparable to noninjected controls and no deaths were reported[35]. In our laboratory we found that TDM/saline at doses of 100 or 200 µg/mouse did not result in locomotor deficits.

S-TDCM (100 µg) offered protection when given 24 hr before radiation and was comparable to 100 µg TDM/oil[20] for γ rays when 30-day survival was used as the end point. S-TDCM (100 µg) was less effective than 100 µg TDM/oil when this preparation was used to protect against mixed-field fission-neutron and γ-photon irradiation (60% versus 90%)[8]. In general, the toxicity of TDM was shown to be associated with the percent of oil used in the emulsion, the strain of the mouse tested, and the number of injections. Further, there appeared to be a species difference since repeated injections of TDM in Drakeol was more toxic to mice than rats[19].

In summary, S-TDCM offers similar levels of radioprotection and therapeutic benefits as naturally occurring TDM. The reduced toxicity of this synthetic analog makes it an ideal compound for continued study.

ACKNOWLEDGMENTS

REFERENCES

1. Lederer, E. (1988) An update on natural and synthetic trehalose diesters. In "Immunomodulators and nonspecific host defense mechanisms against microbial infections." Ed. K. Masihi and W. Lange, pp.73–83, Pergamon Press, Oxford, England.

2. Lemaire, G., Tenu, J.P., Petit, J.F. and Lederer, E. (1986) Natural and synthetic trehalose diesters as immunomodulators. Medicinal Res. Rev. 6: 243–274.

3. Bloch, H. (1950) Studies on the virulence of tubercle bacilli. J. Exp. Med. 2: 197–219.

4. Hayashi, Y., Yamaguchi, I., Kobayashi, M., Shimizu, T., Matsuda, K., Yoshida, M., Kumakura, M. and Hirashima, K. (1990) Effects of Z-100 on mice exposed to -irradiation. J. Radiat. Res. 31: 375–388.

5. Monig . H., Messerschmidt, O. and Streffer, C. (1990) Chemical radioprotection in mammals and man. In "Radiation Exposure and Occupational Risks" Ed. E. Scherer, C. Streffer and K.R. Trott, pp. 97–143, Springer-Verlag, New York.

6. Landauer M.R., Davis, H.D., Dominitz, J.D. and Weiss, J.F. (1988a) Comparative behavioral toxicity of four sulfhydryl radioprotective compounds in mice: WR-2721, cysteamine, diethyldithiocarbamate, and N-acetylcysteine. Pharmacol. Ther. 39: 97–100.

7. Landauer, M.R., Davis, H.D., Kumar, K.S. and Weiss, J.F. (1992) Behavioral toxicity of selected radioprotectors. Adv. Space Res. 12: 273–283.

8. McChesney, D.G., Ledney. G.D. and Madonna, G.S. (1990) TDM enhances survival of fission neutron irradiated mice and *Klebsiella pneumoniae* challenged irradiated mice. Radiat. Res. 121: 71–75.

9. Madonna, G.S., Ledney, G.D., Moore, M.M. and Elliott, T.B. (1991) Treatment of mice with sepsis following irradiation and trauma with antibiotics and synthetic trehalose dicorynomycolate (S-TDCM). J. Trauma. 31: 316–325.

10. Ledney, G.D., Madonna, G.S., Elliott, T.B., Moore, M.M. and Jackson III, W.E. (1991) Therapy of infections in mice irradiated in mixed neutron/photon fields and inflicted with wound trauma: A review of current work. Radiat. Res. 128: S18–S28.

11. Ledney, G.D., Elliott, T.B., Landauer, M.R., Vigneulle, R.M., Henderson, P.L., Harding, R.A. and Tom, Jr., S.P. (1994) Survival of irradiated mice treated with WR-151327, synthetic trehalose dicorynomycolate, or ofloxacin. Adv. Space Res. 14 (10): 583–586.

12. Ribi, E., Ulrich, J.T. and Masihi, K.N. (1987) Immunopotentiating activities of monophosphoryl lipid A. In "Immunopharmacology of infectious diseases: vaccine adjuvants and modulators of non-specific resistance," Ed. J. Majde, pp. 101–112, Alan R. Liss, Inc. New York.

13. Ribi, E. (1986) Structure-function relationship of bacterial adjuvants. In "Advances in Carriers and Adjuvants for Veterinary Biologics," Eds. R. Nevig, P.,Gough, M. Kaeberle and C. Whetstone, pp. 35–49, Iowa State University Press, Ames, IA.

14. Yarkoni, E., Wang, L. and Bekierkunst, A. (1977) Stimulation of macrophages by cord factor and by heat killer and living BCG. Infect. Immun. 16: 1–7.

15. Peterson, V.M., Adamovicz, J.J., Elliott, T.B., Moore, M.M., Madonna, G.S., Jackson, W.E., Ledney, G.D. and Gause, W.C. (1994) Gene expression of hematoregulatory cytokines is elevated endogenously after sublethal gamma irradiation and is differentially enhanced by therapeutic administration of biologic response modifiers. J. Immunol. 153: 2321–2330.

16. Silva, C.L., Ekizlerian, S.M. and Fazioli, R.A. (1985) Role of cord factor in the modulation of infection caused by mycobacteria. Am. J. Pathol. **118**: 238–247.

17. Seggev, J.S., Goren, M.B., Carr R.I. and Kirkpatrick, C.H. (1982) Interstitial and hemorrhagic pneumonitis induced by mycobacterial trehalose dimycolate. Am. J. Pathol. **106**: 348–355.

18. Seggev, J.S., Goren, M.B. and Kirkpatrick, C.H. (1984) The pathogenesis of trehalose dimycolate-induced interstitial pneumonitis. III. Evidence for a role for T lymphocytes. Cell. Immunol. **85**: 428–435.

19. Saito, R., Tanaka, A., Sugiyama, K. and Kato, M. (1975) Cord factor not toxic in rats. American Review of Respiratory Disease **112**: 578–580.

20. Madonna, G.S., Ledney, G.D., Elliott, T.B., Brook, I., Ulrich, J.T. Meyers, K.B., Patchen, M.L. and Walker, R.I. (1989) Trehalose dimycolate enhances resistance to infection in neutropenic animals. Infect. Immun. **57**: 2495–2501.

21. Ferguson, J.L., Kandasamy, S.B., Harris, A.H., Davis, H.D. and Landauer, M.R. (1996) Indomethacin attenuation of radiation-induced hyperthermia does not modify radiation-induced hypoactivity. J. Radiat. Res., **37**, 209–215.

22. Maier, D.A. and Landauer, M.R. (1990) Onset of behavioral effects of mice exposed to 10 Gy 60-Co radiation. Aviat. Space Environ. Med. **61**: 893–898.

23. Landauer M.R., Davis, H.D., Dominitz, J.D. and Weiss, J.F. (1988b) Long-term effects of radioprotector WR-2721 on locomotor activity and body weight of mice following exposure to ionizing radiation. Toxicology **49**: 315–323.

24. McPherson, C.W. (1963) Reduction of *Pseudomonas aeruginosa* and coliform bacteria in mouse drinking water following treatment with hydrochloric acid or chlorine. Lab. Animal Care **13**: 737–744.

25. Elliott, T.B., Ledney, G.D., Harding, R.A., Henderson, P.L., Gerstenberg, H.M., Rotruck, J.R., Verdolin, M.H., Stille, C.M. and Krieger, A.G. (1995) Mixed-field neutrons and γ photons induce different changes in ileal bacteria and correlated sepsis in mice. Int. J. Radiat. Biol. **18**: 85–95.

26. Meulders, J.P. (1988) Dosimetry in mixed n + gamma field. In "Ionizing Radiation: Protection and Dosimetry," Ed. G. Paic, pp. 203–214, CRC Press, Boca Raton, FL.

27. Winer, B.J. (1971) Statistical principles in experimental design. McGraw-Hill, New York.

28. Silva, C.L. and Faccioli, L.H. (1988) Tumor necrosis factor (cachectin) mediates induction of cachexia by cord factor from mycobacteria. Infec. Immun. **56**: 3067–3071.

29. Conn, C.A., McClellan, J.L., Maassab, H.F., Smitka, C.W., Majde, J.A. and Kluger, M.J. (1995) Cytokines and the acute phase response to influenza virus in mice. Am. J. Physiol. **268**: (Pt 2), R78–R84.

30. McCarthy, D.O., Kluger, M.J. and Vander, A.J. (1985) Suppression of food intake during infection: Is interleukin-1 involved? J. Clin. Nutrition **42**: 1179–1182.

31. Plata-Salaman, C.R. (1994) Meal patterns in response to intracerebroventricular administration of interleukin-1 beta in rats. Physiol. Behav. **55**: 727–733.

32. Cockayne, D.A., Bodine, D.M., Cline, A., Nienhuis, A.W., Dunbar, C.E. (1994) Transgenic mice expressing antisense interleukin-3 RNA develop a B-cell lymphproliferative syndrome or neurologic dysfunction. Blood **84**: 2699–2710.

33. Bianchi, M., Sacerdote, P., Ricciardi,-Castagnoli, P., Mantegazza, P. and Panerai, A.E. (1992) Central effects of tumor necrosis factor alpha and interleukin-1 alpha on nociceptive thresholds and spontaneous locomotor activity. Neurosci. Lett. **148**: 76–80.

34. Castro, C.A., Hogan, J.B., Benson, K.A., Shehata, C.W. and Landauer, M.R. (1995) Behavioral effects of vehicles: DMSO, Ethanol, Tween-20, Tween-80, and Emulphor-620. Pharmacol. Biochem. Behav. **50**: 521–526.

35. Orbach-Arbouys, S., Tenu, J.P. and Petit, J.F. (1967) Enhancement of *in vitro* and *in vivo* antitumor activity by cord factor (6-6'-dimycolate of trehalose)administered suspended in saline. Int. Archs. Allergy Appl.Immun. **71**: 67–73.

Paper

PREMATURE CHROMOSOME CONDENSATION ASSAY FOR BIODOSIMETRY: STUDIES WITH FISSION-NEUTRONS

P. G. S. Prasanna,* C. J. Kolanko,*[†] H. M. Gerstenberg,* and W. F. Blakely[‡]

Abstract—Characterization of the premature chromosome condensation assay for radiation quality is needed. To that end, human lymphocytes were exposed *in vitro* to various doses of 250-kVp x rays ($\bar{Y}_D = 4$ keV μm^{-1}, $\bar{Y}_D$ is the dose-mean lineal energy of the absorbed dose distribution, $D(y)$, where y is defined as the energy deposited in a volume by a single event divided by the mean chord length of the volume) and to fission neutrons ($\bar{Y}_D = 65$ keV μm^{-1}). The distribution of prematurely condensed chromosome and fragments following exposure to x rays or to neutrons were non-Poisson after repair at 37°C for 24 h. Dose-response curves were constructed for the yield of excess prematurely condensed chromosome fragments as necessary for biodosimetry applications. The curves were fitted to a weighted linear model by the least-squares regression method. The neutron relative biological effectiveness (RBE) value was estimated to be 2.4 ± 0.39.
Health Phys. 72(4):594–600; 1997

Key words: x rays; neutrons; accidents, nuclear; relative biological effectiveness

INTRODUCTION

BIOLOGICAL DOSIMETRY can make an important contribution to radiological protection in cases where physical dosimetry is lacking or inadequate to quantify exposure doses to different qualities of radiations. A number of methods of quantifying radiation-induced changes at the molecular, cytogenetic, and cellular levels have been considered for biodosimetry (Müller and Streffer 1991; Greenstock and Trivedi 1994). Scoring of dicentrics in metaphase preparations obtained from peripheral blood lymphocyte cultures of accidentally exposed individuals has been considered as a reliable method of cytogenetic dosimetry over the past two decades.

Studies on the relative biological effectiveness (RBE) of neutrons are important for risk assessment in radiological protection and also for the tailoring of neutron therapy protocols. The RBE value for 0.7 MeV peak energy [252]Cf neutrons for the yield of dicentrics and

rings was 12.3 (Tanaka et al. 1994). *In vitro* dose-response curves of unstable chromosome aberrations in human lymphocytes have been obtained for neutron spectra of mean energies 0.7, 7.6, and 14.7 MeV neutrons by Lloyd and Purrot (1981). At low doses, such as those received by radiation workers, RBE values for 0.7, 7.6, and 14.7 MeV neutrons were 17, 10, and 5.5, respectively; at higher doses, these values were 5, 3, and 2 at the 2-Gy equivalent of x rays. The effectiveness of neutrons resembling those that the A-bomb survivors received at Hiroshima was determined in human blood lymphocytes *in vitro* using chromosomal aberrations (dicentrics and rings) endpoint. The "little boy replica" neutrons, with energy approximately 0.2 MeV, were more effective than higher energy (approximately 1 MeV) fission neutrons. The maximum RBE of these neutrons at low doses relative to 250-kVp x rays was estimated to be 22 to 30 (Dobson et al. 1991).

The premature chromosome condensation (PCC) assay is envisaged as an important cytogenetic tool not only in the estimation of radiation dose in cases of whole-body (Pantelias and Maillie 1984, 1985; Zoetelief and Broerse 1990; Pantelias et al. 1993) or partial-body (Blakely et al. 1995) exposure but also in the prediction of human tumor radiosensitivity (Evans et al. 1991; Brown et al. 1992; Sasai et al. 1994). Using x rays, repair kinetics for interphase chromosome breakage (Vyas et al. 1991; Okayasu et al. 1993) and dose-response relationships at different postirradiation time points have been studied (Pantelias and Maillie 1984) in mammalian cells by the PCC assay. But data available on the effect of high-LET (linear energy transfer) radiations appear limited to established cell lines (Bedford and Goodhead 1989; Goodwin et al. 1989; Suzuki et al. 1992). These studies suggested that there is a qualitative difference in the initial chromosome damage caused by high- and low-LET radiations. In this paper, the relationship between excess PCC fragments in human lymphocytes and neutron doses is presented, and a comparison with x-ray dose-response data is made for determining RBE as required for practical biodosimetry applications.

MATERIALS AND METHODS

Mitotic cell collection

Mitotic Chinese hamster ovary (CHO) cells were collected for use as inducers of chromosome condensa-

tion in the PCC assay by the "mitotic shake off" procedure (Pantelias and Maillie 1983), previously described by us (Blakely et al. 1995). Briefly, this procedure, as suggested by E. A. Blakely[||] consists of sequential colchicine inhibition of cell cycle progression in metaphase (two or three times in 3-h windows) and then a collection by "mitotic shake off." The mitotic cells, suspended in mitotic medium containing 10% dimethyl sulfoxide,[¶] were stored in a liquid nitrogen storage container in liquid or vapor phase until later use (Blakely et al. 1995).

Lymphocytes

The experimental design for individual dose-response experiments involved ≥ 4 dose points and used lymphocytes from whole blood obtained from 2 to 3 healthy human donors. In this study the total number of donors was 8. The blood was collected into vacutainers containing ethylenediaminetetraacetic acid.[#] The informed consent form used in this study was approved by the Human Use Committee of the Uniformed Services University of the Health Sciences, Bethesda, MD. Lymphocytes were isolated from whole peripheral blood on a density gradient.[**] Cells were suspended in a tissue-culture medium[††] at an approximate concentration of 1.5×10^6 mL^{-1} for irradiation. For each radiation type, unexposed cells were included to serve as independent controls.

Dosimetry

X-ray irradiation. X-ray irradiations were performed using a 320-kVp Philips industrial x-ray machine[‡‡] with an effective energy of 83 keV (source to sample distance = 55.2 cm, 250 kVp at 12.5 mA, 0.2 mm Cu and 1 mm Al filtration) at doses between 0.5 and 9 Gy. Prior to each day of irradiation, a calibrated 0.5-cc tissue-equivalent ionization chamber (calibration traceable to the National Institute of Standards and Technology) was used to determine dose rate. Dosimetry was performed using ion chambers placed in tissue-culture flasks filled with tissue-equivalent plastic as described by the International Commission on Radiation Units and Measurements (ICRU 1973). Field uniformity was within 2%.

Cells in suspension in 25-cm^2 tissue-culture flasks were placed on a rotating Plexiglas holder for irradiation and exposed at room temperature at a dose rate of 1 Gy min^{-1}. The reported doses were determined as a product of the predetermined dose-rate and exposure time.

Neutron irradiation

Neutron irradiation was performed using the Armed Forces Radiobiology Research Institute (AFRRI) TRIGA Mark-F reactor at doses between 0.25 and 4.0 Gy. Cells were suspended in 15-mL polypropylene centrifuge tubes, placed on a Plexiglas[™] holder, and exposed to neutrons at a dose rate of 0.25 Gy min^{-1}. The radiation field was uniform to within 2.5% across the array. Fluence-weighted mean energies, previously measured for the same configuration, were 0.71 MeV for neutrons (NIST 1991) and 1.80 MeV for gamma rays (Zeman and Ferlic 1984). Samples for irradiation were placed in a lead box built of standard-size lead bricks; the outside dimensions of the box were 71 cm high and 51 cm in width and depth. The distance from the samples to reactor core center was 176.5 cm. Samples were shuttled to and from the box by means of an aluminum extractor tube that penetrated the exposure-room shielding wall (Redpath et al. 1995). The lead box, as well as an additional 15-cm lead shielding wall placed between the box and reactor, enhanced the neutron dose over the gamma dose by selectively shielding the irradiated samples from the reactor gamma rays as well as from the room-scatter radiation. Each run was selectively monitored using fission and ionization chambers in the exposure room. Paired ion chambers, placed at the center of the sample array, were used to determine separately the dose due to gamma and neutron irradiation (Meulders 1988); the neutron to total-dose ratio was measured to be $0.92 \pm 0.07\%$.

Radiation quality and dosimetry parameters

The radiation quality for the two sources was estimated in terms of the frequency-mean lineal energy, $\bar{Y}_f$, where $\bar{Y}_f = \text{LET}_\infty$ (Turner 1992; Rossi 1959).

$\bar{Y}_f$ and $\bar{Y}_D$ were determined from measured or calculated y spectra of the sources used in this study and determined at a 1- and 8-μm equivalent diameter. Estimates of $\bar{Y}_f$ for spherical volumes with 10-μm diameters, the mean diameter of the human lymphocytes used in this work, were obtained in the following way. For the x rays, $\bar{Y}_f$ was measured to be 2 with a tissue-equivalent proportional counter (TEPC) detector with a gas pressure corresponding to 1-μm diameter.[§§] $\bar{Y}_f$ for 10 μm was obtained by comparison of this data with that of Kliauga and Dvorak (1978) to obtain a result at the mean x-ray energy of 83 kVp and 10-μm cell diameter. Kliauga and Dvorak (1978) give results at single energy x-ray lines for diameters between 0.24 and 7.7 μm. Interpolation gave the result at the mean x-ray energy, and extrapolation from 7.7 μm to 10 μm gave the result of 1.53 keV μm^{-1} at a 10-μm diameter.

For the neutron spectrum, our calculated $\bar{Y}_f$ results at 1- and 8-μm diameter were compared to the calculations of Caswell and Coyne (1975), who determined $\bar{Y}_f$ for

---

[||] Personal communication, Lawrence Berkeley Laboratory, Berkeley, CA 94720.
[¶] Aldrich Chemical Co., Milwaukee, WI 55233.
[#] Beckton-Dickinson, Rutherford, NJ 07070.
[**] Histopaque; Sigma Chemical Co., St. Louis, MO 63178.
[††] Karyomax: Life Technologies, Gaithersburg, MD 20877.
[‡‡] GMBH, Hamburg, Germany.

[§§] Available from Benevides, L.A.; Gerstenberg, H.M.; Blakely, W.F. Effect of 250-kVp x-ray and fission-neutron radiations on Chinese hamster V79AO3 cells: I. Characterization of energy deposition and comparison of micronuclei assays (unpublished).

diameters between 0.5 and 32 μm for neutron energy lines having narrow bin widths. Since $\bar{Y}_f$ vs. diameter differed only by a scaling factor, the results of Caswell and Coyne (1975) were then normalized to our data. An interpolation was then made to obtain the 10-μm diameter result of 18 keV μm^{-1}. The mean number of hits per nucleus, based on a mean cell nuclear diameter, Y_f, and radiation dose, is given in Table 1.

PCC assay

The PCC assay was performed after 24 h of repair at 37 °C following irradiation with x rays or neutrons. The lymphocytes were fused with CHO mitotic cells, in the presence of polyethylene glycol,[||||] by the method of Pantelias and Maillie (1983) as adopted by AFRRI (Blakely et al. 1995) for the induction of PCC. Briefly, 2 million mitotic cells were initially washed twice with phosphate buffered saline (PBS) and mixed with lymphocytes isolated from 3–4 mL of blood in a 15-mL round-bottomed test tube. The cells were washed again by the addition of PBS and centrifugation at 200 × g for 8 min. The supernatant was discarded and the pellet was dried by inverting the tube over a blotting paper. The pellet was carefully floated, with a 1-mL syringe, in 0.2 mL of 50% PEG in PBS (w/v). Subsequently, 2 mL of PBS was added to dilute PEG for the next 3 min, and the cells were centrifuged for 200 × g for 8 min. The pellet was resuspended in 0.4 mL of Karyomax and subsequently 50 μL of 20-mM magnesium chloride and 50 μL of 10-μg mL^{-1} colchicine was added. Cell suspension was incubated in a water bath at 37 °C for 30 to 40 min. Chromosome spreads were prepared by the standard air-drying technique on clean grease-free glass slides after hypotonic treatment in 1% sodium citrate and fixation in 1:3 acetic methanol. Slides were stained in 4% Giemsa in distilled water for enumeration of PCCs and fragments under a light microscope[¶¶], at a magnification of 1,500. Total number of PCCs and fragments per cell reflect intact prematurely condensed chromosomes (PCCs) and fragments. The microscope was connected to a video camera,[##] coupled to a monitor (Sony, Japan) and a printer.[***] The number of PCCs and fragments was scored with a video printout as the template for each spread.

Data analysis

Analysis of the yield of PCCs and fragments included determination of the mean ± SE (standard error) and evaluation of the frequency of distribution by use of the σ^2/y and u test (Papworth 1970). The Papworth test, with values of $\sigma^2/y \geq 1$ and $u \geq 1.96$, indicated over dispersion. The dose-effect relationship from this study using pooled data from ≥3 experiments was not significantly different than when analyzed using the means of individual experimental data (data not shown). The data

[||||] PEG, MW 1450; Sigma Chemical Co., St. Louis, MO 63178.
[¶¶] Leitz, GmbH, Germany.
[##] DAGE-MTI Inc., Michigan City, IN 46360.
[***] Seikosha, Tokyo, Japan.

Table 1. Radiation dosimetry parameters used to irradiate human lymphocytes *in vitro*.

| Radiation type	$\bar{y}_f$[a] (keV μm^{-1})	Dose (Gy)	Fluence (hits μm^{-2})	Mean number of hits per nucleus[b]
250-kVp x-rays	1.53	0.00	0.0	0
		0.50	2.0	160
		1.00	4.1	321
		2.00	8.2	642
		3.00	12.3	963
		4.50	18.4	1,444
		6.00	24.6	1,952
		7.50	30.6	2,406
		9.00	36.8	2,887
Neutrons	18.0	0.00	0.00	0
		0.25	0.09	7
		0.50	0.17	14
		1.00	0.35	27
		2.00	0.69	55
		3.00	1.04	82
		4.00	1.39	109

[a] $\bar{y}_f$ is the frequency-mean lineal energy (Turner 1992).
[b] For these calculations, nuclear diameter of a lymphocyte is assumed to be 10 μm. A continuous slowing-down approximation is assumed for the linear energy deposition resulting from 250-kVp x-ray irradiation (ICRU 1973). Cell fractions receiving no hits were negligible (less than 1×10^{-3}) in samples exposed to either type of radiation.

reported here reflect the pooled data set. Dose-response curves for the number of excess PCC fragments were fitted to straight lines by the weighted least-squares regression method. Weights were based on the reciprocal of the SE of the mean squared. Excess PCC fragments per cell were calculated by subtracting 46 from the total number of PCCs and fragments per cell.

RESULTS

Frequency distributions of PCCs and fragments per cell in lymphocytes exposed to representative doses of x rays or neutrons are shown in Figs. 1 and 2. Tables 2 and
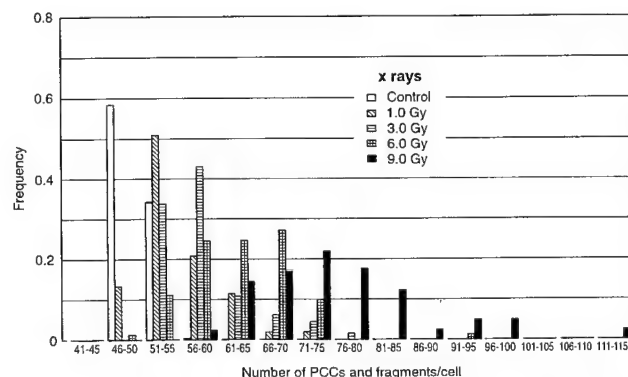
Fig. 1. Distribution, after 24 h of repair at 37 °C, of PCCs and fragments in lymphocytes exposed to different doses of x rays. The number of PCC fragments expressed per cell were grouped in increments of 5. These results represent the pooled data from ≥ 3 experiments.
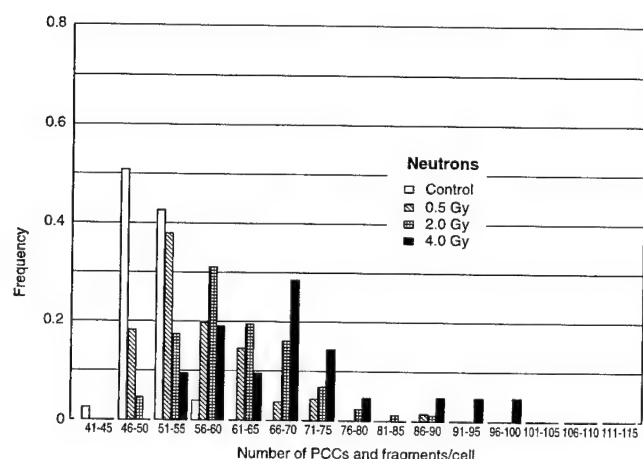
Table 2. Distribution analysis of x-ray dose-response data.

Dose (Gy)	Number of cells	PCCs and fragments/cell Mean ± SE	σ^2/y ± SE	u^a
0	79	47.62 ± 0.32	1.09 ± 0.16	0.55
0.5	77	50.43 ± 0.68	3.37 ± 0.16	4.62
1.0	53	50.76 ± 0.69	2.37 ± 0.20	7.00
2.0	49	54.94 ± 0.87	2.51 ± 0.20	7.40
3.0	65	54.45 ± 0.72	2.36 ± 0.18	7.72
4.5	79	59.10 ± 1.10	4.97 ± 0.16	24.81
6.0	81	59.19 ± 0.77	2.53 ± 0.16	9.66
7.5	56	62.32 ± 1.29	4.15 ± 0.19	16.51
9.0	41	71.56 ± 1.78	4.14 ± 0.22	14.03

[a] The values of u for the number of PCCs and fragments ≥ 1.96, indicate overdispersion based on Papworth criteria (1970). See legend to Fig. 1 for additional experimental details.

Table 3. Distribution analysis of fission-neutron dose-response data.

Dose (Gy)	Number of cells	PCCs and fragments/cell Mean ± SE	σ^2/y ± SE	u^a
0	75	46.57 ± 0.30	1.02 ± 0.16	0.10
0.25	92	49.73 ± 0.69	4.46 ± 0.15	23.37
0.50	137	52.84 ± 0.73	5.61 ± 0.12	38.06
1.0	55	54.02 ± 0.91	3.27 ± 0.19	11.81
2.0	87	57.34 ± 0.81	3.28 ± 0.15	14.94
3.0	34	62.00 ± 1.33	2.72 ± 0.25	6.99
4.0	21	64.19 ± 2.63	5.98 ± 0.32	15.78

[a] For other explanations see Table 2 and the legend to Fig. 2.

3 summarize the radiation doses and the number of PCCs and fragments observed after 24 h of repair at 37 °C following exposure to x rays and to fission neutrons. Based on the Papworth (1970) test, excess PCC fragments in the sham-treated or unirradiated cells are uniformly distributed around 46 to 47. These results fit a Poisson distribution (Figs. 1 and 2, and Tables 2 and 3). Exposure to x rays followed by 1 d repair resulted in overdispersion (Fig. 1). Table 2 shows the results of the distribution analysis of the frequency of an excess number of PCC fragments after exposure to x rays. The σ^2/Y values ranged between 2.37 and 4.97, and u values ranged between 7 and 24.81 for the excess number of PCC fragments (Table 2), which clearly indicates an overdispersion or non-Poisson distribution. For neutrons the distribution was non-Poisson (Fig. 2) as indicated by the σ^2/Y values ranging between 2.72 and 5.98, and u values between 6.99 and 38.06 (Table 3). The number of PCCs and fragments observed after 24 h of repair at 37 °C following exposure to radiation demonstrated a progressive increase with doses from 47.62 ± 0.32 at 0 Gy to 71.56 ± 1.78 at 9 Gy for x rays (Table 2). Similarly,

exposure to neutrons resulted in an increase from 46.57 ± 0.30 at 0 Gy to 64.19 ± 2.63 at 4 Gy (Table 3).

Exposure to 4.5-Gy x rays and 2-Gy neutrons, which induced a significant elevation of total PCCs and fragments above background levels (Table 2 and 3), showed approximately similar means (Fig. 3). Fig. 3 shows the frequency distributions for these doses. Dose-effect relationships were fitted to a weighted linear model for the two qualities of radiation as shown in Fig. 4. The dose-response relationships for excess PCC fragments, in the region 0 to 9 Gy of x rays, and 0 to 4 Gy of neutrons, are described by the straight-line equations. Table 4 provides the coefficients of the straight line (Y = a + bD) and the ratio of the slope and intercept between these two types of radiation. An RBE value of 2.4 ± 0.39 was estimated for neutrons when compared to x rays.

Table 4 also provides the microdosimetric quantity, $\bar{Y}_D$, the dose-mean lineal energy of the absorbed dose distribution, $D(y)$, where y is defined as the energy deposited in a volume by a single event divided by the mean chord length of the volume. Previous microdosimetry measurements have been made for both the x rays and neutrons by use of a TEPC filled with tissue-equivalent gas and corresponding to a diametric path length of 1 μm. These results show that the energy spectrum of radiation events for both the x rays and neutrons scan several orders of magnitude, but the mean event size for the neutrons, 65 keV μm^{-1}, is more than 16 times that of the x rays, 4 keV μm^{-1}. Cell fractions

Fig. 2. Distribution, after 24 h of repair at 37 °C, of PCCs and fragments in lymphocytes exposed to different doses of neutrons. (See other explanations in Fig. 1.)
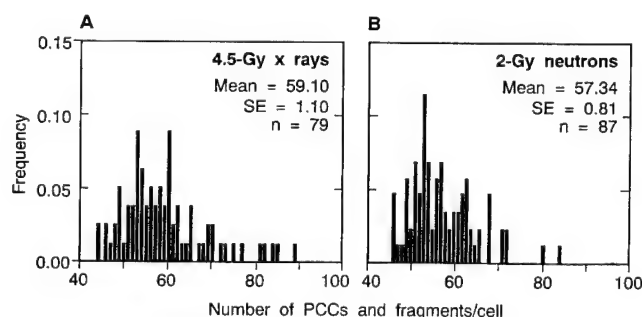
Fig. 3. Frequency distributions of PCCs and fragments following (A) 4.5-Gy x rays and (B) 2-Gy neutrons that demonstrate approximately equivalent yields of excess PCC fragments.
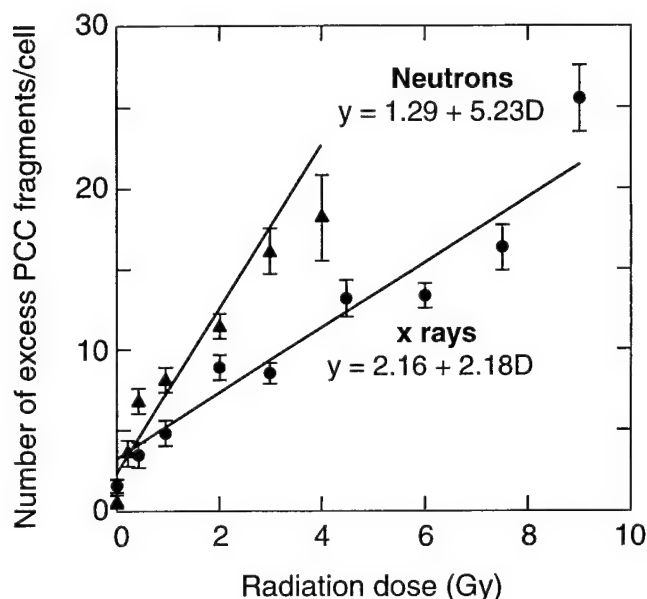
Fig. 4. Dose-response relationship for the yield of excess PCC fragments after 24 h repair at 37 °C. The bars represent SE of the mean.

Table 4. Values of $\bar{y}_D$[a] coefficients, and ratio of dose-response data.

	Radiation type		
	Neutrons	X rays	Ratio
$\bar{y}_D$ (keV μm^{-1})	65	4	—
Slope	5.23 ± 0.717	2.18 ± 0.195	2.40 ± 0.39
Intercept	1.29 ± 0.65	2.16 ± 0.544	0.60 ± 0.34

[a] Microdosimetry measurements, $\bar{y}_D$, were obtained as described in the Methods section. The slope and intercepts ($\pm$SE) are obtained from the fitted curves shown in Fig. 4.

that were not hit by radiation were negligible (less than 1×10^{-3}) in samples exposed to radiation.

DISCUSSION

The premature chromosome condensation assay, performed on peripheral blood lymphocytes of exposed individuals, is a promising direct and sensitive cytogenetic tool for biodosimetry purposes (Cornforth and Bedford 1983; Pantelias and Maillie 1985). Absorbed radiation doses can be predicted rapidly (within 24 h of the receipt of the blood sample in the laboratory) as is needed by the clinician for an effective treatment. Since it is conducted on peripheral blood lymphocytes, which are in G_0/G_1 (resting) phase of cell cycle, and does not require cell division, confounding factors such as mitotic delay (Poncelet et al. 1988) and interphase death (Natarajan et al. 1996) do not appear to interfere with dose estimates.

The background number of PCCs and fragments observed was slightly higher than the expected 46 for human lymphocytes, corresponding to the diploid chromosome number. These results are comparable with earlier observations (Pantelias and Maillie 1985). The slightly elevated background levels, observed in the present and· earlier studies, may be attributed to the effects of macrophages contaminated in lymphocyte culture, which is a known source of peroxides and oxygen free radicals. Studies on the effects of oxygen tension similar to the *in vivo* conditions and of peroxide detoxifiers, such as peroxidase or catalase, are warranted.

Overdispersion of excess PCC fragments in lymphocytes at various times following exposure to up to 8 Gy of x rays has been reported (Pantelias and Maillie 1985). The present distribution analysis indicates overdispersion 24 h after x-ray exposure in a broader dose range and supports these observations (Table 2). Further, our studies with high-LET radiations also demonstrate similar overdispersion of excess PCC fragments (Table 3 and Fig. 2). Distributions of PCCs and fragments following exposures to doses that demonstrate approximately equivalent yields are shown in Fig. 3, which reflects the qualitative difference between these radiation types as seen after repair by this assay. These doses represent mid-values in the respective dose range for these two radiation qualities. Earlier studies, conducted on Syrian hamster embryo cells, with heavy ions and gamma rays, suggested that initial chromosome damage produced by high- and low-LET radiation are qualitatively different (Suzuki et al. 1992). Overdispersion, similar to the present observations for PCCs and fragments, has also been seen for other cytogenetic end points, such as for the frequencies of acentric fragments (Edwards et al. 1979; Virsik and Harder 1981) and micronuclei in cytokinesis-blocked human lymphocytes (Littlefield et al. 1989; Thierens et al. 1991) following exposure to radiation. However, distribution of dicentric aberrations in lymphocytes was described by Poisson statistics after low-LET radiations (Edwards et al. 1979).

The frequency of excess PCC fragments per cell following exposure to 0–9 Gy x rays and to 0–4 Gy neutrons is shown in Fig. 4. The data were fitted by the weighted least-squares regression method to straight lines having a slope of 2.18 ± 0.195 fragments per cell per Gy for x rays, and 5.23 ± 0.717 for neutrons. These data indicate that neutrons are more than twice as efficient as x rays as reflected in this assay; this is consistent with the considerably larger $\bar{Y}_D$ for the neutrons (Table 4). Earlier, the PCC technique was used to study the efficiency of slow alpha particles (3.2 MeV, 128 keV μm^{-1}) relative to 250 kVp in noncycling HF-19 human diploid fibroblasts. For both qualities of radiation, the dose-effect relationship was linear, similar to our present observations. A RBE value of 2.16 ± 0.13 was estimated for alpha particles for the early formation of chromosome breaks (Bedford and Goodhead 1989).

The observation that linearity of the dose-effect relationship for initial induction of chromosome breaks is preserved even after 24 h of repair (Iliakis et al. 1988) is supported by our present studies using x rays. This is also true for neutrons (Fig. 4). A linear dose-effect relation-

ship for this bioindicator endpoint for dose assessment facilitates the practical use of this technique in cases of accidental exposures.

The linear dose-effect relationship observed in the dose range of 0 to 9 Gy for x rays (Fig. 4) agrees in general with previously published work from laboratories using human lymphocytes (Pantelias and Maillie 1985; Vyas et al. 1991) and HF19 human diploid fibroblasts (Bedford and Goodhead 1989). These previously described dose-effect relationships in interphase cells have demonstrated the potential use of this assay for dose estimates in cases of uniform whole-body exposure to a low-LET radiation. However, application of this assay for biodosimetry purposes necessitates a characterization of the effects of partial-body exposure and high-LET radiations. Recently, we suggested the possible use of this assay to predict irradiated fraction and dose to the fraction after high-dose partial-body exposures to a low-LET radiation, based on simulated partial-body exposure studies conducted with mixed cultures (Blakely et al. 1995). Although most accidental overexposures involve x rays or gamma rays, the growth of the nuclear power industry and the use of neutron sources in therapy increase the risk of accidents involving other radiation qualities (Zoetelief and Broerse 1990; Müller and Streffer 1991). Two practical difficulties associated with dose reconstruction in accidents involving mixed radiation qualities are (a) the uncertainties associated with assessment of components of radiation quality and (b) the choice of an RBE for high-LET radiations (IAEA 1986; UNSCEAR 1988). These difficulties warrant the characterization of effects due to individual components of mixed radiation fields. While the effects of radiation quality on the dicentric assay have been extensively studied (IAEA 1986; UNSCEAR 1988) and RBE is dependent on the end points studied (UNSCEAR 1988), investigations of the effects of radiation quality on the PCC assay are relatively sparse. This fact attests to the relevance of these findings on the estimation of neutron RBE value, after 24 h repair, as applicable to practical biodosimetry. Further planned studies will involve the effects of mixed radiation fields on this bioindicator endpoint.

REFERENCES

Bedford, J. S.; Goodhead, D. T. Breakage of human interphase chromosomes by alpha particles and X-rays. Int. J. Radiat. Biol. 55:211–216; 1989.

Blakely, W. F.; Prasanna, P. G. S.; Kolanko, C. J.; Pyle, M. D.; Mosbrook, D. M.; Loats, A. S.; Rippeon, T. L.; Loats, H. Application of premature chromosome condensation assay in simulated partial-body exposures: Evaluation of the use of an automated metaphase-finder. Stem Cells 13(Suppl.1):223–230; 1995.

Brown, J. M.; Evans, J.; Kovacs, M. S. The prediction of human radiosensitivity in situ: An approach of using chromosome aberrations detected by fluorescence in situ hybridization. Int. J. Radiat. Oncol. Biol. Phys. 24:279–286; 1992.

Caswell, R. S.; Conyne, J. J. Microdosimetric spectra and parameters of fast neutrons. In: Proceedings of the Fifth Symposium on Microdosimetry, 22–26 September 1975. Italy: Verbania Pallanza; EUR 5452 d-e-f; 1975.

Cornforth, M. N.; Bedford, J. S. X-ray induced breakage and rejoining of human interphase chromosomes. Science 222:1141–1143; 1983.

Dobson, R. L.; Straume T.; Carrano, A. V.; Minkler, J. L.; Deaven, L. L.; Littlefield, L. G.; Awa, A. A. Biological effectiveness of neutrons from Hiroshima bomb replica: results of a collaborative cytogenetic study. Radiat. Res. 128:143–149; 1991.

Edwards, A. A.; Lloyd, D. C.; Purrot, R. J. Radiation-induced chromosome aberrations and the Poisson distribution. Radiat. and Environ. Biophys. 16:89–100; 1979.

Evans, J. W.; Chang, J. A.; Giaccia, A. J.; Pinkel, D.; Brown, J. M. The use of fluorescence in situ hybridization combined with premature chromosome condensation for the identification of chromosome damage. Br. J. Cancer 63:517–521; 1991.

Goodwin, E.; Blakely, E.; Ivery, G.; Tobias, C. Repair and misrepair of heavy-ion-induced chromosomal damage. Adv. Space. Res. 9:83–89; 1989.

Greenstock, G. L; Trivedi, A. Biological and biophysical techniques to assess radiation exposure: A perspective. Prog. Biophys. Molec. Biol. 61:81–130; 1994.

Iliakis, G.; Pantelias, G. E.; Seaner, A. Effect of arabinofurasyladenine on radiation-induced chromosome damage in plateau-phase CHO cells measured by premature chromosome condensation: Implications for repair and fixation of α-PLD. Radiat. Res. 114:361–378; 1988.

International Atomic Energy Agency. Biological dosimetry: Chromosomal aberration analysis for dose assessment. Vienna: International Atomic Energy Agency; IAEA Technical Report Series No. 260:1–69; 1986.

International Commission on Radiation Units and Measurements. Measurement of absorbed dose in a phantom irradiated by a single beam of x or gamma rays. Washington, DC: ICRU; Publication 23; 1973.

Kliauga, P.; Dvorak, R. Microdosimetry measurements of ionization by monoenergetic photons. Radiat. Res. 73:1–20; 1978.

Littlefield, L. G.; Sayer, A. M.; Frome, E. L. Comparison of dose-response parameters for radiation-induced acentric fragments and micronuclei observed in cytokinesis-arrested lymphocytes. Mutagenesis 4:265–270; 1989.

Lloyd, D. C.; Purrot, R. J. Chromosome aberration analysis in radiological protection dosimetry. Radiat. Prot. Dosim. 1:19–28; 1981.

Meulders, J. P. Dosimetry in mixed n + γ field. In: Ionizing radiation: Protection and dosimetry. Boca Raton, Florida: CRC Press Inc.; 1988: 203–215.

Müller, W. U.; Streffer, C. Biological indicators of radiation damage. Int. J. Radiat. Biol. 59:863–873; 1991.

Natarajan, A. T.; Darroudi, F.; Ramalho, A. T. Cytogenetic indicators of radiation exposure. In: Advances in the treatment of Radiation Injuries. Oxford: Elsevier Science; 1996:263–269.

National Institute of Standards and Technology. Annual progress report in support of neutron dosimetry. Gaithersburg, MD: NIST; 1991.

Okayasu, R.; Cheong, N; Iliakis, G. Comparison of yields and repair kinetics of interphase chromosome breaks visualized by Sendai-virus or PEG-mediated cell fusion in irradiated CHO cells. Int. J. Radiat. Biol. 64:689–694; 1993.

Pantelias, G. E.; Iliakis, G. E.; Sambani, C. D.; Politis, G. Biological dosimetry of absorbed radiation by C-banding of interphase chromosomes in peripheral blood lymphocytes. Int. J. Radiat. Biol. 63:349–354; 1993.

Pantelias, G. E.; Maillie, H. D. A simple method for premature chromosome condensation induction in primary human and rodent cells using polyethylene glycol. Somatic Cell Genetics 9:533–547; 1983.

Pantelias, G. E; Maillie, H. D. The use of peripheral blood mononuclear cell prematurely condensed chromosomes for biological dosimetry. Radiat. Res. 99:140–150; 1984.

Pantelias, G. E.; Maillie, H. D. Direct analysis of radiation-induced chromosome fragments and rings in unstimulated human peripheral blood lymphocytes by means of the premature chromosome condensation technique. Mutat. Res. 149:67–72; 1985.

Papworth, D. G.; In: Savage, J. R. K. Sites of radiation-induced chromosome exchanges. Curr. Topics in Radiat. Res. 6:129–194; 1970 (Appendix).

Poncelet, E.; Leonard, A.; Leonard E. D.; Dutrillaux, B. Biological dosimetry: Radiation-induced mitotic delay can lead to underestimate of the part of the body exposed after nonuniform irradiation. Strehlanther. und Onkol. 164:542–543; 1988.

Redpath, J. L.; Antoniono, R. J.; Sun, C.; Gerstenberg, H. M.; Blakely, W. F. Late mitosis/early G_1 phase and mid-G_1 phase are not hypersensitive cell cycle phases for neoplastic transformation of HeLa x skin fibroblast human hybrid cells induced by fission-spectrum neutrons. Radiat. Res. 141:37–43; 1995.

Rossi, H. H. H. Specification of radiation quality. Radiat. Res. 10:522–531; 1959.

Sasai, K.; Evans, J. W.; Kovacs, M.S.; Brown, J. M. Prediction of human cell radiosensitivity: Comparison of clonogenic assay with chromosome aberrations scored using premature chromosome condensation with fluorescence in situ hybridization. Int. J. Radiat. Oncol. Biol. Phys. 30:1127–1132; 1994.

Suzuki, M.; Watanabe, M.; Suzuki, K.; Nakano, K.; Matsui, K. Heavy ion-induced chromosome breakage studied by premature chromosome condensation (PCC) in Syrian hamster embryo cells. Int. J. Radiat. Biol. 62:581–586; 1992.

Tanaka, K.; Hoshi, M.; Sawada, S.; Kamada, N. Effects of ^{252}Cf neutrons, transmitted through an iron block on human lymphocyte chromosome. Int. J. Radiat. Biol. 66:391–397; 1994.

Thierens, H.; Vral, A.; de Ridder, L. Biological dosimetry using the micronucleus assay for lymphocytes: Interindividual differences in dose response. Health Phys. 61:623–630; 1991.

Turner, J. E. An introduction to microdosimetry. Radiat. Protect. Management 9:25–58; 1992.

United Nations Scientific Committee on the Effects of Atomic Radiation. Sources, effects and risks of ionizing radiation. New York: United Nations; 1988.

Virsik, R. P.; Harder, D. Analysis of radiation-induced acentric fragments in human G_0 lymphocytes. Radiat. Environ. Biophys. 19:29–40; 1981.

Vyas, R. C.; Darroudi, F.; Natarajan, A. T. Radiation-induced chromosomal breakage and rejoining in interphase-metaphase chromosomes of human lymphocytes. Mutat. Res. 249:29–35; 1991.

Zeman, G. H.; Ferlic, K. P. Paired ion chamber constants for fission gamma-neutron fields. Bethesda, MD: Armed Forces Radiobiology Research Institute; AFRRI TR84-8; 1984.

Zoetelief, J.; Broerse, J. J. Dosimetry for radiation accidents: Present status and prospects for biological dosimeters. Int. J. Radiat. Biol. 57:737–750; 1990.

■ ■

Thiol WR-1065 and disulphide WR-33278, two metabolites of the drug Ethyol (WR-2721), protect DNA against fast neutron-induced strand breakage

C. SAVOYE, C. SWENBERG†, S. HUGOT, D. SY, R. SABATTIER‡, M. CHARLIER and M. SPOTHEIM-MAURIZOT*

Abstract. The main metabolites of the cytoprotective drug Ethyol (Amifostine, WR-2721) are the thiol WR-1065 and the disulphide WR-33278 (formed by the oxidation of WR-1065). Both metabolites are well-known protectors against DNA damage induced by γ-rays. Using supercoiled plasmid DNA and restriction fragments we show that they protect efficiently also in the case of fast neutrons. In anoxic conditions WR-1065 ($Z = +2$) protects by scavenging of $OH^{\bullet}$ and by 'chemical repair' (by H donation from its SH function). WR-33278 ($Z = +4$) protects by scavenging of $OH^{\bullet}$ and, in the case of the supercoiled plasmid DNA, by reducing the accessibility of radiolytic attack sites via the induction of packaging of DNA in liquid-crystalline condensates (observed by circular dichroism). Because of this second mechanism, the plasmid DNA is more efficiently protected by WR-33278 than by WR-1065, at concentration ratios > 1 drug/4 nucleotides. Moreover, using sequencing gel electrophoresis of irradiated fragments of known sequence, we show that the protection by the two metabolites is non-homogeneously distributed along the DNA sequence, with 'hot spots' of protection and with unprotected regions. Based on presented molecular modelling results we explain the sequence dependence of radioprotection by structural variations induced by the binding of the drugs.

1. Introduction

Ethyol (Amifostine) is a new promising cytoprotective drug containing the phosphorothioate WR-2721 (Capizzi and Oster 1995). In most cases, it protects specifically normal cells without diminishing the damaging effect of chemo- and radiotherapies on tumour cells (Washburn *et al.* 1974, Yuhas *et al.* 1980, Brown *et al.* 1984, van der Vijght and Peters 1994, Wasserman 1994). This interesting property is partially due to better penetration of the drug into normal than into tumour cells (Yuhas 1980). The main cellular radioprotective metabolite of WR-2721 is the thiol WR-1065 (Calabro-Jones *et al.* 1988, Smoluk *et al.* 1988). The conversion of the phos-phorothioate into its thiol occurs by the dephos-phorylation with alkaline phosphatase, an enzyme generally more abundant in normal tissues than in tumours (Calabro-Jones *et al.* 1985).

Strand breaks of DNA, critical radiation-induced damages, are mainly due to the abstraction of an H atom from the 4' position of deoxyribose by the $OH^{\bullet}$ radicals produced by the radiolysis of water (Giese *et al.* 1995). The well-known radioprotective ability of thiols is explained by the scavenging of radiation induced $OH^{\bullet}$ radicals and by the 'chemical repair' of the damaged deoxyriboses of DNA, by H atom donation from the SH function (Fahey 1988, Held 1988). The most efficient radioprotectors are the positively charged thiols that concentrate close to DNA due to electrostatic attraction (Vasilescu *et al.* 1986, Zheng *et al.* 1988, Spotheim-Maurizot *et al.* 1991). It was shown that WR-1065, which has an electric charge $Z = +2$ at neutral pH (Newton *et al.* 1992), is a better radioprotector than the thiol cysteamine ($Z = +1$) in the case of irradiation of cells and of plasmid DNA with γ-rays. It is also a much better protector than the disulphide cystamine with $Z = +2$ (Aguilerra *et al.* 1992, Zheng *et al.* 1992).

Carnes and Grdina (1992) reported a significant protection by WR-2721 also against the mice neoplastic mortality induced by high LET neutrons. However, the drug seems to protect less efficiently against the cytotoxic and mutagenic effects of neutrons than against those of γ-rays (Sigdestadt *et al.* 1986, Kataoka *et al.* 1992). This can be due to a lower protection of DNA by the thiol metabolite WR-1065 against neutrons than against low LET radiations since, generally, thiols protect less efficiently from high LET than from low LET radiations (Bird 1980, Sigdestadt *et al.* 1986). In a previous work we have shown that cysteamine protects less efficiently from fast neutrons- than from γ-ray-induced DNA strand breaks only in anoxia (Spotheim-Maurizot *et al.* 1991). We explained this discrepancy by a possible competition between the 'chemical

*Author for correspondence.
Centre de Biophysique Moléculaire, CNRS, rue Charles Sadron, 45071 Orléans Cedex 2, France.
†Applied Cellular Radiobiology Department, Armed Forces Radiobiology Research Institute, Bethesda, MD 20889, USA.
‡Service d'Oncologie et de Radiothérapie, Centre Hospitalier Régional d'Orléans, 45067 Orléans Cedex 2, France.

repair' (occurring for both radiations) and the 'fixation' of damages by the oxygen that in initially anoxic solution is produced in the secondary, dense ionization tracks of neutrons (by protons, α particles and heavy ions).

Using plasmid DNA, we evaluate in the present work the ability of the thiol WR-1065 to protect DNA from fast neutron-induced strand breaks. Anoxic conditions were employed since WR-1065 gets easily oxidized and converts into several products, from which the main one is the highly charged disulphide WR-33278 ($Z = +4$). This disulphide is also a metabolites of WR-2721 *in vivo*, but its role in the radioprotection is not yet clearly established (Smoluk *et al.* 1986, 1988, Shaw *et al.* 1994). We checked also its effect on the plasmid DNA radiolysis. The effects of WR-1065 and WR-33278 are compared with those of cysteamine and cystamine.

The radiation-induced strand breakage of DNA in solution is non-homogeneously distributed along the molecule. This modulation of radiosensitivity can be explained by sequence-dependent variations of DNA structure. For instance, the reported radioresistance of the AATT regions (Franchet-Beuzit *et al.* 1993, Isabelle *et al.* 1995, Spotheim-Maurizot *et al.* 1995a) is consistent with the reduced accessibility of the $4'$ positions located in the reputed narrow minor groove of this sequence (Fratini *et al.* 1982). The radioprotection by proteins is also non-homogeneous. It occurs at and around their sites of binding to DNA. This protection can be explained by the local scavenging of $OH^{\bullet}$ radicals, by the physical screening of the binding site (inaccessibility of the radiolytic attack site) and by an eventual structural change of the DNA binding region (Franchet-Beuzit *et al.* 1993, Isabelle *et al.* 1993). The radioprotection by the positively charged thiols and disulphides can also be non-homogeneous if their binding to DNA modifies the conformation of the binding site and of the neighbouring zones. Vasilescu *et al.* (1986) have shown that the electrostatic binding of WR-1065 to DNA occurs at two neighbouring phosphates of the same strand or of opposite strands, as previously suggested for a polyamine of a closely related chemical structure, the spermine (Feuerstein *et al.* 1986). As for putrescine or spermine, the binding of WR-1065 and WR-33278 can induce distortions of the B-DNA helix (Feuerstein *et al.* 1986, Lavery *et al.* 1986) that can lead to variations of DNA radiosensitivity and radioprotection.

We have determined the distribution of the protection by WR-1065 and WR-33278 along an 80-bp restriction fragment containing two radioresistant bent AATT sequences. The results are discussed in relation to those of a molecular modelling study of DNA–WR drugs complexes.

2. Materials and methods

2.1. *Chemicals*

The pOP203 plasmid (Fuller 1982) was prepared according to Sambrook *et al.* (1989). Before irradiation, plasmid DNA was dialysed extensively against $1\,\text{mmol}\,\text{dm}^{-3}$ phosphate buffer, pH 7·25. DNA was irradiated at a concentration of $50\,\mu\text{g}\,\text{ml}^{-1}$ ($1·4 \times 10^{-4}\,\text{mol}\,\text{dm}^{-3}$ nucleotide).

The fragment of 80 bp was prepared from the plasmid DNA and labelled as previously described (Franchet-Beuzit *et al.* 1993).

Solutions of cysteamine, cystamine (Merck), WR-1065 and WR-33278 (Walter Reed Army Institute, Washington, DC, USA) were prepared in $1\,\text{mmol}\,\text{dm}^{-3}$ potassium phosphate, pH 7·25 buffer. The solutions of drugs and of DNA were separately deoxygenated by flushing with pure argon, mixed and kept under argon flushing until irradiation. DNA solutions irradiated without additives were deoxygenated in the same conditions.

The possible oxidation of the thiols during the experiment was measured for cysteamine by the 5,5'-dithio-bis-(2-nitrobenzoic acid) (DTNB) method. In the argon-flushed solution of $0·1\,\text{mmol}\,\text{dm}^{-3}$ cysteamine and at 273 K, 10% of the cysteamine became oxidized during the irradiation with 30 Gy of fast neutrons.

2.2. *Irradiations*

Irradiations were performed with fast neutrons obtained by the nuclear reaction of 34 MeV protons on a semithick beryllium target (Centre d'Etude et de Recherche par Irradiation, CNRS, Orléans). For experiments with plasmids the mean dose-rate of fast neutrons monitored with transmission chambers was 0·3 Gy/min and the dose mean lineal energy in water at the point of interest was 87·7 KeV/μm. For experiments with fragments the mean dose-rates were 10 Gy/min.

The samples were contained in polypropylene tubes (Eppendorf, 0·4 ml) immersed 1 cm below the surface of an ice bath.

2.3. *Electrophoresis*

Horizontal agarose (1·2%, Gibco BRL) minigels in Tris-acetate buffer (Tris $20\,\text{mmol}\,\text{dm}^{-3}$, sodium acetate $10\,\text{mmol}\,\text{dm}^{-3}$, EDTA $1\,\text{mmol}\,\text{dm}^{-3}$, pH 8·1) were run for 2 h at $830\,\text{Vm}^{-1}$ at 293 K. The electrophoresis separates the supercoiled, the circular

relaxed and the linear forms of the plasmid. The fractions of the three forms in each lane were assayed, after ethidium bromide staining, using a video-camera system and the DensyLab software (Bioprobe Systems). The average number of single strand breaks (ssb) per plasmid was determined as previously described (Spotheim-Maurizot *et al.* 1991).

The sequencing gel electrophoresis of the 80-bp irradiated fragments was performed as previously described (Franchet-Beuzit *et al.* 1993). To identify the bands, Maxam–Gilbert sequencing of purines and pyrimidines of the same fragment was performed on the same gel.

Gels were fixed in a mixture of 10% acetic acid and 10% ethanol, rinsed with water, dried onto Whatman 3MM paper. They were then exposed onto PhosphorImager, which allows scanning and quantitative analysis using the ImageQuant software (Molecular Dynamics).

2.4. *Circular dichroism*

The circular dichroism spectra were recorded at 277 K with a Jobin–Yvon autodichrograph Mark V. In each case, the spectra were recorded after complete stabilization of the signal.

2.5. *Molecular modelling*

A molecular modelling study was carried out with SYBYL software (TRIPOS 6.2 (1995) St Louis, MO, USA). A DNA sequence of 30 bp was initially built up in the standard B conformation and the thiol and disulphide molecules were built separately. The thiol molecules with positive charges on its two amine groups was anchored electrostatically on the negatively charged phosphates of two successive nucleotides. Three different positions were explored, with the thiol located: (1) longitudinally in the minor groove, (2) longitudinally in the major groove and (3) transversally across the minor groove. The energy calculations were performed with the Amber force field using the Kollman's charges (Weiner *et al.* 1984). The solvent effect was implicitly taken into account by introducing a distance-dependent dielectric constant. The disulphide molecule was anchored electrostatically on the negatively charged phosphates of four successive nucleotides. The naked DNA or the DNA–WR complexes were energy minimized with the Powell method (Powell 1977). The main feature of the analysis was the minor groove width, which was measured at each pair of nucleotide as the mean distance between the H5′ atom on one strand and the H4′ atom on the other strand (Edwards *et al.* 1992).

3. Results

3.1. *Radiolysis of plasmid DNA*

Deoxygenated solutions of supercoiled plasmid DNA (4362 bp) were irradiated at 273 K with 30 Gy fast neutrons. The irradiation induced 0·02 ssb/plasmid/Gy. The number of ssb decreases when DNA is irradiated in the presence of increasing amounts of WR-1065, WR-33278, cysteamine and cystamine. The ratios of the number of ssb induced in the presence and in the absence of the drugs ($1/PF$) as a function of R (concentration of added drug/concentration of nucleotides) are shown in Figure 1. The protection efficiencies are in the order WR-1065 > cysteamine > cystamine. For WR-33278, the shape of the protection curve is different from those of the three other drugs. At low concentrations (first part of the curve) it protects less efficiently than WR-1065. At high concentrations of drug the situation is inverted.

To search for eventual WR-33278-induced conformational changes, we have performed CD measurements. Figure 2 shows the CD spectra of DNA in the presence of increasing amounts of the disulphide. We observe large changes in the spectrum from $R = 0·26$, thus in the concentration range where radioprotection by WR-33278 overpasses that by WR-1065. The variation of the intensity of the CD signal at 260 nm and of the $1/PF$ as a function of R are shown in Figure 3.

3.2. *Radiolysis of the 80-bp restriction fragment*

Deoxygenated solutions of ^{32}P-labelled 80-bp restriction fragments were irradiated with 80 Gy fast
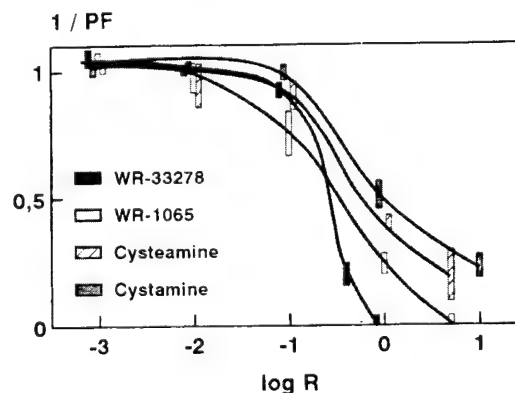

Figure 1.   Variation of the inverse of the SSB protection factor (1/PF) as a function of the number of drug molecules per nucleotide, R. Irradiation, 30 Gy fast neutrons. Buffer, 1 mmol dm^{-3} potassium phosphate, pH 7·25. Curves are the best smoothing of the experimental values (averages of at least three experiments).
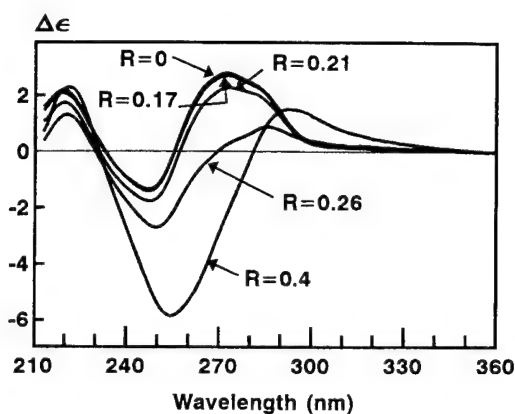
Figure 2.   Modification of the circular dichroism spectra of the supercoiled plasmid DNA in the presence of increasing amounts of WR-33278. DNA was in 1 mmol dm^{-3} potassium phosphate buffer, pH 7·25.
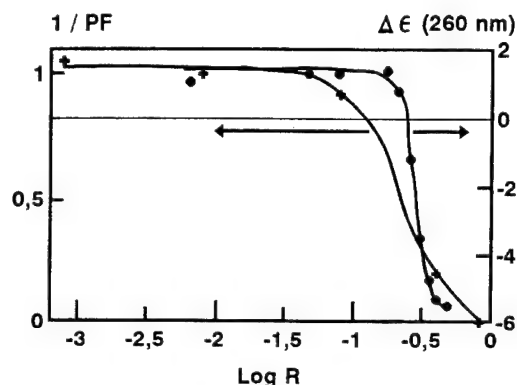

Figure 3.   Variation of the circular dichroism signal at 260 nm (circles) and the SSB protection curves in 1 mM potassium phosphate buffer (crosses) as a function of the WR-33278 concentration.

neutrons. The sequencing gel electrophoresis of the irradiated fragments shows the induction of frank strand breaks at all nucleotide sites. The probability of breakage varies along the fragment. The breakage pattern of DNA (probability of breakage at each nucleotide site) reveals the previously reported relative radioresistance of the AATT sequences. When the fragments were irradiated in the presence of drugs, the breakage patterns are modified. Figure 4 shows as an example the breakage patterns of DNA irradiated without additive and in the presence of 0·1 WR-1065/nucleotide.

The protection patterns (ratio of the breakage probabilities for DNA with and without drug) calculated from the breakage patterns of 'naked' DNA and of DNA irradiated in presence of the drugs are presented in Figures 5 and 6. They reveal a non-homogeneous protection by both WR drugs.

For WR-1065 at $R = 0·1$, two 'hot spots' of protec-

tion (M and O) are observed along the analysed sequence, the strongest being at the sequence M. A protection lower than the average value is observed for the sequence N. At $R = 1$ the pattern is modified and a new, but less intense, 'hot spot' of protection appears at a TGT sequence (P) and the low-protected region is shortened and shifted in the 5′ direction to the sequence Q (Figure 5).

The pattern for WR-33278 at $R = 0·1$ shows a globally low protection. Protection occurs at the sequence X and at a GTC triplet (Y). The rest of the analysed sequence is not protected. At $R = 1$, almost the entire fragment is protected. The strongest protection occurs at the TCCT sequence belonging to the region X. One nucleotide every 9–12 nucleotides is unprotected. This renders a wave-like shape to the protection pattern (Figure 6). The period does not change with increasing disulfide concentration.

3.3. *Molecular modelling*

The molecular modelling of a 30-bp sequence of our 80-bp fragment shows that the two AATT zones exhibit a minor groove restricted width. This result is in good agreement with the crystallographic data (Fratini *et al.* 1982). The zones with a narrow minor groove are the zones of low probability of radiation induced strand breakage in the naked DNA (Figure 7).

We have constructed DNA–WR-1065 complexes and observed that the longitudinal location of the thiol in the minor groove (around $-209 \text{ kJ} \cdot \text{mol}^{-1}$) is energetically more favourable than that in the major groove (around $-167 \text{ kJ} \cdot \text{mol}^{-1}$) and than the transversal location across the minor groove (around $-155 \text{ kJ} \cdot \text{mol}^{-1}$).

The DNA–WR-1065 complex with the thiol molecule electrostatically anchored along the minor groove at T24C25 site (belonging to the 'hot spot' of protection M; Figure 5, top) shows a narrowing of the minor groove in and around the binding zone. Moreover the thiol masks the H4′ atoms of the nucleotides to which it is anchored (Figure 8). On the contrary, the minor groove is widened when one molecule of WR 1065 is anchored at the T7G8 site (belonging to the only slightly protected region N; Figure 5, top). Since in this case the thiol is deeply inserted in the groove, the H4′ atoms of the nucleotide to which it is anchored, are not masked by the ligand (Figure 9). When six molecules of thiol are bound to the 30 bp oligonucleotide, the conformation of the complex is different: the minor groove in the zone around T7G8 (which at high concentration belongs to the 'hot spot' of protection P; Figure 5) becomes also narrower than in the naked DNA (data
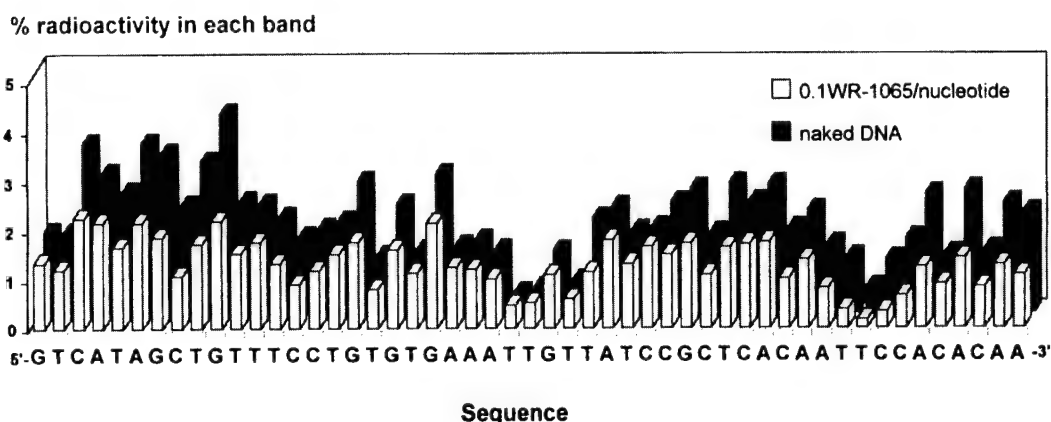
% radioactivity in each band

Sequence

Figure 4.   Probability of strand breakage at each nucleotide irradiated in the presence (clear bars) and in the absence (dark bars) of 0·1 WR-1065/nucleotide along a part of the 80 bp DNA fragment. Irradiation dose, 80 Gy fast neutrons. Anoxic conditions. The results are those of one typical experiment out of five rendering similar patterns. The experimental error in the determination of area of peaks in the densitogram of gels is < 3%.

Sequence

Sequence

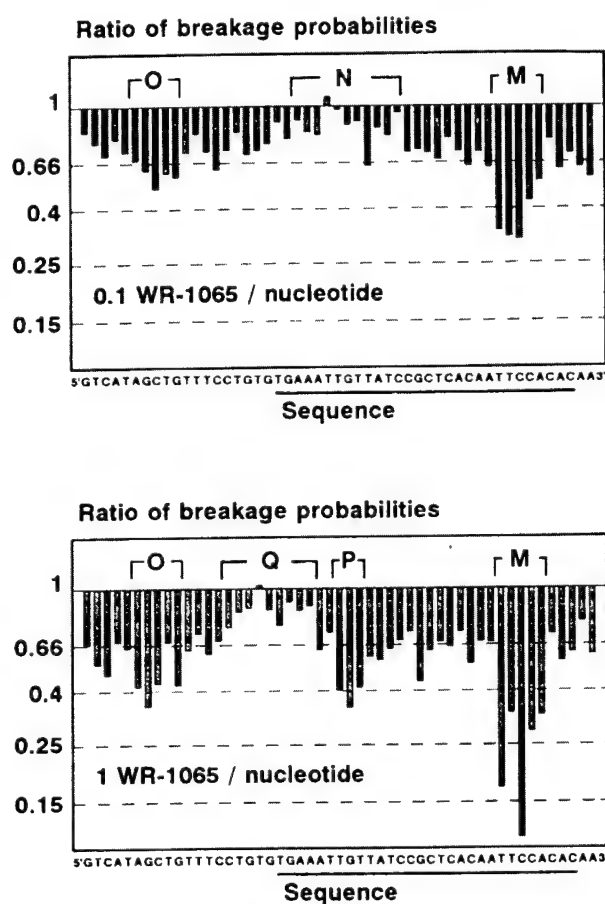**Sequence**

Sequence

Figure 5.   Ratios of the probability of strand breakage at each nucleotide along a part of the 80 bp DNA fragment irradiated in the presence and in the absence of WR-1065. Irradiation dose, 80 Gy of fast neutrons. Anoxic conditions. The results are those of a typical experiment out of five rendering similar patterns. The experimental error in the determination of the areas of peaks in the densitogram of gels is < 3%. Underlined, the sequence of the modelized 30 bp fragment.
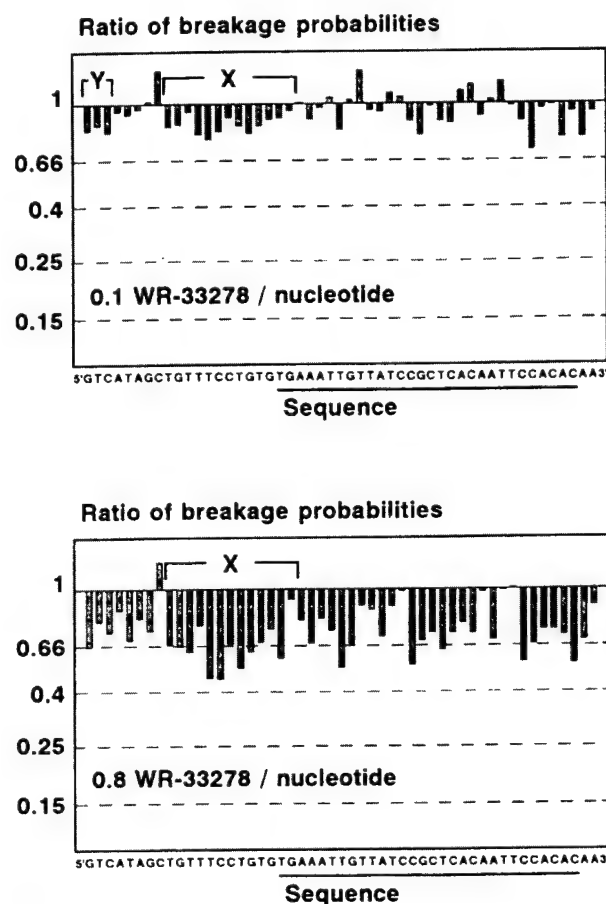
Figure 6.   Ratios of the probability of strand breakage at each nucleotide along a part of the 80 bp DNA fragment irradiated in the presence and in the absence of WR-33278. Irradiation dose, 80 Gy fast neutrons. Anoxic conditions. The results are those of a typical experiment out of five rendering similar patterns. The experimental error in the determination of the areas of peaks in the densitogram of gels is < 3%. Underlined, the sequence of the modelized 30 bp fragment.
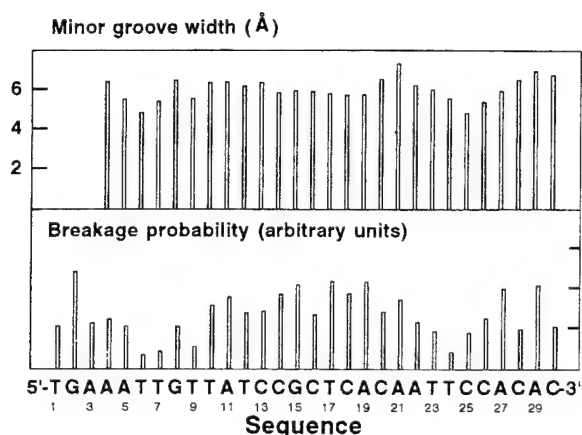
Figure 7.   Variation of the minor groove width of a naked 30 bp DNA calculated by molecular modelling (up) and the probability of strand breakage at each nucleotide along the irradiated naked DNA, from Figure 4 (down).

not shown). In all discussed locations, the SH function, which moreover can rotate around the terminal C-S, is close enough to the 4' position to allow the H donation and thus the chemical repair.

We have modelled the DNA–WR-33278 complex with one disulphide molecule electrostatically anchored along the minor groove at T24C25C26A27 site. This site belongs in this case to an unprotected region (in the case of WR-1065 it belongs to the 'hot spot' of protection M). The final structure exhibit a widening of the minor groove in and around the binding zone. The disulphide molecule is deeply inserted in the groove and the H4' atoms of the nucleotide to which it is anchored are not masked.

When six molecules of disulphide are bound to the 30 bp oligonucleotide, the minor groove width is strongly reduced all along the 30 bp fragment with minima at the sites of anchorage and maxima at the uncovered nucleotides (periodic variation with period of 4 bp). The total length of the fragment is decreased by 0·18 nm (0·006 nm/bp). When eight molecules are bound, the variation of the minor groove width exhibit a periodicity of 3 bp.

4. Discussion

4.1. *Mechanisms of protection*

The anoxic radioprotection by the metabolites WR-1065 and WR-33278 of the drug WR-2721 can be explained by:

(i)   the scavenging of OH$^{\bullet}$ radicals,
(ii) the 'chemical repair' of damaged sugars (for the thiol WR-1065),
(iii) the packaging of plasmid DNA into a radio-

resistant condensate (for high concentrations of the disulfide WR-33278).

4.1.1. *Scavenging of OH$^{\bullet}$ radicals and 'chemical repair' of damaged sugars* The rate constant of the reaction of WR-1065 with OH$^{\bullet}$ radicals ($9{\cdot}2 \times 10^9$ dm^3 mol s^{-1}; Ward and Mora-Arellano 1984) is lower than that of cysteamine ($1{\cdot}8 \times 10^{10}$ dm^3 mol s^{-1}; Buxton *et al.* 1988). Nevertheless, WR-1065 protects more efficiently than cysteamine: at 1 drug/nucleotide, $PF_{\text{WR-1065}} \approx 2 \times PF_{\text{cysteamine}}$ (Figure 1). This can be due to its higher charge and thus to its higher degree of condensation around DNA (Manning 1978). Thus WR-1065 can more efficiently repair the damaged sugars and scavenge the OH$^{\bullet}$ radicals reaching DNA. Cystamine is a disulphide with the same positive charge as WR-1065 ($Z = +2$), with a similar chemical structure (diamine), but missing the SH function. Although its reaction rate with OH$^{\bullet}$ radicals is the same as that of cysteamine (Buxton *et al.* 1988) and its charge is higher, it protects slightly less than cysteamine since it is unable to 'chemically repair' the damaged sugars. Thus, in spite of its lower OH$^{\bullet}$ scavenging ability, WR-1065 is the best radioprotector. The mechanism of protection by scavenging of radicals and by 'chemical repair' was already proposed by Zheng *et al.* (1988) for the protection by WR-1065, cysteamine and cystamine against γ-rays in aerobic conditions.

The results of molecular modelling are in good agreement with the mechanisms of protection discussed above. The energetically most favourable location of the thiol and of the disulphide in the minor groove allows the interference with the initial damaging process, the abstraction of a H atom from the 4' position situated in the minor groove (by OH$^{\bullet}$ radicals) with formation of a 4' sugar radical. Therefore they can efficiently scavenge the OH$^{\bullet}$ radicals and repair the sugar radical. In addition, the drug molecules can protect particular sequences also by masking the 4' positions and by narrowing the minor groove. Such sequence-dependent effects can account for the variations of protection along the molecule (see discussion below).

4.1.2. *Packaging of DNA into a radioresistant condensate.* Although cystamine protects plasmid DNA less efficiently than cysteamine, WR-33278 protects more efficiently than WR-1065 at $R > 0{\cdot}25$. To explain the radioprotection by WR-33278 we propose, together with the scavenging of OH$^{\bullet}$ radicals, another type of mechanism which involves also the charge of the drug, $Z = +4$. The modifications of the shape and intensity of CD spectra at drug concentrations that strongly radioprotect are similar to those previously
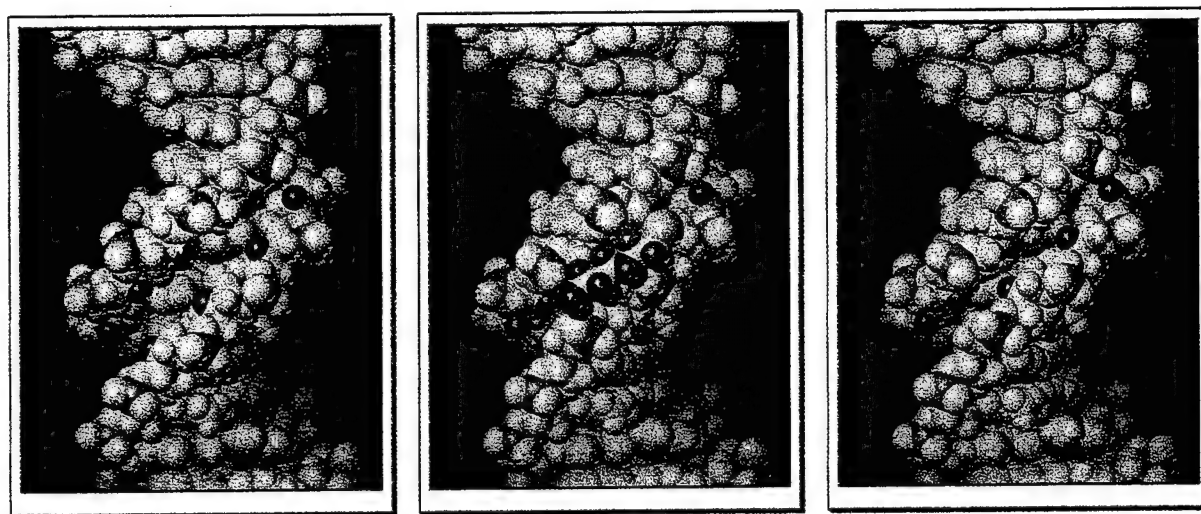
Figure 8.   A part of the model of the 30 bp DNA with one WR-1065 molecule bound at the T24C26 sequence. (left) Naked DNA, (centre) DNA-WR 1065 complex, (right) DNA-WR 1065 complex with hidden thiol. Colours: P, orange; H'4, magenta; S, yellow; N, blue; H atoms of the thiol, cyan; all other atoms, white.
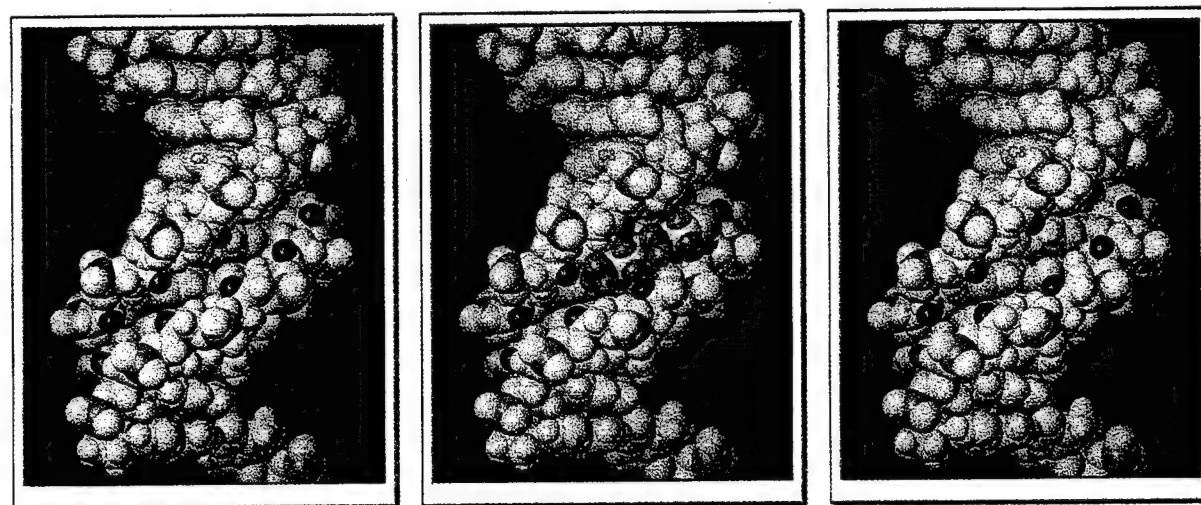

Figure 9.   A part of the model of the 30 bp DNA with one WR-1065 molecule bound at the T7G8 sequence. (left) Naked DNA, (centre) DNA-WR 1065 complex, (right) DNA-WR 1065 complex with hidden thiol. Colours: P, orange; H'4, magenta; S, yellow; N, blue; H atoms of the thiol, cyan; all other atoms, white.

observed for other radioprotective molecules with closely related chemical structures, the polyamines spermidine $(\mathcal{Z} = +3)$ and spermine $(\mathcal{Z} = +4)$ (Spotheim-Maurizot *et al.* 1995b, Newton *et al.* 1996). The modifications of CD spectra (at drug concentrations corresponding to an extensive neutralization of the negative charge of DNA) may reflect the same important conformational changes as for the polyamines: the formation of liquid–crystalline structures of toroidal or rod-like shape. The packaging of DNA molecules longer than 400 bp into such condensed structures is triggered by the extensive neutralization of the negative charges of DNA (92% for the ligands with $\mathcal{Z} = +3$ and 94% for ligands with $\mathcal{Z} = +4$;

Manning 1978) that render possible intra- and inter-molecular interactions (Bloomfield 1991, and references herein). We have explained the 'simultaneous' radioprotection of DNA by spermidine or spermine, by the reduction of the accessibility of $OH^{\bullet}$ radicals to the attack sites (nucleotides) in the condensates. We suggest here that WR-33278 radioprotects DNA by the same mechanism. Shigematsu *et al.* (1994) have shown similarities in the radioprotection by spermine and WR-33278 against mutagenesis at the *hprt* locus in Chinese hamster AA8 cells.

In the case of fragments, WR-33278 protects less efficiently than WR-1065 even at high concentration. This can be due to the fact that the 80 bp

oligonucleotides is too short to condense into the same type of highly radioresistant structure as the plasmid (Bloomfield 1991).

4.2. *Sequence-modulated protection*

The electrostatic binding of a small positively charged molecule to one or more neighbouring phosphates (on the same strand or on opposite strands) is *a priori* non-specific and therefore it is expected to be sequence-independent. Nevertheless, it was shown that the polyamines bind preferentially to particular sequences. The preferential binding was explained by sequence-dependent variations of DNA structure and electrostatic potential (Feuerstein *et al.* 1986, Lavery *et al.* 1986).

The non-homogeneous protection by WR-1065 and WR-33278 cannot be simply explained by a sequence-dependent binding to DNA, since no clear sequence similarity appears between the observed 'hot spots' of protection.

Our results of molecular modelling suggest another (or an additional) explanation of the sequence-dependence of the radioprotection. It would be due to structural variations induced by the binding of the drugs and to the eventual masking of radiolytic attack sites. The electrostatic binding of WR-1065 to two nucleotides belonging to the 'hot spot' M, in the energetically most favourable location (longitudinally in the minor groove), triggers the narrowing of the minor groove at and around the bound nucleotides, and masks the H4' position of the bound nucleotides (Figure 8). Both effects can explain the increased radioprotection in this zone.

The low protection of the region N can be explained by the increase of accessibility of the 4' positions in the minor groove widened by the deep insertion of the thiol. Moreover these positions are not masked by the thiol as in the 'hot spot'. The deep insertion can also diminish the radioprotective effect of OH$^\cdot$ scavenging (Figure 9).

The modification of the radioprotection pattern with increasing thiol concentration can be explained by a concentration-dependent conformational change of the helix (Vasilescu *et al.* 1986, Mallet *et al.* 1994). Moreover, Lavery *et al.* (1986) have shown modifications of the binding-induced distortion with increasing the concentration of putrescine. Such effects can either increase or decrease the radiosensitivity of the affected region.

According to our results, at high thiol concentration, the protection of the region P (unprotected at low concentrations) can be explained by the narrowing of the minor groove observed in the model of the 30 bp DNA with six bound thiols (see § 3).

The emergence of a new hot spot of protection, at a TGT triplet may be related to the flexibility of this sequence (Folta-Stogniew and Russu 1995) and thus to its facility to undergo structural changes.

The lack of protection of certain zones by the deep insertion of the disulphide WR-33278 can be explained, like in the case of the WR-1065, by the widening of the minor groove, by the lack of masking the H4' atoms and by the reduced effect of OH$^\cdot$ scavenging (see § 3).

The protection by high concentrations of WR-33278 involves the calculated narrowing of the minor groove all along the model of DNA with six disulphide molecules (see § 3).

The molecular modelling does not account for the constant periodicity of 10 bp of the wave-like shape of the protection pattern. This periodicity recalls the one observed in the case of the 146 bp DNA of irradiated core nucleosome (Franchet *et al.* 1993) or of shorter DNA fragments irradiated with bound charged proteins (Isabelle *et al.* 1993) or with compounds such as distamycine (experiments with chemically produced OH$^\cdot$ radicals; Churchill *et al.* 1990) and polyamines (spermidine and spermine; Savoye *et al.* in preparation). The common point of all these systems is the extensive symmetrical or asymmetrical neutralization (until 94% in the case of spermine and WR-33278) of the negative charge of the phosphates. According to the hypothesis of Manning (1989) such uncharged DNA, if > 60 bp, would contract along its axis ($0\cdot1$ Å/bp), buckle and form a bent 'spring-like' structure. Our results of modelling agree with the contraction, since a shortening of the helix is observed with WR-33278 ($0\cdot06$ Å/bp). It is possible that, in the proposed regularly bent structure, the width of the minor groove varies with a period of 10 bp corresponding to the pitch of B-DNA. This will lead to a periodically variable accessibility of the H4' atom and thus will explain the observed wave-like pattern of radioprotection by WR-33278 and, may be, by other charged molecules.

5. Conclusion

The two studied metabolites of Ethyol (Amifostine, WR-2721), the thiol WR-1065 and the disulphide WR-33278 formed by the oxidation of WR-1065, protect efficiently against the DNA strand breakage induced by fast neutrons. The fact that at relatively high concentrations WR-33278 is an even better protector than WR-1065 can contribute to the explanation of the differential radioprotection of normal and tumour cells by Ethyol (WR-2721). Since normal tissues are better vascularized (and thus better oxygenated), more WR-33278 may be generated in

the normal than in tumoral cells. Thus normal cells can be better protected than the tumour cells.

Moreover, the protection by the two metabolites of Ethyol is non-homogeneously distributed along DNA: some sequences are more efficiently protected than others. We explain this sequence-dependence by various structural changes induced by the binding of the two main metabolites.

The thiol-induced and the even stronger disulphide-induced modification of DNA structure can also influence (diminish) the subsequent binding of some anti-tumour drugs. This may explain why Ethyol is not only a good radioprotector but also an efficient cytoprotector in the chemotherapy with a large variety of drugs (Capizzi and Oster 1995).

Acknowledgements

References

AGUILERA, J. A., NEWTON, G. L., FAHEY, R. C. and WARD, J. F., 1992, Thiol uptake by Chinese hamster V79 cells and aerobic radioprotection as a function of the net charge on the thiol. *Radiation Research*, **130**, 194–204.

BIRD, R. P., 1980, Cysteamine as a protective agent with high-LET radiations. *Radiation Research*, **82**, 290–296.

BLOOMFIELD, V. A., 1991, Condensation of DNA by multivalent cations: consideration of mechanism. *Biopolymers*, **31**, 1471–1481.

BROWN, D. Q., YUHAS, J. M., MACKENZIE, L. J., GRAHAM III, W. J. and PITTOCK III, J. W., 1984, Differential radioprotection of normal tissues by hydrophilic chemical protectors. *International Journal of Radiation Oncology, Biology, Physics*, **10**, 1581–1584.

BUXTON, G. V., GREENSTOCK, C. L., HELMAN, W. P. and ROSS, A. B., 1988, Critical review of rate constants for reactions of hydrated electrons, hydrogen atoms and hydroxyl radicals ($^{\bullet}$OH/$^{\bullet}$O^{-}) in aqueous solution, *Journal of Physical and Chemical Reference Data*, **17**, 513–886.

CALABRO-JONES, P. M., AGUILERA, J. A., WARD, J. F., SMOLUK, G. D. and FAHEY, R. C., 1988, Uptake of WR-2721 derivatives by cells in culture: identification of the transported form of the drug. *Cancer Research*, **48**, 3634–3640.

CALABRO-JONES, P. M., FAHEY, R. C., SMOLUK, G. D. and WARD, J. F., 1985, Alkaline phosphatase promotes radioprotection and accumulation of WR-1065 in V79-171 cells incubated in medium containing WR-2721. *International Journal of Radiation Biology*, **47**, 23–27.

CAPIZZI, R. L. and OSTER, W., 1995, Protection of normal tissues from the cytotoxic effects of chemotherapy and radiation by Amifostine: clinical experiences. *European Journal of Cancer*, **31A**(suppl. 1), S8–13.

CARNES, B. A. and GRDINA, D. J., 1992, *In vivo* protection by the aminothiol WR-2721 against neutron-induced carcinogenesis. *International Journal of Radiation Biology*, **61**, 567–576.

CHURCHILL, M. E. A., HAYES, J. J. and TULLIUS, T. D., 1990, Detection of drug binding to DNA by hydroxyl radical footprinting. Relationship of distamycin binding site to DNA structure and positioned nucleosome on 5S RNA genes of *Xenopus. Biochemistry*, **29**, 6043–6050.

EDWARDS, K. J., BROWN, D. G., SPINK, N., SKELLY, J. V. and NEIDLE, S., 1992, Molecular structure of the B-DNA dodecamer d(CGCAAATTTGCG)$_2$. An examination of propeller twist and minor groove water structure at 2·2 Å resolution. *Journal of Molecular Biology*, **226**, 1161–1173.

FAHEY, R. C., 1988, Protection of DNA by thiols. *Pharmacology and Therapeutics*, **39**, 101–108.

FEUERSTEIN, B. G., PATTABIRAMAN, N. and MARTON, L. J., 1986, Spermine-DNA interactions: a theoretical study. *Proceedings of the National Academy of Sciences, USA*, **83**, 5948–5952.

FRANCHET-BEUZIT, J., SPOTHEIM-MAURIZOT, M., SABATTIER, R., BLAZY-BAUDRAS, B. and CHARLIER, M., 1993, Radiolytic footprinting. Beta rays, gamma photons and fast neutrons probe DNA–protein interactions. *Biochemistry*, **32**, 2104–2110.

FRATINI, A. V., KOPKA, M. L., DREW, H. R. and DICKERSON, R. E., 1982, Reversible bending and helix geometry in a B-DNA dodecamer: CGCGAATT^{Br}CGCG. *Journal of Biological Chemistry*, **257**, 14686–14707.

FOLTA-STOGNIEW, E. and RUSSU, I. M., 1995, Sequence-dependence of base-pair opening in a DNA dodecamer containing the CACA/GTGT sequence motif. *Biochemistry*, **33**, 11016–11024.

FÜLLER, F., 1982, A family of cloning vectors containing the *lac* UV5 promoter, *Gene*, **19**, 43–54.

GIESE, B., BEYRICH-GRAF, X., ERDMAN, P., PETRETTA, M. and SCHWITTER, U., 1995, The chemistry of single-stranded 4'-DNA radicals: influence of the radical precursor on anaerobic and aerobic strand cleavage. *Chemistry and Biology*, **2**, 367–375.

HELD, K., 1988, Models for thiol protection of DNA in cells. *Pharmacology and Therapeutics*, **39**, 123–131.

ISABELLE, V., FRANCHET-BEUZIT, J., SABATTIER, R., LAINE, B., SPOTHEIM-MAURIZOT, M. and CHARLIER, M., 1993, Radioprotection of DNA by a DNA-binding protein: MC1 chromosomal protein from the archaebacterium *Methanosarcina* sp. *CHT155. International Journal of Radiation Biology*, **63**, 749–758.

ISABELLE, V., PREVOST, C., SPOTHEIM-MAURIZOT, M., SABATTIER, R. and CHARLIER, M., 1995, Radiation-induced damages in single- and double-stranded DNA. *International Journal of Radiation Biology*, **67**, 169–176.

JAYARAM, B., SHARP, K. A. and HONIG, B., 1989, The electrostatic potential of B-DNA. *Biopolymers*, **28**, 975–993.

KATAOKA, Y., BASIC, I., PERRIN, J. and GRDINA, D. J., 1992, Antimutagenic effects of radioprotector WR-2721 against fission-spectrum neutrons and ^{60}Co gamma-rays in mice. *International Journal of Radiation Biology*, **61**, 387–392.

LAVERY, R., SKLENAR, H. and PULLMAN, B., 1986, The flexibility of the nucleic acids: III. The interaction of an aliphatic diamine, putrescine, with flexible B-DNA. *Journal of Biomolecular Structure and Dynamics*, **3**, 1015–1031.

MALLET, G., BEN ABDALLAH, K., COSTA, A. and VASILESCU, D., 1994, Molecular radioprotection of DNA by cysteamine

and WR-1065. A transient electric birefringence study. *Applied Physics Communications*, **13**, 283–298.

MANNING, G. S., 1978, The molecular theory of polyelectrolyte solution with application to the electrostatic properties of polynucleotides. *Quarterly Review of Biophysics*, **11**, 179–246.

MANNING, G. S., 1989, Self-attraction and natural curvature in null DNA, *Journal of Biomolecular Structure and Dynamics*, **7**, 41–61.

NEWTON, G. L., AGUILERA, J. A., WARD, J. F. and FAHEY, R. C., 1996, Polyamine-induced compaction and aggregation of DNA—a major factor of radioprotection of chromatin under physiological conditions. *Radiation Research*, **145**, 776–780.

NEWTON, G. L., DWYER, T. J., KIM, T., WARD, J. F. and FAHEY, R. C., 1992, Determination of the acid dissociation constants for WR-1065 by proton NMR spectroscopy. *Radiation Research*, **131**, 143–151.

POWELL, M. J. D., 1977, Restart procedures for the conjugate gradient method. *Mathematical Programming*, **12**, 241–254.

SAMBROOK, J., FRITSCH, E. F. and MANIATIS, T., 1989, *Molecular Cloning: A Laboratory manual*, 2nd edn (Cold Spring Harbor Laboratory Press, New York), vol. 1.

SHAW, L. M., BONNER, H. S. and BROWN, D. Q., 1994, Metabolic pathways of WR-2721 (Ethyol, Amifostine) in the BALB/c mouse. *Drug Metabolism and Disposition*, **22**, 895–902.

SHIGEMATSU, N., SCHWARTZ, J. L. and GRDINA, D. J., 1994, Protection against radiation induced mutagenesis at the hprt locus by spermine and *N,N*-(dithiodi-2,1-ethandiyl)bis-1,3-propanediamine (WR-33278). *Mutagenesis*, **9**, 355–360.

SIGDESTAD, C. P., GRDINA, D. J., CONNOR, A. M. and HANSON, W. R., 1986, A comparison of radioprotection from three neutron sources and ^{60}Co by WR-2721 and WR-151327. *Radiation Research*, **106**, 224–233.

SMOLUK, G. D., FAHEY, R. C., CALABRO-JONES, P. M., AGUILERA, J. A. and WARD, J. F., 1988, Radioprotection of cells in culture by WR-2721 and derivatives: form of the drug responsible for protection. *Cancer Research*, **48**, 3641–3647.

SMOLUK, G. D., FAHEY, R. C. and WARD, J. F., 1986, Equilibrium dialysis studies of the binding of radioprotector compounds to DNA. *Radiation Research*, **107**, 194–204.

SPOTHEIM-MAURIZOT, M., FRANCHET, J., SABATTIER, R. and CHARLIER, M., 1991, DNA radiolysis by fast neutrons. II. Oxygen, thiols and ionic strength effects. *International Journal of Radiation Biology*, **59**, 1313–1324.

SPOTHEIM-MAURIZOT, M., FRANCHET-BEUZIT, J., ISABELLE, V., TARTIER, L. and CHARLIER, M., 1995a, DNA radiolysis

of the gene regulation domains. *Nuclear Instruments and Methods in Physics Research B*, **105**, 308–313.

SPOTHEIM-MAURIZOT, M., RUIZ, S., SABATTIER, R. and CHARLIER, M., 1995b, Radioprotection of DNA by polyamines. *International Journal of Radiation Biology*, **68**, 571–577.

VAN DER VIJGHT, W. J. F. and PETERS, G. J., 1994, Protection of normal tissues from the cytotoxic effects of chemotherapy and radiation by Amifostine (Ethyol): preclinical aspects. *Seminars in Oncology*, **21**(suppl. 11), 2–7.

VASILESCU, D., BROCH, H. and RIX-MONTEL, M. A., 1986, Mechanism of aminothiol radioprotectors action at the molecular level. *Journal of Molecular Structure (Theochem)*, **134**, 367–380.

VAUGHAN, A. T., GRDINA, D. J., MEECHAN, P. J., MILNER, A. E. and GORDON, D. J., 1989, Conformational changes in chromatin structure induced by the radioprotective aminothiol, WR 1065. *British Journal of Cancer*, **60**, 893–896.

WARD, J. F. and MORA-ARELLANO, V. P., 1984, Pulse radiolysis studies of WR-1065. *International Journal of Radiation Oncology, Biology, Physics*, **10**, 1533–1536.

WASHBURN, L. C. L., CARLTON, J. E., HAYES, R. L. and YUHAS, J. M., 1974, Distribution of WR-2721 in normal and malignant tissues of mice and rats bearing solid tumors: dependence on tumor type, drug dose and species. *Radiation Research*, **59**, 475–483.

WASSERMAN, T. D., 1994, Radiotherapeutic studies with Amifostine (Ethyol). *Seminars in Oncology*, **21**(suppl. 11), 21–25.

WEINER, S. J., KOLLMAN, P. A., CASE, D. A., SINGH, U. C., GHIO, C., ALAGONA, G., PROFETA JR. S. and WEINER, P., 1984, A new force field for molecular mechanical simulation of nucleic acids and proteins. *Journal of American Chemical Society*, **106**, 765–784.

YUHAS, J. M., SPELLMAN, J. M. and CULO, F., 1980, The role of WR-2721 in radiotherapy and/or chemotherapy. *Cancer Clinical Trials*, **3**, 211–216.

YUHAS, J. M., 1980, Active versus passive absorption kinetics as the basis for selective protection of normal tissues by *S*-2-(3-Aminopropylamino)-ethylphosphorothioic acid. *Cancer Research*, **40**, 1519–1524.

ZHENG, S., NEWTON, G. L., GONICK, G., FAHEY, R. C. and WARD, J. F., 1988, Radioprotection of DNA by thiols: relationship between the net charge on a thiol and its ability to protect DNA. *Radiation Research*, **114**, 11–27.

ZHENG, S., NEWTON, G. L., WARD, J. F. and FAHEY, R. C., 1992, Aerobic radioprotection of pBR 322 by thiols: effect of thiol net charge upon scavenging of hydroxyl radicals and repair of DNA radicals. *Radiation Research*, **130**, 183–193.

Radiomodification by Caffeine Alone and in Combination with Phosphorothioates: *In Vivo* and Cell-Free Studies

C.E. Swenberg, M.R. Landauer and J.F. Weiss*

Armed Forces Radiobiology Research Institute, Bethesda, MD 20889-5603, U.S.A.
*Office of International Health Programs, Department of Energy, Germantown, MD 20874-1290, U.S.A.

Abstract. Caffeine is generally considered to result in radiosensitization by affecting the cell cycle. Data from *in vivo* studies, however, do not suggest sensitization; caffeine administration did not adversely affect survival of mice irradiated at doses causing hematopoietic injury, or gastrointestinal injury, or when administered in combination with phosphorothioates. For example, caffeine administration (20 mg/kg IP) in combination with the radioprotector WR-151327, S-2-(3-methylaminopropylamino)propylphosphorothioic acid, (200 mg/kg IP) resulted in a dose modification factor of 1.54 in comparison to 1.51 for WR-151327 treatment alone. In a cell-free system, the active metabolites of phosphorothioates, i.e., free thiols and disulfides, appear to mimic polyamines and modulate enzymes involved in DNA structure and synthesis. The free thiol of WR-151327 (WR-151326) actively enhanced topoisomerase I-mediated unwinding of supercoiled pIBI30 DNA and supercoiling of DNA mediated by DNA gyrase (topoisomerase II). Caffeine, in general, had opposite effects on topoisomerase activities compared to WR-151326. When caffeine was added to the cell-free system together with WR-151326, the stimulatory effects of WR-151326 were suppressed. Further studies are needed in cell-free systems, cells, and animals to elucidate the potential utility of caffeine administration in combination with radiation and other therapeutic agents.

I. INTRODUCTION

A number of phosphorothioates such as WR-151327 (S-3-[3-methylaminopropylamino]propyl-phosphorothioic acid) are capable of protecting normal tissue from damage due to chemotherapy or radiation therapy. WR-151327 has been shown to protect against acute [1] and late effects [2] of both gamma and neutron radiation as well as toxic effects of nitrogen mustard [3]. Our laboratories have been involved in both molecular studies and animal studies aimed at elucidating and improving upon radioprotection afforded by phosphorothioates. Cell-free studies can provide useful models for the assessment of protective agents, e.g., determining how they affect enzymes involved in DNA structure and synthesis [4]. Animal studies, on the other hand, provide useful information on protection relative to toxic effects [5].

One of the principal problems associated with the use of phosphorothioate protectors in humans is their adverse side effects such as hypotension, vomiting, and somnolence [6], which can lead to a degradation in performance. One approach to this problem is to develop combinations of drugs that maximize radioprotection and minimize side effects [7]. Using this paradigm, we found that caffeine was effective in mitigating the motor performance decrement produced by the phosphorothioate WR-3689 [8]. The mechanism by which caffeine reduced this behavioral deficit may be mediated through the adenosine system, since caffeine is a nonspecific A_1 and A_2 adenosine receptor antagonist .

Even though some *in vitro* experiments suggest that caffeine is a radiosensitizer, we have not observed a radiomodifying effect using 30-day survival as an endpoint. For example, 40 mg/kg caffeine administered IP to mice resulted in a dose modification factor (DMF) of 1.03, which was not statistically different from vehicle. Furthermore, caffeine ameliorated the detrimental effects of combined radiation and indomethacin treatment on 7-day survival (GI death) [8]. Kesavan and co-workers in a series of studies also have not observed caffeine radiosensitization, *in vivo*, and have reported protection against radiation-induced chromosomal aberrations in mice [9].

Figure 1. Effects of caffeine (20 mg/kg) alone and in combination with WR-151327 (200 mg/kg) on locomotor activity in nonirradiated mice. Caffeine was administered 30 min before WR-151327. Locomotor activity was assessed immediately following injection of WR-151327. Time intervals are the periods after WR-151327 administration. Data are expressed as percent of vehicle control. Vertical bars represent the SEM. (N = 8-12/ group). * $p < 0.05$ from vehicle control group. † $p < 0.05$ from WR-151327.
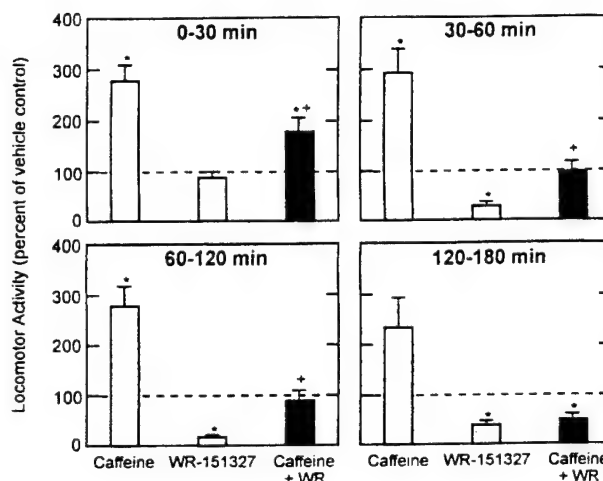
2. *IN VIVO* STUDIES

Locomotor activity and survival were measured in male CD2F1 mice (BALB/c x DBA/2)F1, (Charles River Breeding Laboratory, Raleigh, NC), weighing 24-31 g. All mice were quarantined on arrival and representative animals were screened for evidence of disease. Mice were housed in groups of 10 in Microisolator cages (Lab Products, Maywood, NJ) on hardwood chip contact bedding in a facility approved by the American Association for Accreditation of Laboratory Animal Care. Animal rooms were maintained at $21 \pm 2°$ C with $50 \pm 10\%$ humidity on a 12-h light/dark cycle. Commercial rodent chow and acidified (pH 2.5) water (to control opportunistic infections) were freely available.

Computerized Digiscan activity monitors (Omnitech Electronics, Columbus, OH) were used to quantify locomotor activity. Each monitor used an array of infrared photodetectors, spaced 2.5 cm apart, to determine horizontal locomotor activity, which was expressed as the total distance traveled. Immediately following all injections (IP), mice were placed into individual Plexiglas activity chambers (20 x 20 x 30 cm). Activity was monitored for 3 hr. All testing took place during the dark portion of the light/dark cycle. Each animal was tested only once. Food and water were available throughout the testing period.

Locomotor activity data were log transformed to stabilize the variances. An analysis of variance and the Newman-Keuls multiple range test was used to statistically analyze the data. The data indicate (Fig. 1) that caffeine administration significantly reduced the locomotor decrement observed up to 2 hr. after treatment with WR-151327.

Survival was assessed after irradiation in the bilateral (-radiation field of the Armed Forces Radiation Research Institute (AFRRI) ^{60}Co facility [10]. The mice were confined in a Plexiglas restrainer to limit movement. The midline tissue dose to the animals ranged from 7-16 Gy and was delivered at a dose rate of 1 Gy/min. The dose rate was established in an acrylic mouse phantom using a 0.5 cc tissue-equivalent ionization chamber (calibration factor traceable to the National Institute of Standards and Technology). The tissue-air ratio was 0.96 and the field was uniform to within $\pm$ 3%. Dosimetric measurements were made in accordance with the American Association of Physicists in Medicine protocol for the determination of absorbed dose from high-energy photon and electron beams [11].

All drugs were administered IP. Caffeine (20 mg/kg) or saline were administered 30 min prior to the radioprotector WR-151327 (200 mg/kg) [U.S. Bioscience, West Conshohocken, PA), which was given 30 min before irradiation. Thirty-day survival was analyzed by probit analysis (Fig. 2).

The data indicate that caffeine had no detrimental effect on radioprotection by WR-151327. The $LD_{50/30}$ (Gy) values with [95% Confidence Limits] were: Saline: 8.3 [8.16, 8.56]; Saline/WR-151327: 12.57 [12.44, 12.71]; Caffeine/WR-151327: 12.75 [12.44, 12.71]. Caffeine administered in combination with WR-151327 resulted in a DMF of 1.54 in comparison to 1.51 for WR-151327 treatment alone.

3. CELL-FREE STUDIES

In an attempt to rationalize the effects of caffeine with WR-151327 on radioprotection parameters, we performed several *in vitro* experiments to investigate whether caffeine alters the interaction of topoisomerases with DNA both in the presence and absence of the free thiol (WR-151326) and its disulfide. The motivation for these experiments with topoisomerase I and II is that these enzymes are known to alter a variety of interactions with DNA [12, 13] and thus alter many cellular functions. Furthermore, it is well established that caffeine complexes to a variety of ligands that in turn interact with DNA. For these reasons, it is not unrealistic to expect effects of caffeine on WR-compounds and topoisomerases jointly. The free thiol form of WR-151327 (WR-151326) and its corresponding symmetrical disulfide (WR-25595501) were synthesized [14], and plasmid pIBI30 was isolated by the alkaline lysis procedure from *E. coli* followed by CsCl/EtBr gradient centrifugation.

Samples were electrophoresed using a horizontal submarine gel apparatus. Agarose gels (1.3%) were cast in an electrophoresis buffer (40 mM Tris, 20 mM sodium acetate pH 7.8, and 1.8 mM EDTA). Samples were loaded in 0.1% bromophenol blue buffer and gels were run at 75V for 3 hr in a cold box. Gels were stained with EtBr (1 µg/µl) for 30 min, photographed and scanned using a Molecular Dynamics computing densitometer (Sunnyvale, CA). Topoisomerase I assays contained the following constituents in a total volume of 30 µl: reaction buffer (20 mM Tris-HCl, pH 7.5, 0.5 mM dithiothreitol, 6% glycerol), 20 mM KCl, 1.0 µg (101 µM DNA phosphate) supercoiled DNA, 2.0 units calf thymus topoisomerase I and drug as indicated. Figure 3 illustrates the inhibitory effects of caffeine on topoisomerase reaction with DNA.

Figure 2. Survival of irradiated mice following (A) saline vehicle; (B) WR-151327 alone; and, (C) WR-151327 in combination with caffeine. N = 24/data point.
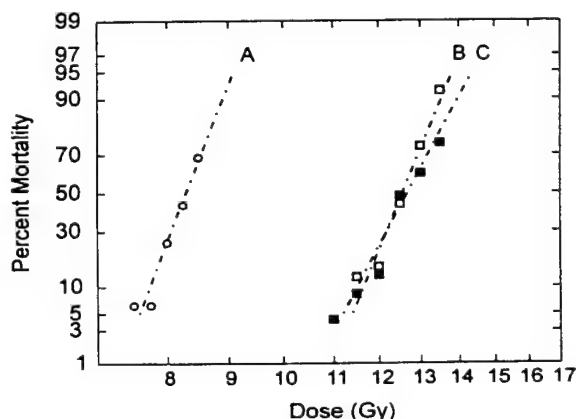
Similar inhibition of the effects of topoisomerase II were observed in the presence of caffeine (data not shown). In the latter experiments, supercoiled pIBI30 was initially relaxed with topoisomerase I under BRL reaction conditions. Here the total volume was 25 µl with reaction buffer (35 mM Tris-HCl, pH 7.5, 0.1mM EDTA, 10 mM 2-mercaptoethanol, 4 µg/ml BSA, 10% glycerol), 2mM $MgCl_2$, 1.5 mM ATP, 0.5 µg relaxed pIBI30, 5 units of topoisomerase II and 160 mM KCL. Samples were incubated at 37°C for 35 min and terminated by the addition of 6.25 µl of loading mixture (5% SDS, 25% glycerol and 0.25 mg/ml bromophenol blue).
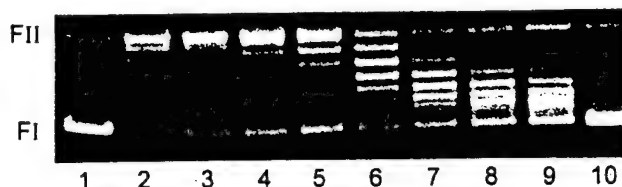

Figure 3. Photograph of a typical gel electrophoresis illustrating the inhibitory effect of topoisomerase I activity on supercoiled pIBI30 with caffeine. FI and FII denote maximum supercoiled form and total relaxed (and nicked circular) form of supercoiled DNA. Bands between these two forms correspond to different topological forms of DNA. Lanes (1) no caffeine, no topoisomerase I; (2) no caffeine, with topoisomerase I, (3-10), 2.5, 5, 10, 25, 40, 55, 70 and 85 mM caffeine with topoisomerase I. See text for further details.
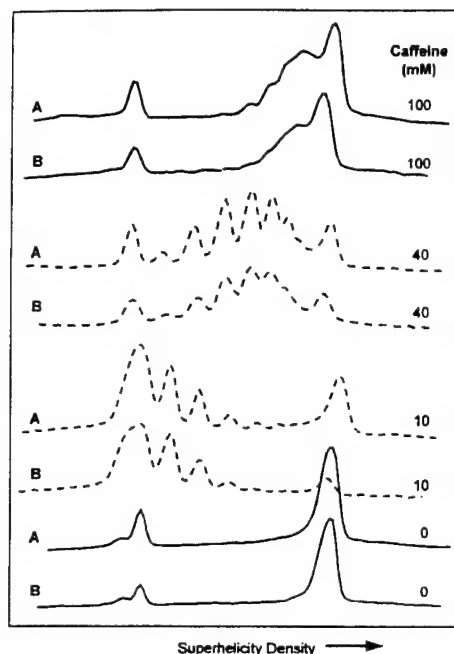
Figure 4. Comparison of densitometric tracings of gel electrophoresis showing modulation of topoisomerase I activity on supercoiled pIBI30 with (A) caffeine (mM); and (B) caffeine (mM) + 400 uM WR-151326. The bottom two curves are controls with no caffeine or topoisomerase. See text for further details.

Of interest here is whether these inhibitory effects of caffeine are altered in the presence of the major metabolites of WR-151327 - the free thiol WR-151326 and its disulfide WR-25595501. We previously demonstrated that the free thiol and disulfide forms of WR-2721 and WR-151327 stimulated topoisomerase-mediated winding and unwinding of supercoiled DNA [4, 15].

In the present study using WR-151326 at a concentration of 400 µM, there was no apparent change in the topological distribution of isomers of supercoiled DNA as illustrated in Fig 4 for the range of caffeine concentrations investigated. Similar results (not shown) were obtained for the disulfide of WR-151326. Although we have illustrated only the inhibitory effects of caffeine on the excitatory effects of thiol on supercoiled DNA, we observed similar results for WR-25595501.

These cell-free experiments clearly indicate that topoisomerase interactions with DNA are inhibited by even small doses of caffeine. In addition, caffeine also inhibits the excitatory effects of WR-compounds on topoisomerases. Whether these are valid conclusions for cellular systems necessitates further experiments. Furthermore, the radiomodifying effects of caffeine *in vivo* may be related to a variety of other pharmacological and physiological properties that are unrelated to its potential interactions with DNA systems.

Acknowledgments

References

[1] Ledney G.D., Elliott T.B., Landauer M.R., Henderson P.L., Harding R.A., Tom S.P., *Adv. Space Res.* **14** (1994) 583-586.

[2] Grdina D.J., Wright B.J., Carnes B.A., *Radiat. Res.* **128** (1991) S124-S127.

[3] Green D., Bensely D., Schein P., *Cancer Res.* **54** (1994) 738-741.

[4] Holwitt E.A., Koda E., Swenberg C.E. *Radiat. Res.* **124** (1990) 107-109.

[5] Weiss J. F., Kumar K. S., Walden T. L., Neta R., Landauer M. R., Clark E.P., *Int. J. Radiat. Biol.* **57** (1990) 709-722.

[6] Kligerman M.M., Turrisi A.T., Urtasun R.C., Norfleet A.L., Phillips T.L., Barkley T. Rubin T., *Int. J. Radiat. Oncol. Biol. Phys.* **14** (1988) 1119-1122.

[7] Landauer M.R., Davis H.D., Kumar K.S., Weiss J.F., *Adv. Space Res.* **12(2)** (1992) 273-283.

[8] Weiss J.F., Landauer M.R., Hogan J.B., Gunter-Smith P.J., Benson K.A., Neta R., Hanson W.R., "Modification of radiation-induced gastrointestinal and hematopoietic injury in mice by combinations of agents: Effects of indomethacin and caffeine," Eicosanoids and Other Bioactive Lipids in Cancer, Inflammation and Radiation Injury, K.V. Honn, L.J. Marnett and S. Nigam Eds. (Kluwer Academic Publ., Boston, MA, in press).

[9] Devasagayam T.P., Kesavan P.C., *Ind. J. Exp. Biol.* **34** (1996) 291-297.

[10] Carter R.E., Verrelli D.M., AFRRI cobalt whole-body irradiation. Technical Report 73-3, (1973) Armed Forces Radiobiology Research Institute, Bethesda, MD.

[11] American Association of Physicists in Medicine, *Med. Phys* **10** (1983) 741-771.

[12] Wang J.C., *Ann. Rev. Biochem.* **5** (1985) 665-692.

[13] Wang J.C., *Biochem. Biophys. Acta* **909** (1987) 1-9.

[14] Vaishnav Y.N., Pendergrass J.A., Clark E.P., Swenberg C.E., *J. Pharm. Biomed. Anal.* **14** (1996) 317-325

[15] Weiss J.F., Pendergrass J.A., von Hanwehr R., Swenberg C.E., "Effects of radioprotectors on DNA topoisomerase activity *in vitro*," *Radiation Research* 1895-1995, Vol. 1, U. Hagen, H. Jung and C. Streffer Eds. (Wurzburg, Germany, 1995) p. 438.

MDR1/P-glycoprotein function. I. Effect of hypotonicity and inhibitors on rhodamine 123 exclusion

JAMES L. WEAVER, LESLIE McKINNEY, PATRICIA V. SCHOENLEIN,
SARAH GOLDENBERG, MICHAEL M. GOTTESMAN, AND ADORJAN ASZALOS
*Molecular Pharmacology, Division of Research and Testing, Center for Drug Evaluation
and Research, Food and Drug Administration, Laurel 20708; Department of Physiology,
Armed Forces Radiation Radiobiology Institute 20889; Laboratory of Cell Biology, National
Cancer Institute, National Institutes of Health, Bethesda, Maryland 20892; and Department
of Anatomy and Cell Biology, Medical College of Georgia, Augusta, Georgia 30912*

Weaver, James L., Leslie McKinney, Patricia V. Schoenlein, Sarah Goldenberg, Michael M. Gottesman, and Adorjan Aszalos. MDR1/P-glycoprotein function. I. Effect of hypotonicity and inhibitors on rhodamine 123 exclusion. *Am. J. Physiol.* 270 (*Cell Physiol.* 39): C1447–C1452, 1996.—The MDR1 protein (P-glycoprotein) is a membrane ATPase whose expression results in resistance to several anti-tumor drugs. It has been proposed that the MDR1 protein, in addition to its pumplike properties, can function as (Gill et al. *Cell* 71: 23–32, 1992; Altenberg et al. *Cancer Res.* 54: 618–622, 1994) or mediate the activity of (Hardy et al. *EMBO J.* 14: 68–75, 1995) a hypotonic stress-induced Cl^- current. In addition, one study found that drug transport and Cl^- channel-associated functions of MDR1 were separable and mutually exclusive and that, when cells were swelled, the MDR1 protein could not transport substrate. This hypothesis was tested in four pairs of isogenic cell lines with *MDR1* transfectants expressing 8,000–55,000 MDR1 antibody binding sites per cell. Cytoplasmic exclusion of rhodamine 123 was used as an indicator of MDR1 function to measure the effect of hypotonic stress, MDR1 inhibitors, and Cl^- channel blockers on MDR1 transport function. It was found that MDR1 activity and its inhibition by cyclosporine A or flufenamic acid were unaffected by hypotonicity alone or in combination with Cl^- channel blockers.

multidrug resistance; chloride channel; drug efflux; cyclosporine A; 4-acetamido-4′-isothiocyanostilbene-2,2′-disulfonic acid; 4,4′-diisothiocyanostilbene-2,2′-disulfonic acid; flufenamic acid

---

THE CELLULAR PHENOTYPE of multidrug resistance (MDR) to anti-cancer chemotherapeutic agents has multiple causes and can be selected for by chronic exposure to cytotoxic drugs such as colchicine and vinblastine. One specific cause is overexpression of the cell surface protein MDR1 (also called P-glycoprotein or p170), a 170-kDa transmembrane protein. The MDR1 protein is thought to mediate the efflux of a variety of drugs out of the cell (see Refs. 13 and 26 for reviews). Cell lines transfected with the *MDR1* cDNA acquire the complete MDR phenotype (20).

On the basis of its structure, the MDR1 protein has been placed in the ATP-binding cassette family of transport proteins that includes the cystic fibrosis transmembrane conductance regulator (CFTR), which is a Cl^- channel (22). Although recent studies have suggested that the MDR1 protein may also have Cl^- channel properties, the mechanism by which the MDR1 protein mediates drug efflux remains unclear (12).

Drug efflux has been shown to be ATP dependent (15). The MDR1 protein has two nucleotide binding sites and has been shown to hydrolyze ATP when reconstituted into lipid vesicles (4) and to support substrate-stimulated ATPase activity (25). Cells expressing MDR1 have reduced accumulation in their cytoplasm of various compounds, many but not all of which are weak bases that are positively charged at neutral pH. Exclusion of cytotoxic agents from cells expressing MDR1 is inhibited by a diverse array of drugs. Some of these, including cyclosporin A (8), verapamil (24), forskolin (19), and several other compounds (5), have been shown to specifically bind to the MDR1 protein.

In addition to its pumplike properties, two recent studies have suggested that the MDR1 protein may also have Cl^- channel activity (11, 29). With the use of whole cell patch-clamp techniques, Gill et al. (11) characterized a Cl^- current that is activated by hypotonic stress in NIH/3T3 and S1 cells transfected with the human *MDR1* gene. The current, which was not present in parental cells, was outwardly rectifying and Cl^- selective. It was inhibited by the Cl^- channel blocker 4,4′-diisothiocyanostilbene-2,2′-disulfonic acid (DIDS) (29), by quinine and verapamil, which inhibit MDR1-associated drug efflux, and by forskolin (FSK) and 1,9-dideoxyforskolin (DDFSK), which affect Cl^- (14, 23) and K^+ channels (9, 17). Perfusion of the cell with the MDR1 substrate vincristine before hypotonic stress prevented activation of the current (11). These findings led to the hypothesis that the MDR1 protein can "switch" among an inactive state, a drug-transporting state, and a Cl^- channel state (11).

The following experiments were designed to test the hypothesis that MDR1 drug-pumping and Cl^--conducting functions are mutually exclusive using intact cells. We measured the ability of *MDR1*-transfected cells to exclude an MDR1 substrate, the fluorescent dye rhodamine 123 (R123), from their cytoplasm while under hypotonic stress. Hypotonic stress causes cell swelling and, if the switch hypothesis is correct, should cause the MDR1 protein to manifest Cl^- channel properties, leading to a cessation of rhodamine efflux and accumulation of the dye inside the cell. Experiments were carried out in four parental cell lines and a stable *MDR1*-transfected derivative of each line: NIH/3T3 and NIH/3T3MDR murine fibroblasts, which are the same as those originally used by Gill et al. (11); FEM-X

and FEM-XvMDR human melanoma cells; and two murine lymphomas: L1210, L1210vMDR and L5178Y, L5178YvMDR. Each MDR1-expressing cell line had easily detectable amounts of the P-glycoprotein on their surface. It was found that, under hypotonic conditions and/or in the presence of Cl^- channel blockers, the four MDR cell lines extruded R123 relative to their parental counterparts, indicating intact transport functions.

MATERIALS AND METHODS

Construction and properties of MDR cell lines. The human *MDR1* cDNA was introduced into the human melanoma cell line FEM-X via transfection with a recombinant *MDR1* retrovirus (pHaMDR1/A) that mediates the integration of the *MDR1* cDNA into the human genome. All of the *MDR1* cDNAs used in this study carry a Gly-Val mutation at position 185. After transduction with the pHaMDR1/A retrovirus as previously described (31), independent drug-resistant FEM-X clones were selected at 4 ng/ml colchicine. One of these clones, FEM-X C14A, was independently subcloned, and cell populations were selected in the following increasing concentrations of colchicine over a 6-mo period: 8, 16, 32, 64, 128, 256, 450, 500, 550, 650, and 900 ng/ml. At various times during this stepwise drug selection, the colchicine-resistant population of cells was recloned. An independent clone selected at 900 ng/ml colchicine (designated FEM-XvMDR) was used for the studies reported here.

The same pHaMDR1/A retroviral vector carrying the human *MDR1* gene was used to transduce the parental L1210 cells. After 48 h, this medium was removed and replaced with RPMI 1640 medium plus 10% horse serum containing 60 ng/ml colchicine. Resistant cells, consisting of 1–10% of the original cell population, were maintained in colchicine thereafter. Killing curves were done to demonstrate the drug resistance of the infected cell populations compared with the parental cells. The *MDR1*-transduced L1210 population had a 50% lethal dose (LD_{50}) of 110 ng/ml colchicine compared with an LD_{50} of 22 ng/ml for the parental cells (5-fold relative resistance to colchicine).

The NIH/3T3 and NIH/3T3MDR cell lines were derived as previously described (5a) by viral transfection with the *MDR1* cDNA. These are the same cell lines used by Valverde et al. (29) in their initial description of the MDR1-associated Cl^- current and were used by Ehring et al. (7) in their studies of this question. The parental NIH/3T3 line has been shown not to express detectable levels of MDR1 by Western blot (28). L5178Y and L5178YvMDR cells were similarly derived as previously described (31).

Growth conditions and inhibitors. The murine lymphomas L5178Y and L5178YvMDR were grown in McCoy's 5A medium with 10% heat-inactivated horse serum as previously described (31), and L1210 and L1210vMDR were grown in RPMI 1640 with 10% heat-inactivated horse serum. FEM-X, FEM-XvMDR, NIH/3T3, and NIH/3T3MDR were grown in Dulbecco's modified Eagle's medium with 10% fetal calf serum.

The cell lines used for data collection were grown without cytotoxic drugs for 3–30 days, to match the substrate-free conditions of Gill et al. (11). No loss of MDR phenotype, as assayed by R123 exclusion, was observed in any cell line. Stock cultures of all MDR cell lines were maintained in 60 ng/ml colchicine, except for FEM-XvMDR, which was maintained in 500 ng/ml colchicine.

Solutions and reagents. NaCl Hanks' solution consisted of (in mM) 145 NaCl, 4.5 KCl, 1.6 $CaCl_2$, 1.3 $MgCl_2$, and 10 N-2-hydroxyethylpiperazine-N'-2-ethanesulfonic acid, pH

7.35. Osmolarity was 290 mosM measured on a Wescor vapor pressure osmometer. NaCl was substituted for KCl to make K^+-free Hanks' solution. All but 10 mM of NaCl was replaced by KCl to make high-K^+ Hanks' solution. Cl^- channel blockers used were DIDS, 4-acetamido-4'-isothiocyanostilbene-2,2'-disulfonic acid (SITS), FSK, DDFSK (23), flufenamic acid, and pentylenetetrazole (21).

MDR cells can be rendered sensitive to cytotoxic agents by various inhibitors of MDR1 protein function. Cyclosporin A (CsA) was used to inhibit MDR1 in all cell lines except NIH/3T3 in which flunarizine was a more effective blocker. All reagents except CsA, which was a Food and Drug Administration reagent standard, were purchased from Sigma Chemical, St. Louis, MO. Fluorescein isothiocyanate (FITC)-labeled MRK-16 antibody (MRK-16-FITC) was produced by labeling the antibody with FITC using a standard protocol. The fluorescein-to-protein ratio of the batch used for these studies was five.

R123 uptake assay. Function of the MDR1 protein was assayed, using a variation of the previously described R123 assay (31). Briefly, cells were removed from culture, washed, and equilibrated in the indicated buffer for 10 min at room temperature. Cells were exposed to solutions in the following sequence: *1*) plus or minus Cl^- channel blockers, 10 min (30 min for DIDS); *2*) plus or minus hypotonic stress by dilution with 50% water for 0, 1, 5, 10, or 15 min; *3*) plus or minus MDR1 inhibitors, 10 min; and *4*) 5.2 µM R123, 20 min at 37°C. Cells were then washed, and the R123 fluorescence of 10,000 cells was measured by flow cytometry. In parental cells, R123 fluorescence levels were stable for at least 1 h (data not shown). In the absence of inhibitors, MDR cells did not accumulate measurable levels of R123 under these conditions. Confocal microscopic observations confirmed no intracellular R123 accumulation in MDR cells when examined within 2 min after rhodamine removal.

Quantitation of MDR1 expression. The measurement of the number of MDR1 molecules expressed on the cell surface of the various cell lines was done using Quantum Simply Cellular Microbeads (Flow Cytometry Standards, Research Triangle Park, NC). These beads have defined numbers of antibody binding sites per bead (0, 5,011, 12,648, 42,414, and 100,785 for the lot used for these experiments) and can be used to generate standard curves of observed fluorescence intensity vs. antibody number. Cells were suspended at 5×10^5 or $1 \times 10^6/0.1$ ml in phosphate-buffered saline (PBS). MRK-16-FITC (3 µg) and 100 µl of bead suspension were combined with the cell suspension in the same tube. After incubating for 30 min at 4°C, cells and beads were washed, resuspended in PBS, and analyzed by flow cytometry. Fluorescence data were simultaneously but independently collected for cells and beads, utilizing differences in light scatter between cells and beads to gate the fluorescence signals. The fluorescence data were analyzed using the program Quickcal supplied by the manufacturer. This program calculates linear regression for the bead data (number of antibody binding sites per bead vs. observed fluorescence) and from this calculates the number of antibody molecules bound to the cells. Data were expressed as the calculated numbers of binding sites minus the calculated numbers of binding sites on unstained cells, which represents normal cellular autofluorescence.

RESULTS

Cell surface expression of MDR1. The number of human MDR1 molecules on the cell surface of each cell line, as indicated by binding of the anti-MDR1 antibody

MRK-16-FITC, is shown in Table 1. The epitope of MDR1 recognized by the anti-MDR1 antibody MRK-16 has recently been described (10) and is consistent with only one extracellular binding site per MDR1 molecule. As expected, all transfected cell lines showed dramatically increased numbers of MRK-16 binding sites compared with nontransfected parental cell lines. The observed fluorescence values for parental cells were very close to the autofluorescence values, and the net values could easily reflect nonspecific binding of the antibody.

Effect of hypotonic stress on R123 exclusion. One measure of the activity of the MDR1 protein is the extent to which cells expressing MDR1 exclude the membrane-permeant fluorescent dye R123 from their interior (16). If activation of the MDR1-associated Cl^- conductance by hypotonic stress precludes substrate transport, then R123 exclusion should be inhibited. Control experiments in the absence of any drugs and under isotonic conditions (Fig. 1, left pair of bars/cell type) show that nontransfected cells were highly fluorescent (solid bars) and that *MDR1*-transfected cells (open bars) accumulated essentially no R123. When cells were exposed to hypotonic stress (50% dilution with water), the ability of *MDR1*-transfected cells to exclude R123 was not affected (Fig. 1, right pair of bars/cell type). Likewise, hypotonic stress did not change the fluorescence of parental cells (Fig. 1). Because the time course of activation of the volume-activated MDR1-associated Cl^- conductance was not precisely known, the time of water addition was varied from a maximum of 20 min before to simultaneously with addition of R123. Figure 2 shows that, when R123 was added 1 min after hypotonic stress when cell swelling is maximal (see Fig. 6 of Ref. 29a for data), MDR1 transport was normal in all four cell types tested. R123 exclusion was unaffected by hypotonic stress between 0 and 20 min before addition of R123 (data not shown). In addition, when L1210 and L1210vMDR cells were incubated in 140 mM K^+ Hanks' buffer and subjected to hypotonic stress, which resulted in an irreversibly swollen cell (see Fig. 7 of Ref. 29a), R123 exclusion was not altered, although accumulation in parental cells was reduced. The R123 fluorescence values in high-K^+ buffer for parental L1210s were 3.84 (isotonic) and 6.21 (hypotonic) and for MDR were 0.179 (isotonic) and 0.175
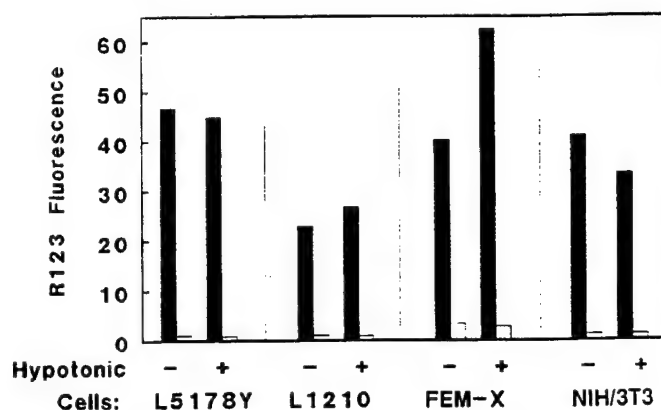

Fig. 1. Effect of hypotonic stress on rhodamine 123 (R123) exclusion in parental (solid bars) and multidrug resistance (MDR; open bars) cell lines. Hypotonic stress was induced by 50% dilution with H_2O. Fluorescence of R123 was in arbitrary units as measured by flow cytometry. Order of treatments: equilibration in phenol red-free RPMI 1640 at 0 min, $\pm H_2O$ at 10 min, +R123 (5.2 µM) at 20 min, wash and analyze by flow cytometry at 40 min.

(hypotonic). Thus, under conditions where a volume-activated Cl^- conductance should be induced, apparent R123 efflux was not affected.

The effects of several MDR1 inhibitors and Cl^- channel blockers on R123 exclusion, alone and in combination, were then tested under normal and hypotonic conditions. The data in Fig. 3 show that, under isotonic conditions (left pairs of bars/cell type), incubation with known MDR1 inhibitors CsA (L5178Y, L1210, FEM-X) or flunarizine (NIH/3T3) reduced the apparent efflux of R123 and resulted in increased fluorescence levels in the MDR cells. As expected, fluorescence levels were comparatively unchanged by MDR1 inhibitors in parental cells. Hypotonic stress did not alter the effect of MDR1 inhibitors on the fluorescence levels of either MDR or parental cells, indicating that, under hypotonic conditions, the sensitivity of MDR1 to its inhibitors was unaffected (Fig. 3, right pairs of bars/cell type).

Likewise, several different Cl^- channel blockers (DIDS, SITS, and flufenamic acid) had no effect on

Table 1. *Expression of cell surface MDR1 molecules*

Cell Type	Calculated Net Number of MRK-16 Binding Sites Per Cell
L5178Y	483
L5178YvMDR	16,815
L1210	218
L1210vMDR	8,382
FEM-X	1,120
FEM-XvMDR	8,055
NIH/3T3	359
NIH/3T3MDR	55,040

Expression was determined by calibration with microbeads with defined numbers of antibody binding sites and represent calculated value minus autofluorescence of unstained cells. MDR, multidrug resistance.
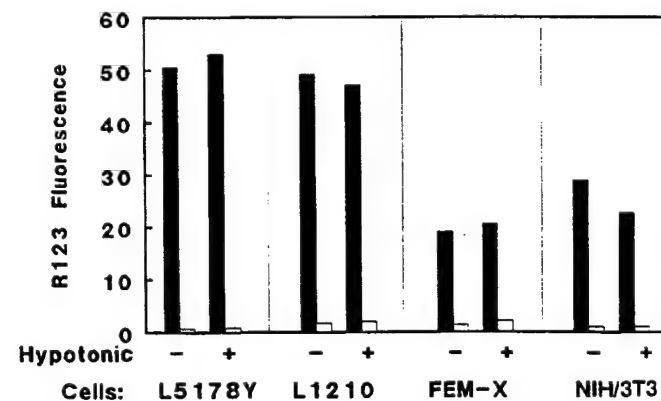

Fig. 2. Effect of hypotonic stress at −1 min on MDR1 function in parental (solid bars) and MDR (open bars) cells. Hypotonic stress was induced by 50% dilution with H_2O. Fluorescence of R123 was in arbitrary units as measured by flow cytometry. Order of treatments: equilibration in Na^+ Hanks'-glucose at 0 min, $\pm H_2O$ at 10 min, +R123 (5.2 µM) at 11 min, wash and analyze by flow cytometry at 31 min.
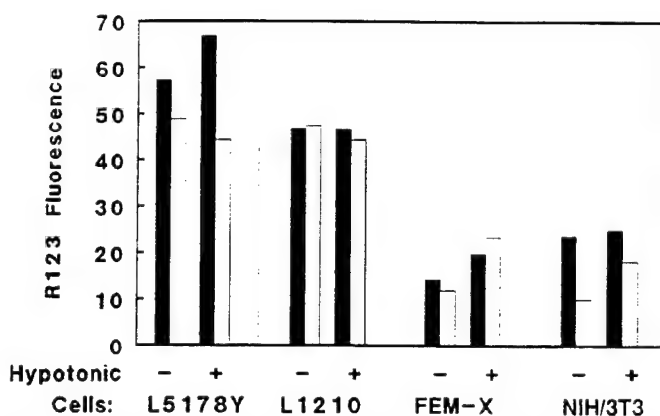
Fig. 3. Effect of MDR inhibitors and hypotonic stress on R123 exclusion in parental (solid bars) and MDR (open bars) cell lines. Hypotonic stress was induced by 50% dilution with H_2O. Fluorescence of R123 was in arbitrary units as measured by flow cytometry. Order of treatments: equilibration in phenol red-free RPMI 1640 at 0 min, $\pm H_2O$ at 10 min, $\pm$cyclosporin A (CsA; 0.8 µM, L5178Y, L1210, FEM-X) or flunarizine (5 µM, NIH/3T3) at 15 min, +R123 (5.2 µM) at 25 min, wash and analyze by flow cytometry at 45 min.

R123 exclusion, with or without hypotonic stress. Figure 4 shows that 100 µM DIDS, which completely inhibits the MDR1-associated Cl^- current in NIH/3T3 cells (29), was unable to affect R123 exclusion in L5178YvMDR under control or hypotonic conditions. DDFSK and FSK, which also block the Cl^- current, did not have consistent effects on R123 efflux. Under isotonic conditions in L1210 cells, DDFSK but not FSK was able to block R123 efflux from MDR cells (data not shown). In L1210 cells, 1 mM SITS, which completely blocks regulatory volume decrease (RVD; see Fig. 4 of Ref. 29a) and should enhance the probability of activating the hypotonic stress-induced Cl^- conductance, had no effect on MDR1-mediated R123 transport under iso- or hypotonic conditions but caused reduced accumula-

tion in parental cells under both conditions. Similar data for FEM-X cells (700 µM SITS) and NIH/3T3 cells (100 µM flufenamic acid) are shown in Fig. 4.

Significantly, after exposure to Cl^- channel blockers as used in Fig. 4, R123 exclusion by MDR cells could still be inhibited by CsA (Fig. 5; L5178Y, L1210, FEM-X) or flunarizine (NIH/3T3). This finding held under both control and hypotonic conditions, further suggesting that hypotonicity alone is not sufficient to inhibit MDR1 function in intact cells.

DISCUSSION

The experiments described here were designed to test the hypothesis that MDR1 substrate pumping and MDR-associated Cl^- channel activity are mutually exclusive. If the MDR1 protein is a volume-activated Cl^- channel, then the hypothesis predicts that, under conditions of hyposmotic stress, MDR1-mediated substrate efflux should not occur (11). With the use of cytoplasmic exclusion of the fluorescent dye R123 as a measure of MDR1 activity, we first demonstrated that *MDR1*-transfected cells showed essentially no accumulated fluorescence compared with parental nontransfected cells (Fig. 1). Under hypotonic conditions that should have led to activation of the MDR-associated Cl^- conductance, R123 efflux was not inhibited, indicating that MDR1 function was intact. This finding was consistent across four cell types, in which expression of cell surface MDR1 protein in transfected lines ranged from ~8,000 to 55,000 per cell. Cell lines from various tissues were used to maximize the probability that an observed effect would be due to the biology of MDR1 and not to a peculiarity of one cell line.

The conditions of the R123 exclusion experiments were designed to mimic those under which the volume-activated MDR-associated Cl^- conductance was origi-
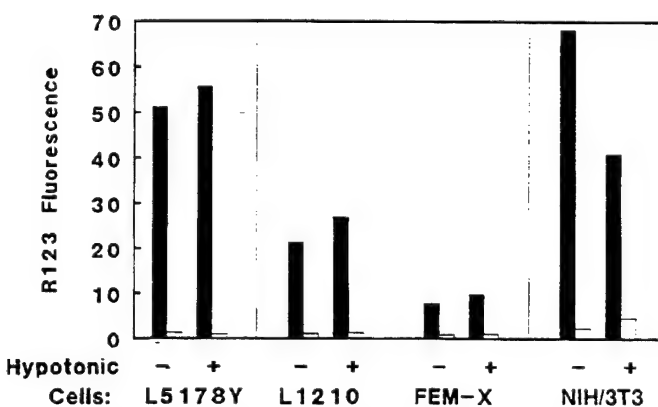

Fig. 4. Effect of Cl^- channel blockers and hypotonic stress on R123 exclusion in parental (solid bars) and MDR (open bars) cell lines. Hypotonic stress was induced by 50% dilution with H_2O. Fluorescence of R123 was in arbitrary units as measured by flow cytometry. Order of treatments: equilibration in phenol red-free RPMI 1640 at 0 min, $\pm Cl^-$ blocker at 10 min, $\pm H_2O$ at 20 min, +R123 (5.2 µM) at 30 min, wash and analyze by flow cytometry at 50 min. SITS incubation was for 30 min, and all other times were adjusted accordingly. Cl^- channel blockers used were: L5178Y cells, DIDS at 150 µM; L1210 cells, SITS at 1 mM; FEM-X cells, SITS at 0.7 mM; NIH/3T3 cells, flufenamic acid at 100 µM.
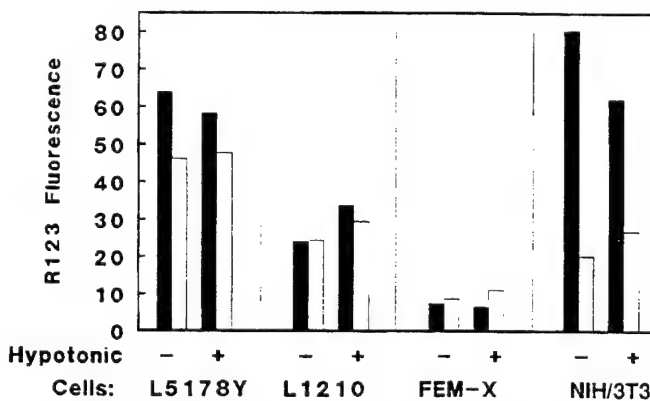

Fig. 5. Effect of MDR inhibitors, Cl^- channel blockers, and hypotonic stress on R123 exclusion in parental (solid bars) and MDR (open bars) cell lines. Hypotonic stress was induced by 50% dilution with H_2O. Fluorescence of R123 was in arbitrary units as measured by flow cytometry. Order of treatments: equilibration in phenol red-free RPMI 1640 at 0 min, $\pm Cl^-$ blocker at 10 min, $\pm H_2O$ at 20 min, $\pm$CsA (0.8 µM, L5178Y, L1210, FEM-X) or flunarizine (5 µM, NIH/3T3) at 25 min, +R123 (5.2 µM) at 35 min, wash and analyze by flow cytometry at 55 min. SITS incubation was for 30 min, and all other times were adjusted accordingly. Cl^- channel blockers used were: L5178Y cells, DIDS at 150 µM; L1210 cells, SITS at 1 mM; FEM-X cells, SITS at 0.7 mM; NIH/3T3 cells, flufenamic acid at 100 µM.

nally observed (11, 29). First, cells were exposed to hypotonic stress before the addition of R123, so that transition of the MDR1 protein into a Cl$^-$-conducting state would not be precluded by the presence of substrate. Second, the time at which R123 was added after hypotonic stress was varied to ensure that the MDR-associated Cl$^-$ current could be activated before the addition of substrate. Patch-clamp and Cl$^-$ efflux studies, including some carried out specifically on NIH/3T3 and NIH/3T3MDR cells, have shown that volume-activated Cl$^-$ currents are usually induced in <1 min (6, 23, 27, 29, 32) and persist while hypotonic stress is maintained (29, 29a). Even if there was only transient "switching" into Cl$^-$ channel mode, this brief interruption in MDR-mediated R123 efflux should have been observed. This is because R123 influx is extremely rapid [half time $\leq$ 2 min (3)] and R123 is rapidly sequestered into the mitochondria. Finally, as an additional means of maximizing the probability that MDR1 would be switched into Cl$^-$-conducting mode, MDR cells were exposed to hypotonic stress in high-K$^-$ buffer, which causes them to swell irreversibly (see Fig. 3 in Ref. 29a) and then were exposed to R123. Cells treated in this way also showed no R123 accumulation, which indicates normal MDR1 function.

A second line of evidence dissociating putative MDR-associated Cl$^-$ channel activity from MDR1 efflux in hypotonically stressed cells was also obtained. Swollen cells remained sensitive to the MDR1 blockers CsA or flunarizine, a second indication of normal MDR1 function (Fig. 3). With one exception (DDFSK), application of Cl$^-$ channel blockers known to inhibit volume-induced Cl$^-$ current (DIDS; Refs. 7, 29) or RVD (SITS; see Fig. 4 in Ref. 29a) in some or all of these cell lines had no effect on R123 accumulation in parental or *MDR1*-transfected cells (Fig. 4). Several Cl$^-$ channel blockers, including DIDS and SITS, have previously been shown to have no effect on R123 transport in either of the L5178Y cell lines (31). Although inhibition of R123 efflux was observed in the presence of DDFSK, this finding was not consistent with those obtained with the other Cl$^-$ channel blockers and might have been secondary to its effects on K$^+$ channels (9, 17). This inhibition of R123 efflux by DDFSK has also been observed in MDR-expressing HT-29 cells (18). Finally, the ability of MDR1 inhibitors to affect MDR1 function was intact in cells that were pretreated with Cl$^-$ channel blockers with or without hypotonic stress (Fig. 5). Taken together, these experiments show that MDR1 function is normal under conditions where Cl$^-$ channel activity is either maximally inhibited or maximally activated, further emphasizing the dissociation between Cl$^-$ channel activity and MDR1 transport activity.

Our findings extend the results of several other groups who have used a somewhat different method to test whether MDR-mediated R123 transport and Cl$^-$ channel function are mutually exclusive. Two groups, one (7) using the same NIH/3T3 and NIH/3T3MDR cells used here and by Valverde et al. (29) and one using Chinese hamster ovary and human breast cancer cell lines (2), measured rates of R123 efflux before,

during, and after hypotonic stress. In cells preloaded with R123, cell swelling did not alter the rates of R123 efflux nor did it prevent inhibition of MDR1 function by verapamil. Furthermore, R123 efflux was not inhibited by Cl$^-$ channel blockers (2, 7) or by the removal of Cl$^-$ (2), in agreement with our previous results (31). However, because cells were preloaded with R123, it was possible that the presence of an MDR1 substrate might have prevented the protein from switching into a Cl$^-$-conducting state.

In summary, our data suggest that MDR1-associated Cl$^-$ channel activity and MDR1-mediated efflux of R123 are independent processes and that, if the MDR1 protein is able to perform both functions, they can be independently induced and regulated and are not mutually exclusive. The accompanying study (29a) more fully examines whether expression of the MDR1 protein confers a new Cl$^-$-conducting pathway on cells.

REFERENCES

1. **Altenberg, G. A., J. W. Deitmer, D. C. Glass, and L. Reuss.** P-glycoprotein-associated Cl$^-$ currents are activated by cell swelling but do not contribute to cell volume regulation. *Cancer Res.* 54: 618–622, 1994.

2. **Altenberg, G. A., C. G. Vanoye, E. S. Han, J. W. Deitmer, and L. Reuss.** Relationship between rhodamine 123 transport, cell volume, and ion-channel function of P-glycoprotein. *J. Biol. Chem.* 269: 7145–7149, 1994.

3. **Altenberg, G. A., C. G. Vanoye, J. K. Horton, and L. Reuss.** Unidirectional fluxes of rhodamine 123 in multidrug-resistant cells: evidence against direct drug extrusion from the plasma membrane. *Proc. Natl. Acad. Sci. USA* 91: 4654–4657, 1994.

4. **Ambudkar, S., I. H. Lelong, J. Zhang, C. O. Cardarelli, M. M. Gottesmann, and I. Pastan.** Partial purification and reconstitution of the human multidrug resistance pump: characterization of the drug-stimulatable ATP hydrolysis. *Proc. Natl. Acad. Sci. USA* 267: 21020–21026, 1992.

5. **Beck, W. T., and X.-D. Quian.** Photoaffinity substrates for p-glycoprotein. *Biochem. Pharmacol.* 43: 89–93, 1992.

5a. **Currier, S. J., S. E. Kane, M. C. Willingham, C. O. Cardarelli, I. Pastan, and M. M. Gottesman.** Identification of residues in the first cytoplasmic loop of P-glycoprotein involved in the function of chimeric human MDR1-MDR2 transporters. *J. Biol. Chem.* 267: 25153–25159, 1992.

6. **Doroshenko, P., and E. Neher.** Volume-sensitive chloride conductance in bovine chromaffin cell membrane. *J. Physiol. Lond.* 449: 197–218, 1992.

7. **Ehring, G. R., Y. V. Osipchuk, and M. D. Cahalan.** Swelling-activated chloride channels in multidrug-sensitive and -resistant cells. *J. Gen. Physiol.* 104: 1129–1161, 1994.

8. **Foxwell, B. M., A. Mackie, V. Ling, and B. Ryffel.** Identification of the multidrug resistance-related P-glycoprotein as a cyclosporin binding protein. *Mol. Pharmacol.* 36: 543–546, 1989.

9. **Garber, S. S., T. Hoshi, and R. W. Aldrich.** Interaction of forskolin with voltage-gated K$^+$ channels in PC12 cells. *J. Neurosci.* 10: 3361–3368, 1990.

10. **Georges, E., T. Tsuruo, and V. Ling.** Topology of P-glycoprotein as determined by epitope mapping of MRK-16 monoclonal antibody. *J. Biol. Chem.* 268: 1792–1798, 1993.

11. **Gill, D. R., S. C. Hyde, C. F. Higgins, M. A. Valverde, G. M. Mintenig, and F. V. Sepulveda.** Separation of drug transport and chloride channel functions of the human multidrug resistance p-glycoprotein. *Cell* 71: 23–32, 1992.

12. **Goldstein, L. J., I. Pastan, and M. M. Gottesman.** Multidrug resistance in human cancer. *Crit. Rev. Oncol. Hematol.* 12: 243–253, 1992.

13. **Gottesman, M. M., and I. Pastan.** Biochemistry of multidrug resistance mediated by the multidrug transporter. *Annu. Rev. Biochem.* 62: 385–427, 1993.

13a. **Hardy, S. P., H. R. Goodfellow, M. A. Valverde, D. R. Gill, F. V. Sepulveda, and C. F. Higgins.** Protein kinase C-mediated phosphorylation of the human multidrug resistance P-glycoprotein regulates cell volume-activated chloride channels. *EMBO J.* 14: 68–75, 1995.

14. **Heuschneider, G., and R. D. Schwartz.** cAMP and forskolin decrease gamma-aminobutyric acid-gated chloride efflux in rat brain synaptoneurosomes. *Proc. Natl. Acad. Sci. USA* 86: 2938–2942, 1989.

15. **Horio, M., M. Gottesman, and I. Pastan.** ATP-dependent transport of vinblastine in vesicles from human multidrug-resistant cells. *Proc. Natl. Acad. Sci. USA* 85: 3580–3584, 1988.

16. **Kessel, D.** Exploring multidrug resistance using rhodamine 123. *Cancer Commun.* 1: 145–149, 1989.

17. **Krause, D., S. C. Lee, and C. Deutsch.** Forskolin effects on the voltage-gated K conductances of human T cells. *Pfluegers Arch.* 412: 133–140, 1988.

18. **Kunzelmann, K., I. N. Slotki, P. Klein, T. Koslowsky, D. A. Ausiello, R. Greger, and Z. I. Cabantchik.** Effects of P-glycoprotein expression on cyclic AMP and volume-activated ion fluxes and conductances in HT-29 colon adenocarcinoma cells. *J. Cell. Physiol.* 161: 393–406, 1994.

19. **Morris, D. I., L. A. Speicher, A. E. Ruoho, K. D. Tew, and K. B. Seamon.** Interaction of forskolin with the P-glycoprotein multidrug transporter. *Biochemistry* 30: 8371–8379, 1991.

20. **Pastan, I., M. M. Gottesman, K. Ueda, E. Lovelace, A. V. Rutherford, and M. C. Willingham.** A retrovirus carrying an MDR1 cDNA confers multidrug resistance and polarized expression of P-glycoprotein in MDCK cells. *Proc. Natl. Acad. Sci. USA* 85: 4486–4490, 1988.

21. **Pellmar, T. C., and W. A. Wilson.** Synaptic mechanism of pentylenetetrazole: selectivity for chloride conductance. *Science Wash. DC* 197: 912–913, 1977.

22. **Riordan, J. R., J. M. Rommens, B. Kerem, N. Alon, R. Rozmahel, Z. Grzelczak, J. Zielenski, S. Lok, N. Plavsci, J.-L. Chou, M. L. Drumm, M. C. Iannuzzi, F. S. Collins, and L.-C. Tsui.** Identification of the cystic fibrosis gene: cloning and characterization of complementary DNA. *Science Wash. DC* 245: 1066–1073, 1989.

23. **Rugolo, M., T. Mastrocola, M. De Luca, G. Romeo, and L. J. Galietta.** A volume-sensitive chloride conductance revealed in cultured human keratinocytes by $^{36}Cl^-$ efflux and whole-cell patch clamp recordings. *Biochim. Biophys. Acta* 1112: 39–44, 1992.

24. **Safa, A. R.** Photoaffinity labeling of the multidrug-resistance-related P-glycoprotein with photoactive analogs of verapamil. *Proc. Natl. Acad. Sci. USA* 85: 7187–7191, 1988.

25. **Sarkardi, B., E. M. Price, R. C. Boucher, U. A. Germann, and G. A. Scarborough.** Expression of the human multidrug resistance cDNA in insect cells generates a high activity drug-stimulated membrane ATPase. *J. Biol. Chem.* 267: 4854–4858, 1992.

26. **Simon, S., and M. Schindler.** Cell biological mechanisms of multidrug resistance. *Proc. Natl. Acad. Sci. USA* 91: 3497–3504, 1994.

27. **Stoddard, J. S., J. H. Steinbach, and L. Simchowitz.** Whole cell Cl^- currents in human neutrophils induced by cell swelling. *Am. J. Physiol.* 265 (*Cell Physiol.* 34): C156–C165, 1993.

28. **Tanaka, S., S. J. Currier, E. P. Bruggermann, K. Ueda, U. A. Germann, I. Pastan, and M. M. Gottesman.** Use of recombinant P-glycoprotein fragments to produce antibodies to the multidrug transporter. *Biochem. Biophys. Res. Commun.* 166: 180–186, 1990.

29. **Valverde, M. A., M. Diaz, F. V. Sepulveda, D. R. Gill, S. C. Hyde, and C. F. Higgins.** Volume regulated chloride channels associated with human multidrug-resistance P-glycoprotein. *Nature Lond.* 355: 830–833, 1992.

29a. **Weaver, J. L., A. Aszalos, and L. McKinney.** MDR1/P-glycoprotein function. II. Effect of hypotonicity and inhibitors on Cl^- efflux and volume regulation. *Am. J. Physiol.* 270 (*Cell Physiol.* 39): C1453–C1460, 1996.

30. **Weaver, J. L., L. McKinney, P. V. Schoenlein, S. Goldenberg, M. M. Gottesman, and A. Aszalos.** Volume regulation and MDR1 protein function in MDR1-transfected and parental cell lines (Abstract). *Biophys. J.* 66: A217, 1994.

31. **Weaver, J. L., G. Szabo, Jr., P. S. Pine, M. Gottesman, S. Goldenberg, and A. Aszalos.** The effect of ion channel blockers, immunosuppressive agents and other drugs on the activity of the multi-drug transporter. *Int. J. Cancer* 54: 456–461, 1993.

32. **Worrell, R. T., A. G. Butt, W. H. Cliff, and R. A. Frizzell.** A volume-sensitive chloride conductance in human colonic cell line T84. *Am. J. Physiol.* 256 (*Cell Physiol.* 25): C1111–C1119, 1989.

MDR1/P-glycoprotein function. II. Effect of hypotonicity and inhibitors on Cl⁻ efflux and volume regulation

JAMES L. WEAVER, ADORJAN ASZALOS, AND LESLIE McKINNEY

*Molecular Pharmacology, Division of Research and Testing, Center for Drug Evaluation
and Research, Food and Drug Administration, Laurel 20708; and Department of
Physiology, Armed Forces Radiation Radiobiology Institute, Bethesda, Maryland 20889*

Weaver, James L., Adorjan Aszalos, and Leslie McKinney. MDR1/P-glycoprotein function. II. Effect of hypotonicity and inhibitors on Cl⁻ efflux and volume regulation. *Am. J. Physiol.* 270 *(Cell Physiol.* 39): C1453–C1460, 1996.— Resistance to anti-tumor drugs can be mediated by overexpression of the multidrug resistance 1 (MDR1) protein (P-glycoprotein). In three MDR1-transfected cell lines (Gill et al. *Cell* 71: 23–32, 1992; Altenberg et al. *Cancer Res.* 54: 618–622, 1994), a hypotonic stress-induced Cl⁻ current has been demonstrated that can be inhibited by MDR1 substrates and Cl⁻ channel blockers. We tested the hypothesis that MDR1 expression confers additional Cl⁻ conductance by measuring regulatory volume decrease (RVD) in four pairs of isogenic cell lines and ³⁶Cl efflux in two cell lines with and without hypotonic stress. The kinetics of RVD and response to Cl⁻ channel blockers were indistinguishable in MDR and parental cells. Additionally, no significant difference was seen between ³⁶Cl efflux rate constants under hypotonic conditions between NIH/3T3 and L1210 parental and MDR cells. We conclude that, in intact cells, the expression of MDR1 does not alter the rate of volume regulation or the rate of ³⁶Cl efflux under hypotonic conditions between parental and MDR cells.

multidrug resistance; P-glycoprotein; chloride channel; chloride efflux; cyclosporin; 4-acetamido-4′-isothiocyanostilbene-2,2′-disulfonic acid; 4,4′-diisothiocyanostilbene-2,2′-disulfonic acid; forskolin; 1,9-dideoxyforskolin

CELLS THAT EXPRESS in their membranes the protein called, variously, multidrug resistance 1 (MDR1), P-glycoprotein, or p170 are able to actively extrude cytotoxic drugs and other compounds from their cytoplasm and are said to be multidrug resistant. The MDR1 protein is a member of the ATP-binding cassette family of transport proteins that includes the cystic fibrosis transmembrane conductance regulator (CFTR), which is a Cl⁻ channel (20). The MDR1 protein functions as an ATP-dependent pump (12) and can extrude drugs against a concentration gradient (21).

Several recent studies have indicated that this protein may also function as or regulate a Cl⁻ conductance. Patch-clamp studies carried out by two different groups have characterized a swelling-activated outwardly rectifying Cl⁻ conductance, present in MDR1-transfected NIH/3T3 fibroblasts (7, 23) and BC 19/3 breast cancer cells (1), which was not present in the corresponding parental cell lines. In contrast, studies comparing NIH/3T3 and a colchicine-selected MDR1-expressing derivative (COL1000; Ref. 16) showed that both parental and MDR1-expressing cells have swelling-induced Cl⁻ currents. However, the MDR cells exhibited a greater sensitivity to osmotic stress and showed increased anion efflux for a given degree of hypotonicity in the external solution than their parental counterparts. Also, in contrast to the original observations, Ehring et al. (5) carried out patch-clamp experiments on the same transfected NIH/3T3 cell lines used above and observed similar large swelling-induced Cl⁻ conductances in both parental and transfected lines. Kunzelmann et al. (14) measured ³⁶Cl⁻ efflux in HT-29 cells and found no difference in the rates of Cl⁻ efflux between MDR1-expressing and MDR1-negative cell lines under isotonic or hypotonic conditions. Finally, Rasola et al. (19) measured Cl⁻ currents in four MDR1-expressing cell lines and found no association between the amount of MDR1 protein present and the size of the Cl⁻ currents.

Given these conflicting reports, we carried out two functional assays of Cl⁻ conductance using intact cells to determine whether differences between *MDR1*-transfected vs. nontransfected lines could be observed. First, the ability of MDR1-expressing vs. parental cells to carry out a regulatory volume decrease (RVD) after osmotic stress was measured. Hypotonic swelling activates various forms of ion transport, leading to net loss of ions with concomitant loss of water and a return to normal cell size (hence the term RVD). If it is assumed, by analogy to a number of other cell types (see Refs. 4 and 9 for reviews), that a volume-activated Cl⁻ current is necessary for RVD, and then MDR1-expressing cells might show an increased rate of RVD compared with parental cells if they also express additional Cl⁻ conductance. Experiments were carried out in various combinations of four parental cell lines and a stable *MDR1*-transfected derivative of each line: NIH/3T3 and NIH/3T3MDR murine fibroblasts, FEM-X and FEM-XvMDR human melanoma cells, and two murine lymphomas. L1210, L1210vMDR and L5178Y, L5178YvMDR.

Second, the release of ³⁶Cl⁻ from two pairs of cell lines under isotonic and hypotonic conditions was compared to determine whether *MDR1*-transfected cells would show increased rates of Cl⁻ efflux after cell swelling.

No difference in the regulatory volume response between the parental and MDR cell lines was found. Consistent with these results, no significant differences in the rate constants for swelling-induced Cl⁻ efflux between the *MDR1*-transfected and parental lines of two cell types, NIH/3T3 and L1210, were found. A small but significant difference in the rate constant for Cl⁻ efflux was noted under isotonic conditions for NIH/3T3 but not L1210 cells.

MATERIALS AND METHODS

Growth conditions, inhibitors, and reagents. The cell lines, drugs, and solutions used for these experiments are described in the accompanying study (23a).

Cl⁻ efflux measurements. Cl⁻ efflux was measured using Na^{36}Cl (Amersham, Arlington Heights, IL). NIH/3T3 parental or MDR cells were plated in 24-well plates at 4×10^5/well and allowed to settle overnight. Two wells of either parental or MDR cells were labeled by incubation in Dulbecco's modified Eagle's medium (DMEM) with 20 µCi/ml ^{36}Cl⁻ for 90 min at 37°C. Cells were washed three times with Na⁻ Hanks'-glucose solution plus or minus drugs. Next, 0.5 ml of Na⁻ Hanks'-glucose solution was added to each well. Every 2 min, this buffer was removed to a scintillation vial and fresh buffer was added. After 16 min, one well was switched to hypotonic buffer [50% Na⁺ Hanks'-glucose (drugs), 50% water]. At the 28-min time point, the cells were lysed with 0.5 ml of 5% Triton X-100 and the wells were scraped, and all cells and supernatant were removed to a scintillation vial. The counts per minute (cpm) of ^{36}Cl⁻ remaining in the cell layer at each time point were calculated, and the data were normalized and represented as the fraction of the total cpm remaining in the cells. For the 8- to 16-min (isotonic and hypotonic) and 18- to 30-min (hypotonic only) time points, the data were fitted to this single exponential equation using the program NFIT (University of Texas Medical Branch, Galveston, TX)

$$y = A + B \times \exp^{(-x/T)}$$

where A is background, B is starting value minus background, and T is the time constant. Efflux rate constants were calculated as $1/T$, and means $\pm$ SE were obtained for each experiment. Statistical significance was calculated using Student's t-test. All calculations were performed using Quattro Pro for Windows version 5.0 (Borland, Scotts Valley, CA).

For the nonadherent L1210 and L1210vMDR cells, methods were adapted from Grinstein et al. (8). For each run, ~100 × 10⁶ cells were washed once and resuspended in DMEM with 45 µCi/ml Na^{36}Cl. After 60 min of incubation, the cells were quickly washed twice and resuspended in two tubes in DMEM to a concentration of 10×10^6/ml. Aliquots of 100 µl were taken at the start and at 1-min intervals for 10 min. Each aliquot was centrifuged through a mixture of 10 parts dibutyl phthalate and 3 parts corn oil. The supernatant was removed to one scintillation vial and the pellet resuspended in 0.5 ml of 5% Triton X-100 and transferred to a separate scintillation vial. After 4 min, an equal volume of water or DMEM was added to the hypotonic or isotonic tubes, respectively. Data from 10-min counts were expressed as the normalized fraction of cpm in the cell pellet. Data were fitted by a single exponential, using the 1- to 4-min or 1- to 10-min data points for isotonic and 5- to 10-min data points for hypotonic data. Rate constants were calculated as described above for the NIH/3T3 cells.

Measurement of membrane potential. Membrane potential was measured by flow cytometry using the positively charged cyanine dye DiOC(6)$_3$ (Molecular Probes, Eugene, OR) using the method of Wilson et al. (26).

Measurements of cell volume. Most cell volume measurements were obtained on a Coulter ZM cytometer connected to a Zenith 286 computer containing a PCA II interface board from The Nucleus, Oak Ridge, TN. Volume data were collected on ~1 × 10⁴ cells and mean volume calculated using commercial software written for the PCA II interface. Cells were suspended at ~2 × 10⁶/ml in Na⁺ Hanks' buffer with 5 mM glucose unless otherwise noted and were equilibrated for 10 min (L1210, L5178, FEM-X) or 30 min (NIH/3T3). The baseline was established by measuring the mean volume of

control cells in triplicate every 10 min. A test sample was diluted 50% with water and volume measurements taken at 1- to 3-min intervals. The results are expressed normalized to the initial control volume, which varied by <5% over 30 min.

In some experiments on the lymphoid cell lines, changes in cell volume were estimated by quantitating changes in forward angle light scatter (FS) over time. This is a variation on the system that McManus et al. (17) used to measure cell volume regulation. Changes in light scatter were measured by flow cytometry on an Epics Elite cell sorter (Coulter, Hialeah, FL) equipped with a Time Zero module (Cytek, Fremont, CA). Cells were resuspended in the indicated buffers at a concentration of ~2 × 10⁶/ml. Data were collected for 5 min to establish a baseline, then water was added to dilute the cell suspension by 50%. Data were collected for an additional 20 min and analyzed using Multitime software, version 2.5 (Phoenix Flow Systems, San Diego, CA). The data were automatically binned into 64 groups so that each data point represents the average for 23.4 s.

Figure 1 shows a comparison of the FS and Coulter cytometer data in L5178Y cells as they respond to hypotonic stress. Coulter volume measurements show that, as expected, the cells initially swell and then regulate back toward their original volume. Changes in the FS signal occur on a similar time scale but in the opposite direction. After addition of water, the FS signal, which usually increases with particle size, instead drops abruptly before returning toward baseline and seems to show that the cells are shrinking in response to hypotonic stress. A possible explanation for this apparently anomalous change in FS has to do with the surface morphology of lymphoid cells. Grinstein et al. (10) have observed by scanning electron microscopy that the surface of resting peripheral blood lymphocytes is covered with many fingerlike processes. After exposure to hypotonic stress the cell expands and the "fingers" are diminished in size relative to the expanded cell volume. As the cells return toward their original size during RVD, the villi return to their original size. This type of change in cell surface morphology after hypotonic stress has also been observed in Erlich ascites cells (11). The resting cell has a very rough surface that is effective at light scatter, and the swollen cell has a much smoother surface that is less likely to scatter light. Thus the forward light scatter signal was inversely correlated with changes in cell volume but only in L1210 and L5178 cells. In NIH/3T3 and FEM-X cells, the observed changes in FS were too small to be practically useful.
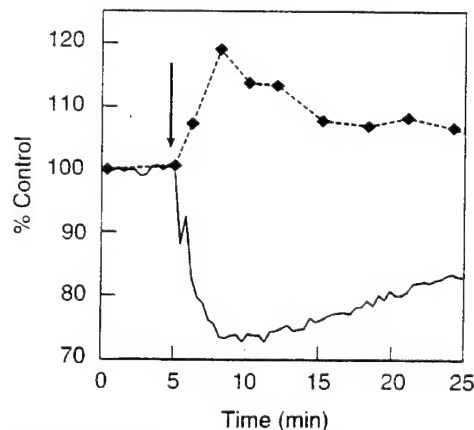

Fig. 1. Kinetics of forward scatter and Coulter volume changes in response to hypotonic stress in L5178Y cells. Solid line, forward angle light scatter (FS) signal; dashed line, Coulter volume response. Arrow, dilution with 50% H$_2$O.

RESULTS

RVD in MDR and parental cells. Cells that are exposed to hypotonic stress swell and then undergo an RVD to recover their original volume. In many cell types, RVD involves the activation of K^+ and Cl^- conductances, leading to net efflux of KCl and the passive loss of water (9). If the MDR1 protein functions as or regulates a volume-activated Cl^- channel, then RVD could be faster in MDR cells, assuming that the induced Cl^- conductance is a significant fraction of the total cellular Cl^- conductance and is rate limiting for volume regulation. Figure 2 shows the time course of the RVD in parental and MDR cells using four pairs of cell lines. Cells were equilibrated in NaCl Hanks' solution and then diluted to 50% with water. Coulter volume measurements showed that cells swelled to 120–130% of their initial volume within ~5 min and recovered within 20–30 min. In all four cell lines, there was no significant difference in the rate of RVD between parental and *MDR1*-transfected cells. Although the FS measurements are continuously acquired, we verified their accuracy for the initial stage of volume regulation by taking frequent Coulter volume measurements (10- to 12-s intervals for 5–7 min) on the L1210 cell lines. This experiment showed no difference in the rates of RVD ($n = 3$). The MDR cells showed slightly greater initial swelling, which is the opposite of what would be expected if the MDR cells had a significantly greater Cl^- conductance (data not shown).

Resting volumes for each cell line were very consistent on a given day (<5% variability) but showed greater variation across days. Values for NIH/3T3 and FEM-X cells ranged from ~1,600 to 2,800 fl and for L1210 and L5178Y ranged from 470 to 830 fl. No consistent differences in resting volume were noted between parental and MDR cells from any of these cell lines.

The rate of RVD is not increased by increasing cation conductance. Given the lack of difference in the rates of

RVD between parental and *MDR1*-transfected cells, several assumptions underlying the RVD experiments were more directly examined. Was it possible that Cl^- conductance was not rate limiting for RVD? To address this question, cells were exposed to the K^+ ionophore valinomycin to artificially increase K^+ permeability. The effectiveness of valinomycin in altering K^+ permeability was confirmed using the membrane potential-sensitive cyanine dye $DiOC(6)_3$ to show that 1 µM valinomycin caused hyperpolarization of L5178Y and L1210 cells in 4.5 mM K^+ Hanks' solution (data not shown). Even if K^+ is not the normal cation used in RVD, the increased permeability to K^+ should still increase the rate of RVD if cation conductivity is rate limiting. In parental L1210 and L5178Y cells, the rates of RVD in control and valinomycin-treated cells were found to be similar (Fig. 3A). Increasing valinomycin concentration to 20 µM caused no alteration in the rate of RVD (data not shown). Similar experiments were not carried out on MDR cells because valinomycin is a substrate for the MDR1 protein (15, 22, 25) and results would not be interpretable.

Because valinomycin had no effect on RVD, one experiment was carried out to determine whether RVD was discernibly sensitive to the gradient for K^+ and whether parental and MDR cells responded similarly to altered K^+ gradients. Cells were exposed to high-K^+ Hanks' solution and then subjected to hypotonic stress (Fig. 3B). Under these conditions, the driving force for K^+ is inward, and, if K^+ conductance is sufficiently large, then K^+ will go into the cell accompanied by anions and water and produce a second phase of swelling after the initial response to hypotonicity. The data show that cells placed in high-K^+ solution initially swelled to ~120% of resting volume after hypotonic stress. Three of the four parental cell lines then underwent a secondary swelling over the next 30 min (Fig. 3B) to a maximum of 150%. Secondary swelling was also observed in *MDR1*-transfected L1210 (Fig. 3C)
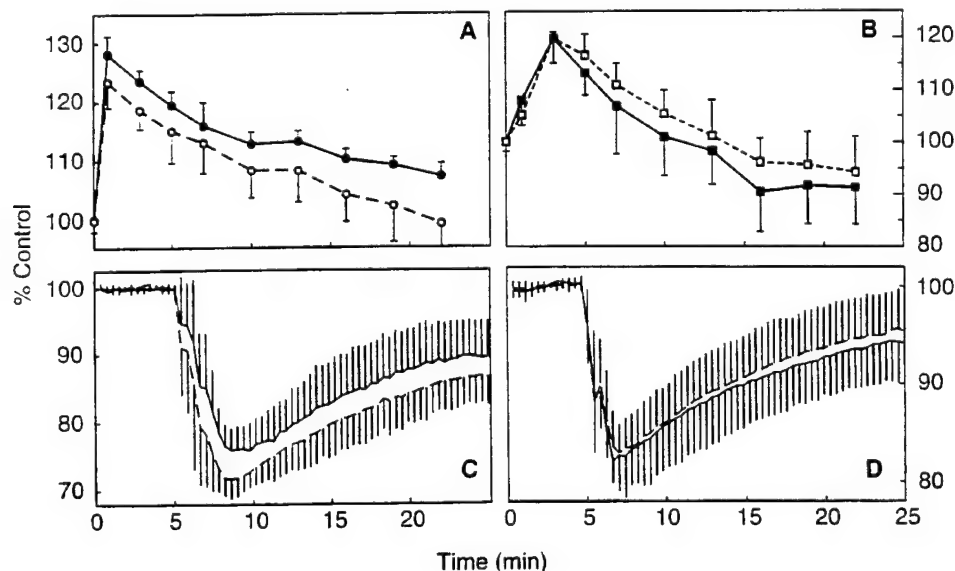

Fig. 2. Regulatory volume decrease (RVD) response in parental and multidrug resistant (MDR) cell lines. All values are means of 4–8 experiments; error bars represent SD. *A*: changes in Coulter volume with 50% H_2O at 0 min ($n = 4$). Solid line, NIH/3T3; dashed line, NIH/3T3MDR. *B*: changes in Coulter volume with 50% dilution with H_2O at 0 min ($n = 4$). Solid line, FEM-X; dashed line, FEM-XvMDR. *C*: changes in FS with 50% dilution with H_2O at 5 min ($n = 5$). Solid line, L5178Y; dashed line, L5178YvMDR. *D*: changes in FS with 50% dilution with H_2O at 5 min ($n = 8$). Solid line, L1210; dashed line, L1210vMDR.
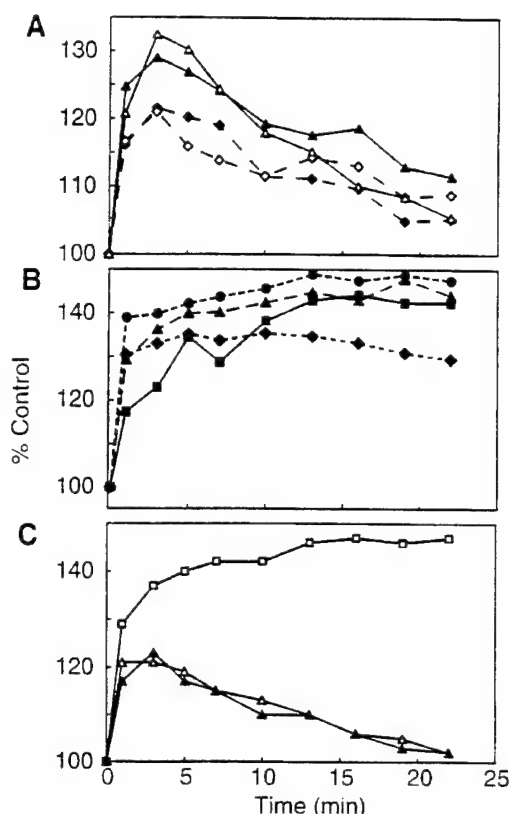
Fig. 3. Effect of various treatments affecting K⁺ flux on RVD measured by Coulter volume. A: RVD with valinomycin. Solid lines, L1210; dashed lines, L5178Y; ■ or ▲. no drug; □ or △, 1 μM valinomycin at −5 min. B: RVD in 140 mM K⁺ Hanks'-glucose solution. Solid line, FEMX; dashed line/triangles, L1210; dashed line/circles, NIH/3T3; dashed line/diamonds, L5178Y. C: RVD of L1210vMDR cells. ▲, Na⁺ Hanks'-glucose solution; △, 0 mM K⁺ in Na⁺ Hanks'-glucose solution; □, 140 mM K⁺ Hanks'-glucose solution.

and NIH/3T3 cells (maximum = 140%; data not shown). These data indicate that volume regulation can be altered by the direction of the driving force for K⁺ in both parental and MDR cells but do not prove that K⁺ is necessarily the primary cation involved in volume regulation.

Cl⁻ channel blockers and RVD. An alternative approach to testing whether an MDR1-associated Cl⁻

channel participates in RVD was to try to block RVD using compounds known to block the volume-activated Cl⁻ current in *MDR1*-transfected NIH/3T3 cells: 1,9-dideoxyforskolin (DDFSK; effective at 50 μM), forskolin (FSK; 50 μM), and 4,4'-diisothiocyanostilbene-2,2'-disulfonic acid (DIDS; 100 μM) (6, 23). In NIH/3T3 and FEM-X cells, 50 μM DDFSK produced some slowing of RVD, but the amount of inhibition was similar in parental and *MDR1*-transfected cells (data not shown). A complete block of RVD in both NIH/3T3 and NIH/3T3MDR cells resulted from treatment with 100 μM DDFSK (data not shown). In contrast, DDFSK had no effect on RVD in either parental or *MDR1*-transfected L1210 cells. No effect on RVD was seen in L1210 cells with FSK at a higher concentration of 150 μM. DIDS was tested in both L1210 and L5178Y cells, at 500 and 150 μM, respectively (Fig. 4, *A* and *C*). Although DIDS reduced the extent of initial swelling in each cell line, there was no differential effect on the MDR cells compared with parental cells. The rates of recovery were also not noticeably affected. In the L5178Y cell lines, DIDS was tested at concentrations between 50 and 700 μM, with no differential effect on RVD observed (data not shown).

As a positive control, we tested the effect of the Cl⁻ channel blocker 4-acetamido-4'-isothiocyanostilbene-2,2'-disulfonic acid (SITS) on RVD. Figure 4, *B* and *D*, shows that, in L1210 and L5178Y cells, 700 or 1,000 μM SITS inhibited RVD. In addition, Coulter volume data showed that 700 μM SITS blocked RVD in both NIH/3T3 cell lines (data not shown). Finally, the Cl⁻ channel blockers niflumic acid (90 μM, L1210) and pentylenetetrazole (2 mM, L1210) were tested for their effects on RVD and had no differential effect.

Cyclosporin A (CsA), at a concentration that completely inhibits rhodamine 123 (R123) exclusion (0.8 μM), was tested for its affect on RVD. In L5178Y or L5178YvMDR cells this MDR1 inhibitor had no effect on the kinetics of RVD (data not shown).

Cl⁻ efflux measurement in NIH/3T3 and NIH/3T3MDR cells. Given the lack of difference in RVD between parental and MDR cell lines, a series of Cl⁻ efflux experiments was carried out to directly measure
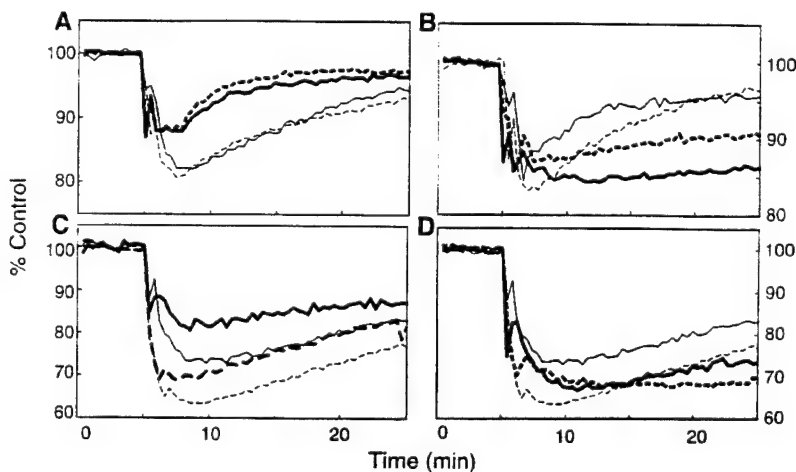
Fig. 4. Effect of SITS or DIDS on volume regulation by FS. A: DIDS and L1210 cells. Solid lines, L1210. Dashed lines, L1210vMDR. Light lines, no drug; heavy lines, 500 μM DIDS. Cells were exposed 30 min before data collection. B: SITS and L1210 cells. Same line scheme as A, except that cells were exposed to 700 μM SITS 10 min before data collection. C: DIDS and L5178Y cells. Solid lines, L5178Y; dashed lines, L5178YvMDR. Light lines, no drug. Heavy lines, 150 μM DIDS at 30 min before data collection. D: SITS and L5178Y cells. Same line scheme as C, except that cells were exposed to 1 mM SITS 10 min before data collection.

the changes in Cl^- permeability after hypotonic stress. The time course of efflux of $^{36}Cl^-$ from NIH/3T3 parental and NIH/3T3MDR cell lines under isotonic and hypotonic conditions was measured. Data from a representative experiment are shown in Fig. 5, expressed as the fraction of labeled Cl^- remaining in the cells with time. Under isotonic conditions, after an initial period of rapid $^{36}Cl^-$ efflux (0–6 min), the efflux rate became monoexponential. Dilution of the bathing medium by 50% (at ~17 min) led to an increase in the rate of $^{36}Cl^-$ efflux, as would be expected if cell swelling activated a Cl^- conductance.

Efflux rate constants, calculated as described in MATERIALS AND METHODS and averaged for five experiments, are shown in Fig. 6A for each cell line before and after the dilution of the medium. No significant difference in the efflux rate constant was observed between parental and MDR cell lines under hypotonic conditions. Under isotonic conditions, a small but statistically significant increase in the efflux rate constant was noted in MDR vs. parental cells. In one experiment, as a point of reference, fractional Cl^- efflux was converted to a true efflux rate by normalizing cpm values to specific activity, cell number, and cell volume (obtained from Coulter counter measurements). Values for parental NIH/3T3 cells ranged from 1.79 mmol·l cell

Fig. 6. Values of fitted efflux rates for NIH/3T3 (open bars) and NIH/3T3MDR (solid bars) $^{36}Cl^-$ efflux data. Because isotonic/hypotonic runs were paired, for each measurement of the hypotonic rate constant, two rate constants for isotonic conditions were obtained. A: no drug treatment; isotonic mean, $n = 10$; hypotonic mean, $n = 5$. B: 5 µM valinomycin; isotonic mean, $n = 8$; hypotonic mean, $n = 4$. C: 50 µM bumetanide; isotonic mean, $n = 8$; hypotonic mean, $n = 4$. Error bars indicate SE. *Significant differences (at $P < 0.05$) between parental and MDR; ☆ significant differences between drug treated (B or C) and no drug (A).

water^{-1}·min^{-1} under isotonic conditions to 3.33 mmol·l cell water^{-1}·min^{-1} under hypotonic conditions.

Because it was possible that, under hypotonic conditions, anion permeability was not rate limiting and an MDR-associated Cl^- conductance was masked, efflux experiments were repeated in the presence of 5 µM valinomycin. No significant difference in rate constants between parental and MDR cells under isotonic or hypotonic conditions was observed after valinomycin treatment ($n = 4$, Fig. 6B). Likewise, there was no significant difference between rate constants of untreated vs. valinomycin-treated cells under hypotonic conditions for either parental or MDR cell lines. Under isotonic conditions, there was no significant change in the rate constant for parental cell lines, but the rate constant for valinomycin-treated MDR cells showed a slight but significant decline. Together, these data indicate that cation permeability was not rate limiting for Cl^- efflux.

Last, to determine whether another Cl^- transport system might be masking an MDR-associated Cl^- pathway, efflux experiments were repeated in the presence of bumetanide, an inhibitor of the Na^+-K^+-Cl^- cotransporter. A concentration of 50 µM was used that
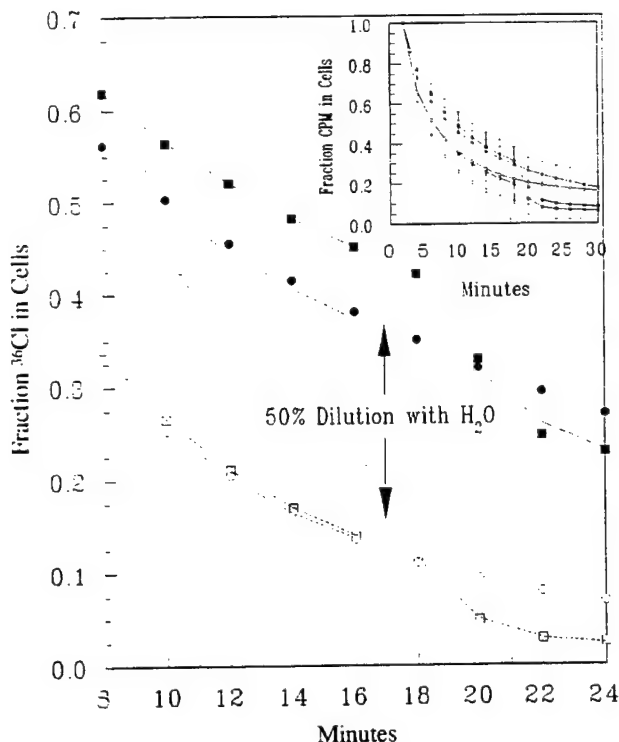

Fig. 5. Representative data of efflux of ^{36}Cl from NIH/3T3 and NIH/3T3MDR cells. Values are normalized counts/min (cpm) of ^{36}Cl remaining in the cells at each time point. ●, NIH/3T3 isotonic conditions; ■, NIH/3T3 with 50% hypotonicity after 16-min time point; ○, NIH3T3/MDR isotonic conditions; □, NIH/3T3MDR 50% hypotonicity after 16-min time point. Solid lines, fitted curves for parental data; dashed lines, fitted curves for MDR data. *Inset*: averaged data ($n = 5$ experiments) for entire time period; error bars represent SE.
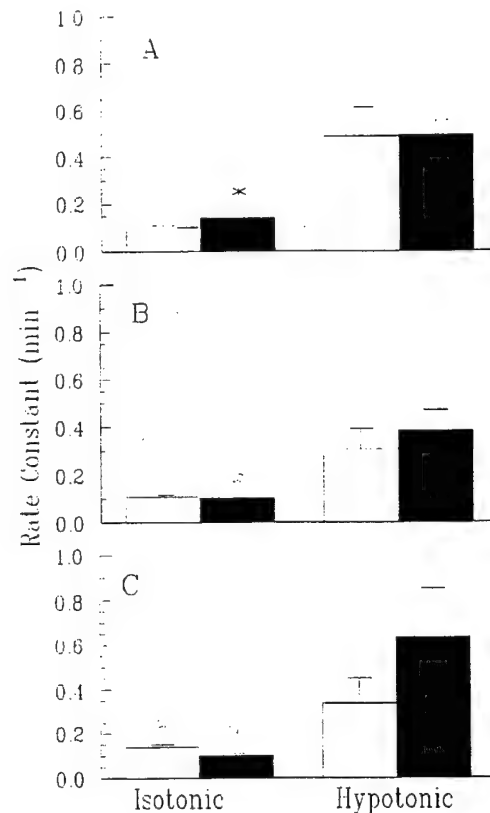
has been shown to effectively block activity of the transporter without blocking other Cl⁻ efflux pathways (18). No significant difference in the rate constants between parental and MDR cells under isotonic or hypotonic conditions was revealed by this treatment (Fig. 6C; $n = 4$). Small but significant increases in the rate constants for both parental and MDR cell lines were observed in bumetanide-treated compared with untreated control, but only for the isotonic condition.

Cl⁻ efflux measurements in L1210 and L1210vMDR cells. Efflux measurements were also performed on the L1210 and L1210vMDR cell lines. Representative efflux data are shown in Fig. 7 and show the same pattern of increased Cl⁻ efflux after hypotonic stress as the NIH/3T3 cells. Comparison of efflux rate constants (Fig. 8A) indicates that there was no significant difference between parental and MDR cells under isotonic or hypotonic conditions ($n = 3$). Addition of 5 µM valinomycin did not significantly affect the rate constants of ³⁶Cl⁻ efflux in either cell type ($n = 2$, Fig. 8B).

DISCUSSION

The hypothesis that expression of MDR1 protein is associated with increased Cl⁻ conductance was tested by measuring RVD and ³⁶Cl⁻ efflux in parental and *MDR1*-transfected cell lines. After hypotonic stress, parental and *MDR1*-transfected cells underwent RVD with similar kinetics (Fig. 2). However, since none of these cell lines approached their predicted van t'Hoff volumes after exposure to hypotonic solution, it was possible that the MDR-associated Cl⁻ conductance was only transiently activated and affected only the early
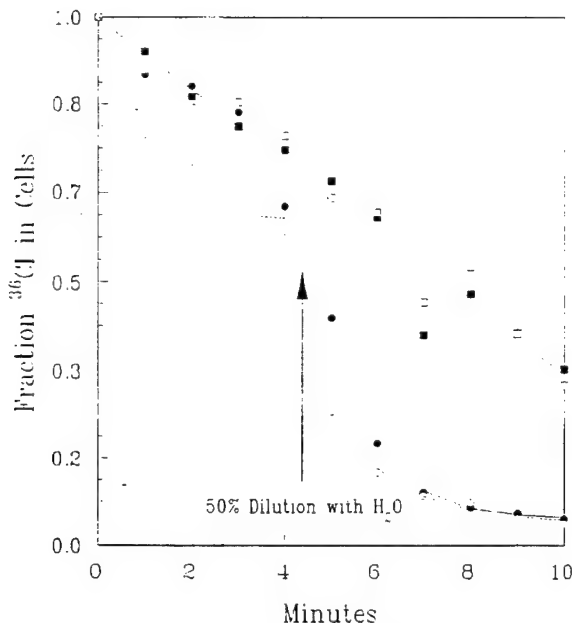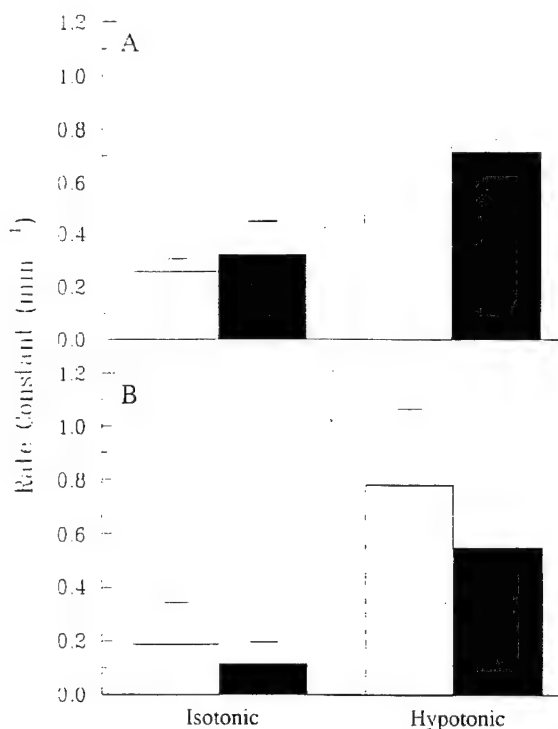

Fig. 8. Values of fitted efflux rates for L1210 (open bars) and L1210vMDR (solid bars) ³⁶Cl⁻ efflux data. A: no drug treatment. B: 5 µM valinomycin. Differences between parental and MDR or no drug and valinomycin were not significantly different at $P < 0.05$.

phase of the RVD process. However, rapid measurements of RVD over the first 5 min with the L1210 cell lines showed that no previously undetected RVD was occurring in the MDR cell line. Data from NIH/3T3 lines were more variable but did not reliably show large early differences in RVD.

It is unlikely that the lack of observed difference in the rate of RVD between parental and MDR1-expressing cells was due to absent or insufficient (i.e., rate-limiting) cation conductive pathways. Parental cells exposed to the K⁺ ionophore valinomycin did not show an increased rate of RVD in hypotonic NaCl Hanks' solution compared with untreated controls even at high (20 µM) doses of ionophore. In addition, experiments carried out in high-K⁺ solutions showed that volume regulation in both parental and MDR1 cells could be altered in a similar manner by changing the direction of the K⁺ gradient (Fig. 3).

Attempts to unmask an MDR1-associated Cl⁻ conductance using reported blockers of MDR1-associated Cl⁻ current were also unsuccessful. Neither DDFSK, FSK, nor DIDS produced differential inhibition of RVD in any of the cell lines tested, although partial inhibition of RVD in paired MDR and parental cell lines was seen (Fig. 4 and see text). This partial inhibition may have been due to other nonspecific actions of these blockers. For example, FSK blocks "n" type K⁺ channels in T lymphocytes that are known to participate in volume regulation (13). In contrast, SITS, a Cl⁻ channel blocker known to inhibit RVD in other cells types, also blocked RVD in the cell lines used here. In agreement with our observations, it has been shown recently (5) that, in the

Fig. 7. Representative data of efflux of ³⁶Cl⁻ from L1210 and L1210vMDR cells. Values are normalized cpm of ³⁶Cl⁻ remaining in the cells at each time point. ■, L1210 isotonic conditions; ●, L1210 with 50% hypotonicity after 4-min time point; □, L1210vMDR isotonic conditions; ○, L1210vMDR 50% hypotonicity after 4-min time point. Solid lines, fitted curves for parental data; dashed lines, fitted curves for MDR data.

NIH/3T3 parental and MDR cell lines, DIDS and 5-nitro-2-(3-phenylpropylamino)benzoic acid block volume-activated Cl⁻ channels to a similar extent in both parental and MDR lines.

To more directly measure the effect of MDR1 expression on Cl⁻ permeability, ^{36}Cl efflux was evaluated in two pairs of cell lines, NIH/3T3, NIH/3T3MDR and L1210, L1210vMDR. The results showed no significant difference in ^{36}Cl efflux rate constants in NIH/3T3MDR or L1210vMDR compared with parental cells under hypotonic conditions (Figs. 6 and 8). A small but significant difference in the isotonic rate constant between parental and MDR cells was observed in NIH/3T3 but not L1210 cells. Neither basal nor hypotonic-induced rates of ^{36}Cl efflux were increased by valinomycin (Figs. 6B, 8B). Although this indicates that cation conductance was not rate limiting for ^{36}Cl⁻ efflux, this interpretation is complicated by the fact that valinomycin is also an inhibitor of MDR1 transport function (5a, 25). However, since treatment with CsA also had no effect on ^{36}Cl efflux (data not shown), it appears that competitive inhibition of MDR1 transport does not alter the availability of Cl⁻ efflux pathways. Confirming this observation, treatment with CsA had no effect on RVD in the L5178Y and L5187YvMDR cell lines at a concentration that blocks R123 efflux completely (data not shown).

Our data support the findings of Ehring et al. (5) who, with the use of the same *MDR1*-transfected NIH/3T3 cells that were used by us and by Valverde et al. (23), found no difference in the levels of swelling-induced Cl⁻ conductance. Our findings differ from those of Luckie et al. (16) who found a differential anion efflux between parental and colchicine-selected NIH/3T3 cells at levels of osmotic stress >30% dilution.

Given the lack of difference between parental and transfected cells, was it possible that there were simply too few MDR1-associated Cl⁻ channels to significantly increase total cellular Cl⁻ conductance relative to parental cells? The data from the accompanying study (23a) indicate that the number of MDR1-binding sites per cell is 8,000–55,000. Several estimates of the number of Cl⁻ channels necessary to account for Cl⁻ efflux (3) or current (27) observed during RVD range from 350 to 1,000 channels per cell. Thus, in all cell lines tested, the numbers of MDR1 antibody binding sites per cell are significantly in excess of the number of Cl⁻ channels per cell likely to be needed for all of the Cl⁻ channel activity needed to carry out RVD. The lack of effect of valinomycin on both RVD and ^{36}Cl efflux shows that cation permeability is not likely to be rate limiting.

In summary, we have found that RVD and ^{36}Cl efflux rate constants were not different in several lines of parental vs. MDR1-expressing cells. Drugs reported to inhibit MDR1-associated Cl⁻ channel activity were not able to differentially affect RVD in parental vs. MDR cells. If the MDR1 protein is associated with a volume-activated Cl⁻ transport pathway, it is not detectable in intact cells using these functional assays.

REFERENCES

1. **Altenberg, G. A., J. W. Deitmer, D. C. Glass, and L. Reuss.** P-glycoprotein-associated Cl⁻ currents are activated by cell swelling but do not contribute to cell volume regulation. *Cancer Res.* 54: 618–622, 1994.

2. **Altenberg, G. A., C. G. Vanoye, E. S. Han, J. W. Deitmer, and L. Reuss.** Relationship between rhodamine 123 transport, cell volume, and ion-channel function of P-glycoprotein. *J. Biol. Chem.* 269: 7145–7149, 1994.

3. **Cahalan, M. D., and R. S. Lewis.** Role of potassium and chloride channels in volume regulation by T lymphocytes. In: *Cell Physiology of Blood,* edited by R. B. Gunn and J. C. Parker. New York: Rockefeller Univ. Press, 1988, p. 281–301.

4. **Deutsch, C., and S. C. Lee.** Cell volume regulation in lymphocytes. *Renal Physiol. Biochem.* 11: 260–276, 1988.

5. **Ehring, G. R., Y. V. Osipchuk, and M. D. Cahalan.** Swelling-activated chloride channels in multidrug-sensitive and -resistant cells. *J. Gen. Physiol.* 104: 1129–1161, 1994.

5a. **Eytan, G. D., M. J. Borgnia, R. Regev, and Y. G. Assaraf.** Transport of polypeptide ionophores into proteolipsomes reconstituted with rat liver P-glycoprotein. *J. Biol. Chem.* 269: 26058–26065, 1994.

6. **Gallin, E. K.** Ion channels in leukocytes. *Physiol. Rev.* 71: 775–811, 1991.

7. **Gill, D. R., S. C. Hyde, C. F. Higgins, M. A. Valverde, G. M. Mintenig, and F. V. Sepulveda.** Separation of drug transport and chloride channel functions of the human multidrug resistance p-glycoprotein. *Cell* 71: 23–32, 1992.

8. **Grinstein, S., C. A. Clarke, A. Dupre, and A. Rothstein.** Volume-induced increase of anion permeability in human lymphocytes. *J. Gen. Physiol.* 80: 801–823, 1982.

9. **Grinstein, S., and J. K. Foskett.** Ionic mechanisms of cell volume regulation in leukocytes. *Annu. Rev. Physiol.* 52: 399–414, 1990.

10. **Grinstein, S., A. Rothstein, B. Sarkadi, and E. W. Gelfand.** Responses of lymphocytes to anisotonic media: volume-regulating behavior. *Am. J. Physiol.* 246 (*Cell Physiol.* 15): C204–C215, 1984.

11. **Hoffmann, E. K., I. H. Lambert, and L. O. Simonsen.** Mechanisms of volume regulation in Erlich ascites tumor cells. *Renal Physiol. Biochem.* 11: 221–247, 1988.

12. **Horio, M., M. Gottesman, and I. Pastan.** ATP-dependent transport of vinblastine in vesicles from human multidrug-resistant cells. *Proc. Natl. Acad. Sci. USA* 85: 3580–3584, 1988.

13. **Krause, D., S. C. Lee, and C. Deutsch.** Forskolin effects on the voltage-gated K conductances of human T cells. *Pfluegers Arch.* 412: 133–140, 1988.

14. **Kunzelmann, K., I. N. Slotki, P. Klein, T. Koslowsky, D. A. Ausiello, R. Greger, and Z. I. Cabantchik.** Effects of P-glycoprotein expression on cyclic AMP and volume-activated ion fluxes and conductances in HT-29 colon adenocarcinoma cells. *J. Cell. Physiol.* 161: 393–406, 1994.

15. **Lincke, C. R., A. M. van der Bliek, G. J. Schuurhuis, T. van der Velde Koerts, J. J. Smit, and P. Borst.** Multidrug resistance phenotype of human BRO melanoma cells transfected with wild-type human mdr1 complementary DNA. *Cancer Res.* 50: 1779–1785, 1990.

16. **Luckie, D. B., M. E. Krouse, K. L. Harper, T. C. Law, and J. J. Wine.** Selection for MDR1/P-glycoprotein enhances swelling-activated K⁺ and Cl⁻ currents in NIH/3T3 cells. *Am. J. Physiol.* 267 (*Cell Physiol.* 36): C650–C658, 1994.

17. **McManus, M., J. Fischbarg, A. Sun, S. Herbert, and K. Strange.** Laser light-scattering system for studying cell volume

regulation and membrane transport processes. *Am. J. Physiol.* 265 (*Cell Physiol.* 34): C562–C570, 1993.

18. **Owen, N. E.** Regulation of Na/K/Cl cotransport in vascular smooth muscle cells. *Biochem. Biophys. Res. Commun.* 14: 500–508, 1984.

19. **Rasola, A., L. J. V. Galietta, D. C. Gruenert, and G. Romeo.** Volume-sensitive chloride currents in four epithelial cell lines are not directly correlated to the expression of the MDR-1 gene. *J. Biol. Chem.* 209: 1432–1436, 1994.

20. **Riordan, J. R., J. M. Rommens, B. Kerem, N. Alon, R. Rozmahel, Z. Grzelczak, J. Zielenski, S. Lok, N. Plavsci, J.-L. Chou, M. L. Drumm, M. C. Iannuzzi, F. S. Collins, and L.-C. Tsui.** Identification of the cystic fibrosis gene: cloning and characterization of complementary DNA. *Science Wash. DC* 245: 1066–1073, 1989.

21. **Schlemmer, S. R., and F. M. Sirotnak.** Functional studies of p-glycoprotein in inside-out plasma membrane vesicles derived from murine erythroleukemia cells overexpressing MDR 3. *J. Biol. Chem.* 269: 31059–31066, 1994.

22. **Ueda, K., A. M. Shimabuku, H. Konishi, Y. Fujii, S. Takebe, K. Nishi, M. Yoshida, T. Beppu, and T. Komano.** Functional expression of human P-glycoprotein in *Schizosaccharomyces pombe*. *FEBS Lett.* 330: 279–282, 1993.

23. **Valverde, M. A., M. Diaz, F. V. Sepulveda, D. R. Gill, S. C. Hyde, and C. F. Higgins.** Volume regulated chloride channels associated with human multidrug-resistance P-glycoprotein. *Nature Lond.* 355: 830–833, 1992.

23a. **Weaver, J. L., L. McKinney, P. V. Schoenlein, S. Goldenberg, M. M. Gottesman, and A. Aszalos.** MDR1/P-glycoprotein function. I. Effect of hypotonicity and inhibitors on rhodamine 123 exclusion. *Am. J. Physiol.* 270 (*Cell Physiol.* 39): C1447–C1452, 1996.

24. **Weaver, J. L., L. McKinney, P. V. Schoenlein, S. Goldenberg, M. M. Gottesman, and A. Aszalos.** Volume regulation and MDR1 protein function in MDR1-transfected and parental cell lines (Abstract). *Biophys. J.* 66: A217, 1994.

25. **Weaver, J. L., G. Szabo, Jr., P. S. Pine, M. Gottesman, S. Goldenberg, and A. Aszalos.** The effect of ion channel blockers, immunosuppressive agents and other drugs on the activity of the multi-drug transporter. *Int. J. Cancer* 54: 456–461, 1993.

26. **Wilson, H. A., B. E. Seligmann, and T. M. Chused.** Voltage-sensitive cyanine dye fluorescence signals in lymphocytes: plasma membrane and mitochondrial components. *J. Cell. Physiol.* 125: 61–71, 1985.

27. **Worrell, R. T., A. G. Butt, W. H. Cliff, and R. A. Frizzell.** A volume-sensitive chloride conductance in human colonic cell line T84. *Am. J. Physiol.* 256 (*Cell Physiol.* 25): C1111–C1119, 1989.

This article was altered to
correct typographical errors.

Effects of Nitrogen Mustard Alone and in Combination with Ionizing Radiation on Guanine

Yashesh N. Vaishnav and Charles E. Swenberg

Applied Cellular Radiobiology Department
Armed Forces Radiobiology Research Institute
Bethesda, MD 20889-5603

Abstract

Mustard agents are known to interact with cellular macromolecules such as DNA by forming covalent adducts. Using guanine as our DNA model, we have optimized the products formed by the interaction of guanine with nitrogen mustard mechlorethamine (HN_2) and examined the radiation sensitivity of guanine in the presence and absence of HN_2 using different qualities and quantities of radiations. Briefly, in an equimolar solution (0.5 mM) the pH-dependence (pH 3.0-12.0) and time-dependence (0-36 h) of alkylation of guanine at room temperature were determined using a reverse-phase high-performance liquid chromatography (HPLC) column. Based on the HPLC peak areas of the product and intact guanine, the optimal pH for alkylation was determined to be 8.0 and the time required for alkylation was 10 h in triethanolamine buffer (100 mM). Two products, alkylated guanines, were detected (10:1, peak areas measured at 260 nm) and purified. Structural studies of the products were performed by mass spectrometry. At optimal conditions, samples of either guanine or an equimolar solution of guanine and HN_2 were either ^{60}Co (γ ray) or fission neutron irradiated at 25 Gy min^{-1} at doses up to 400 Gy. Samples were analyzed by HPLC. In each case, the sole radiation product observed and characterized was 8-hydroxy-guanine. Dose-yield plots were linear and showed that HN_2 enhanced the radiation sensitivity of guanine. This increase in radiation sensitivity is attributed to the difference in electrophilic properties of nitrogen mustard to guanine.

1. Background

Mustard gas has a long history, having been used in World War I as a powerful chemical weapon. Though mustard gas has been known for a long time, it was Berenblum in 1929 who first reported dichlorodiethyl-sulfide-induced tumors in mice. There are two standard types of mustard agents: the sulfur mustards and their analogs nitrogen mustards. Both have structural similarities, and basic chemical reactions are common between them and both exhibit vesicant properties. In the interval between World War I and II, extensive studies of the biological and chemical actions of nitrogen mustards were undertaken. The marked cytotoxic action on lymphoid tissue encouraged Gilman and Phillips (1946) to study the effect of nitrogen mustards on transplanted lymphosarcoma in mice, and in 1942 clinical studies were initiated by Gilman (1963) and this launched the era of modern cancer therapy.

Although known as a strong vesicant, bifunctional nitrogen mustard mechlorethamine [(bis-2-chloroethyl)methyl amine, HN_2] was the first effective anticancer agent employed clinically (Mattes et al., 1986). Derivatives of HN_2, such as L-phenylalanine mustard, chlorambucil, and cyclophosphamide are also effective therapeutic agents (Masta et al.,1984) even though they are carcinogenic. Chemotherapeutic agents have the common property of undergoing strongly electrophilic chemical reaction through the formation of carbonium ion intermediates or transition complexes with target molecules. These interactions lead to the formation of covalent linkages with various nucleophilic substances. Numerous nucleophilic sites in nucleic acid have been recognized as locations where the monofunctional or bifunctional alkylating agent interact: in adenine, N-1, N-3 and N-7, in guanine N-3, N-7 and O-6, in cytosine, N-1, N-3 and O-2 and for thymine N-3 and O-4 are possible locations (Lawley and Martin, 1975; Ehrenberg, 1961). Other biologically important groups for alkylation include phosphate, amino, sulfhydryl, hydroxyl and carboxyl moieties. However, the major site for DNA alkylation is the N-7 position of guanine (Tomaz, 1969, 1970; Roberts, 1978). This particular interaction accounts for approximately 90% of the total. Fig. 1 summarizes the actions of nitrogen mustard HN_2 with guanine residues in DNA chain and their possible consequences (Calabresi and Park, 1988). Evidence indicates that the cytotoxic and other effects of the alkylating agents are directly related to the alkylation of components of DNA as illustrated in Fig. 1. Overall it is important to note that bifunctional agents are closely associated with cytotoxic effects whereas monofunctional agents are more related to the capacity for mutagenesis and carcinonesis. This observation suggests that cross-linking of DNA strands by bifunctional agents is directly linked to cellular survival compared to effects such as depurination and strand scission, which are the precursors that lead to mutagenesis and carcinogenesis.

Soon after World War II cytotoxic chemotherapy for various cancers increased and a number of alkylating agents, including nitrogen mustards were used alone (Povirk and Schuker, 1994) or in combination with radiotherapy and/or other drugs (Farmer, 1994). Case reports of leukemia in treated patients soon appeared and revealed a consistent and definite increase in second malignancies following combined radio- and chemotherapy for Hodgkin's disease (Povirk and Schuker, 1994). Paradoxically, it was the success of cancer therapy both in increased cure rates and long-term survival that has led to the carcinogenesis of a number of chemotherapeutic agents such as HN_2 in man.
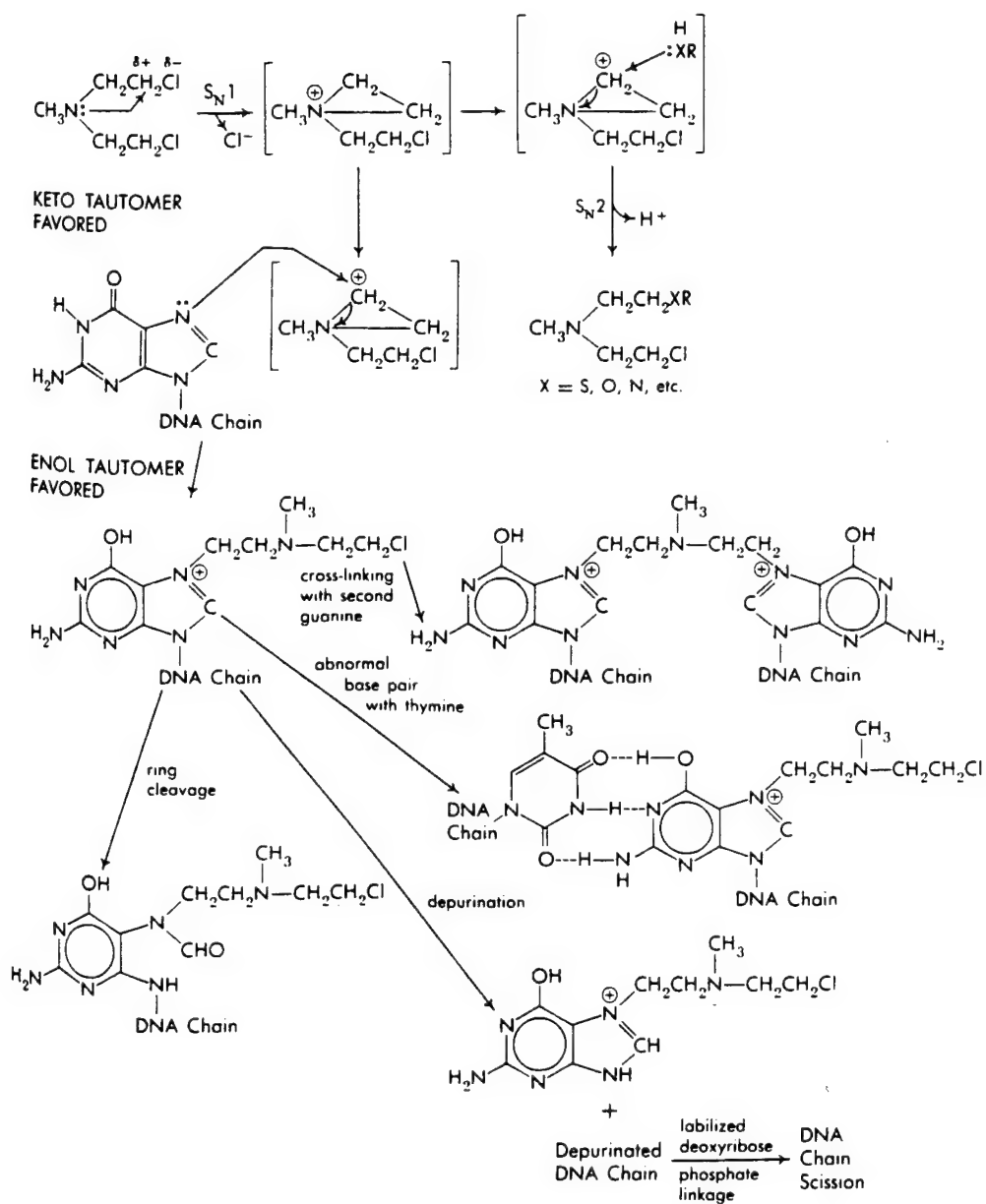
Fig. 1. Chemical and biochemical mechanisms of actions of akylating agents [Redrawn from Calabresi and Parks, 1988].

1131

Fig. 2 summarizes toxicodynamics of sulfur mustard-induced cell damage/death according to Somani (1993). The scheme in Fig. 2 is based on pioneering work of many investigators including Roberts (1971), Ludlum (1978), Gross (1981), Meier (1987), Smith (1991), Papirmeister (1991) and Somani (1993). Although the nitrogen mustards are slightly less reactive than sulfur mustard agents they, nevertheless, in the majority of instances exhibit similar consequences at cellular levels.
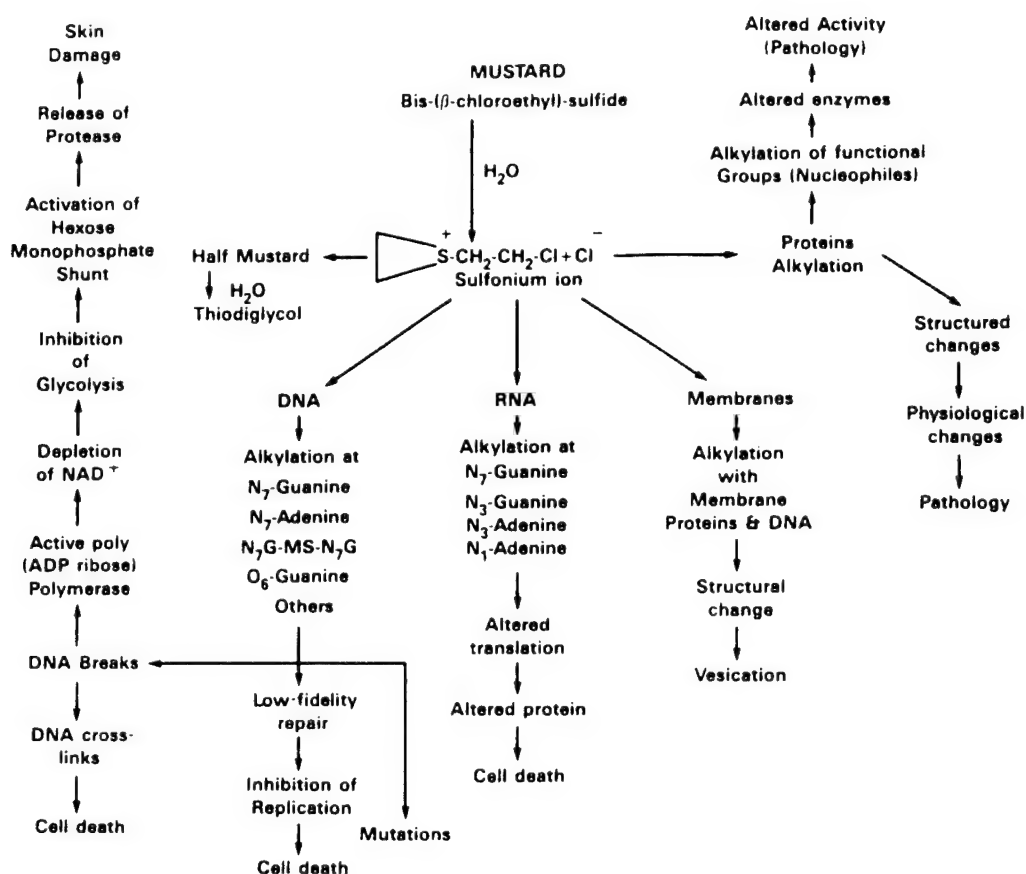

Fig. 2. Possible toxicodynamics of mustard [Redrawn from Somani, 1993].

1. Introduction

Depending on their chemical structures vesicant mustard agents can be monofunctional or bifunctional alkylating agents and due to their electrophilic nature, they may alkylate any accessible nucleophilic sites in nucleic acids, proteins or other biomolecules. All bifunctional nitrogen mustards including HN_2 are chemotherapeutic agents. The nitrogen mustards are also carcinogenic and mimic ionizing radiation in many respects, e.g., produce similar DNA lesions, including modified bases, base-free sites, and single and double strand breaks. Nevertheless, their actions are not quantitatively similar in that important differences exist in their combined toxicities with ionizing radiation. As nitrogen mustards and ionizing radiation remain parts of the radiotherapeutic and chemotherapeutic regimen for several malignant diseases, it is important to understand molecular events involved in combined exposures. Clarifications of the microscopic events should be helpful in elucidating any adverse reactions and in the development of countermeasures. As guanine is known to be the DNA target most susceptible to alkyl modification, our initial experiments concerned the response of dilute solution of guanine to the combined modalities. In this report, the products of HN_2 interactions with guanine are optimized, and the radiation sensitivity (γ ray and neutrons) and radiation chemistry of guanine in the absence and presence of HN_2 are presented.

2. Material and Methods

2.1. *Reagents and instruments*

Guanine, mechlorethamine hydrochloride and triethanolamine hydrochloride were purchased from Sigma Chemical Co. (St. Louis, MO). HPLC-grade acetonitrile was obtained from Aldrich Chemical Co., N-O-bis-(trimethylsilyl)-trifluoroacetamide (BSTFA) was purchased from Supelco, Inc., (Belfonte, PA). All HPLC analyses were performed using a Kratos Analytical Spectroflow 400 solvent delivery system (Ramsey, NJ) on-line with model SP-4100 computing integrator and Applied Biosystems model 783 absorbance detector gradient controller. Mass spectral analysis were performed on the Kratos Analytical 25 RFA mass spectrometer using a direct insertion probe (DIP)-electron impact (EI) mode. Experiments using γ and neutron irradiation were performed using AFRRI ^{60}Co and TRIGA facility, respectively.

## 2.2. *Detection, isolation and characterization of the products from interaction of guanine with HN_2*

Solution of guanine (0.5 mM) alone and equimolar mixture of guanine and HN_2 (0.5 mM each) in triethanolamine hydrochloride (TA buffer) (100 mM, pH 7.5 adjusted with 0.5 M NaOH) were allowed to stand at room temperature for 3 h. Subsequently, aliquots (10 µl) from each solution were analyzed by high-performance liquid chromatography (HPLC) using a reverse-phase semipreparatory column (Speris, Clwyd, UK; 250 mm x 4.6 mm) in an isocratic eluent mode (water-acetonitrile-acetic acid in 85:13:2, v/v/v). HPLC peak profiles of both samples were recorded by optical detection at 260 nm. Products were collected and freeze-dried for subsequent mass spectral (MS) analysis.

HPLC-purified products 1 and 2 (P-1 and P-2 in Fig. 3) were transformed into their corresponding trimethylsilyl (TMS) derivatives. In reaction vials, approximately 100-μg sample of either P-1 or P-2 was dissolved in 25-μl mixture of acetonitrile-BSTFA (1:2, v/v). The resulting mixture was subsequently heated to 65°C for 45 min and then allowed to stand at room temperature for an additional 40 min to equilibrate the mixture. Using DIP, 3-4 μl of the silylated product was analyzed in an EI/MS mode (70 eV; source temperature 270°C), and mass spectra were recorded as previously described (Vaishnav et al., 1991; Vaishnav and Swenberg, 1993).

2.3. Interaction of guanine with HN₂: pH dependence

A solution of triethanol amine hydrochloride (TA) (100 mM, 100 ml) was equally divided into 10 fractions. The pH of the fractions was adjusted from 3.0 to 12.0 respectively, with either 0.1 M NaOH or 0.1 M HCl and then each fraction was made 0.5 mM (equimolar) with respect to guanine and HN₂. The resulting mixtures were allowed to incubate at room temperature for a period 3 h, and then placed in an ice-bath until all samples were analyzed. The progress of the reaction for each pH value was monitored by a reverse-phase HPLC column as described. The peak areas for each product were determined by triangulation. Following initial analysis, samples were allowed to incubate at room temperature (72 h) and were subsequently reanalyzed.
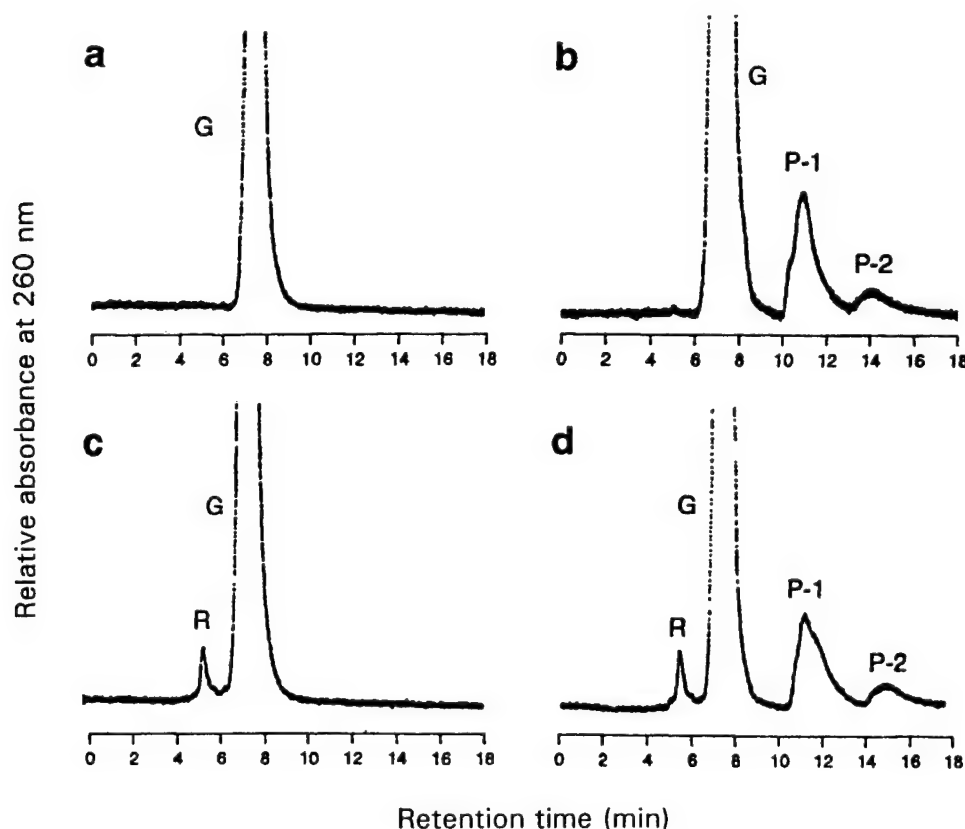
Fig. 3. Representative HPLC product profiles: (a) Guanine standard, (b) interaction products of guanine with mechlorethamine, (c) irradiated guanine (100 Gy/min), and (d) irradiated equimolar mixture of guanine and mechlorethamine at optimal conditions. Here G, P-1, P-2 and R denote guanine, product 1, product 2, and radiation products, respectively.

2.4. *Interaction of guanine with HN_2: Time dependence*

An equimolar mixture of guanine and HN2 (0.5 mM) in 100 mM TA buffer (pH 8.0) was allowed to incubate at room temperature, and aliquots (10 μl each) were withdrawn periodically between 0 and 40 h from the incubating mixture and analyzed on a reverse-phase HPLC column as described. Peak areas for the P-1, P-2 and unreacted guanine (G) were determined.

2.5. *Irradiation of guanine in the absence/presence of HN_2*

Solution of guanine and HN-2 (0.5 mM each) were prepared in 100 mM TA buffer (pH 7.5). The solutions were allowed to stand overnight at room temperature. Aliquots (200 μl each) from these solutions were withdrawn and placed individually into irradiation vials (micropolypropylene tubes, 500 μl, Marsch Biomedical Products, Rochester, NY). The air-saturated samples were bilaterally exposed to different doses of ^{60}Co (γ) or fission neutrons at approximately 25 Gy/min. Irradiated samples and unirradiated controls were allowed to stand at 4°C until analysis. Both sets of samples were analyzed using a reverse-phase HPLC as described previously.

Dosimetry: For γ ray irradiation, the desired dose rate was established using 0.5 cc tissue equivalent (TE) ionization chamber. The ionization chambers were previously calibrated by factors traceable to the National Institutes of Standards and Technology. Dosimetric measurements were made in accordance with the American Association of Physicists in Medicine (AAPM Task Group 21, 1983) protocols for the determination of absorbed dose from high-energy photon and electron beams. For mixed-field neutron and γ ray radiation the dose rate was 23.5 Gy/min ± 6% with neutron dose to total dose approximately 0.94 ± 8%. Dosimetry measurements were made using TE and magnesium ion chamber pairs.

3. Results

3.1. *Product detection, isolation and characterization*

From the HPLC product profiles (Fig. 3) at equimolar mixture of guanine and HN_2 at room temperature (pH = 7.5) results in two new products, P-1 (RT = 11.82 min) and P-2 (RT = 14.44 min), in addition to unaltered intact guanine, G (RT = 7.90 min). The intact product labeled G, P-1, and P-2 were isolated and purified on a HPLC reverse-phase column. The purified samples were freeze-dried and transformed into their corresponding TMS derivatives. The TMS derivatives of P-1, P-2, and G were analyzed.

The mass spectrum of the TMS derivative of P-1 showed the molecular ion (M^{+}) at m/z=414, consistent with the molecular formula of the diTMS derivative (2TMS-$C_{10}H_{13}N_6Cl$) of a monoalkyl adduct of guanine with HN-2. Further fragmentation of the M^{+} resulted in several prominent ions (m/z= 399, 352, 248, 246, 205, 203, and 147) characteristic of the diTMS derivative (McCloskey et al., 1968; McCloskey, 1974; Vaishnav and Swenberg, 1993).

The DIP/EI mass spectrum of the TMS derivative of the HPLC-purified P-2 showed M^+ at m/z 468 to be consistent with the molecule $3TMS-C_{10}H_{13}N_2O_2$. Other characteristic fragment ions were at m/z 367, 352, 295, 248, 246, and 170; silyl group migration (McLaferty, 1980) and other characteristic losses from silyl derivatives (McCloskey, 1974: McLafferty, 1980) were utilized to elucidate the chemical structure of P-2.

Under our mass spectral conditions, no extensive fragmentation of the tri-TMS derivative of G was observed. The M^+ was observed at m/z 367, which corresponds to tri-TMS derivative of guanine. In addition to the prominent M^+, the low intensity ions included m/z 295, 294, 281, and 221. These fragmentation patterns are identical to that previously reported (McCloskey et al., 1968) for the TMS derivative of guanine.

3.2. pH-Dependent formation of guanine-HN_2 adducts

Equimolar mixtures of guanine and HN_2 at different pHs (between 3.0 and 12.0) were allowed to stand at room temperature for either 3 or 72 h prior to reverse-phase HPLC analysis. From the resulting chromatograph, peak area (p-1, p-2) of P-1 and P-2, and (g) of unaltered guanine (G) were determined for each pH value and the percent of product, [p x $(p+g)^{-1}$ x 10^2] formed was derived. Fig. 4 data showed that the maximum product formation occurred between pH 7.5 and 8.5. Furthermore, significant qualitative differences were observed in product formation for samples incubating between 3 and 72 h; although, at pHs between 7.5 and 8.5, there were differences in the amounts of product formed when incubations times were longer.
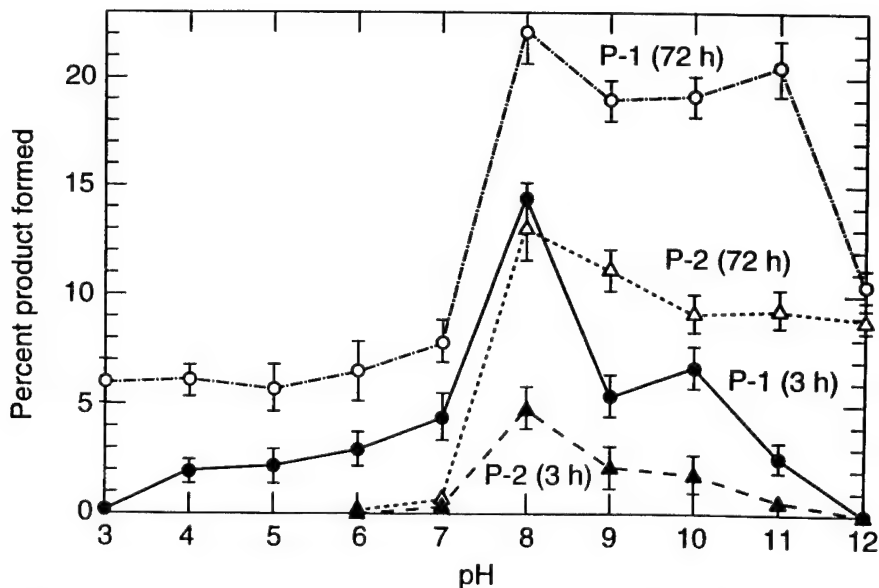

Fig. 4. pH-Effects on product formation in the interaction of guanine with mechlorethamine.

3.3. Time-dependent formation of guanine-HN₂ adduct

Equimolar mixture of guanine and HN_2 at optimal pH in 100 mM TA buffer was allowed to interact at room temperature for a period of 48 h. The interaction was monitored on a reverse-phase HPLC column. From the HPLC peak area values for P-1, P-2, and G, % formation of P-1 and P-2 were determined and plotted against time (Fig. 5). As evident from data in Fig. 5, saturation of P-1 and P-2 formation was achieved only after 8 h. Under more physiologically relevant conditions (10 mM sodium phosphate buffer, pH 7.4), P-1 and P-2 are observed but with lower yields (data not shown).

3.4. Irradiation of guanine in the absence/presence of HN₂

Gamma and fission neutron irradiations of guanine alone and in the presence of equimolar HN_2 were performed as described in Materials and Methods. Samples were analyzed on a reverse-phase HPLC column. Under the described experimental protocol, the peak labeled R in the representative chromatograph (Fig. 3) was the only radiation product detected and was common to both sets. Peak areas for each peak representing irradiation product R and intact guanine (G), (peak area r and g, respectively) were determined and %
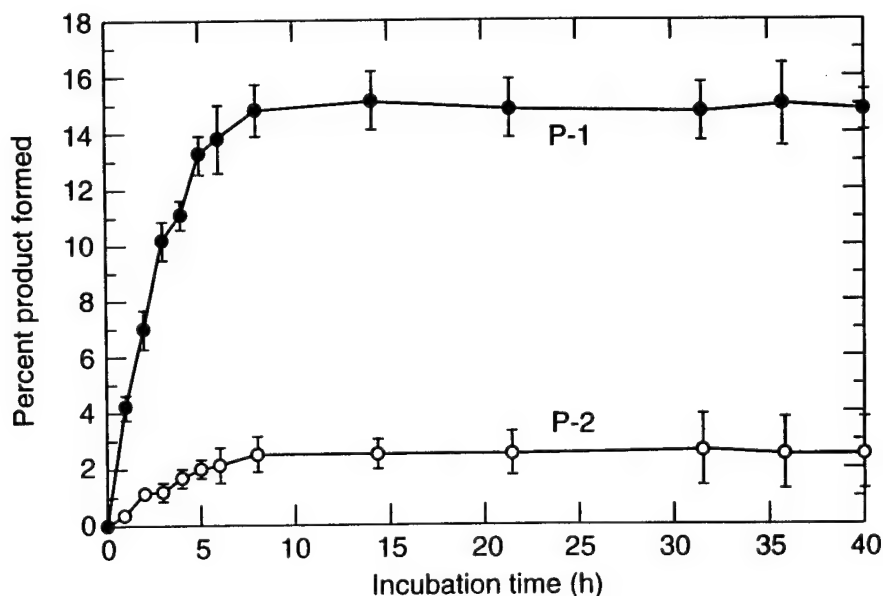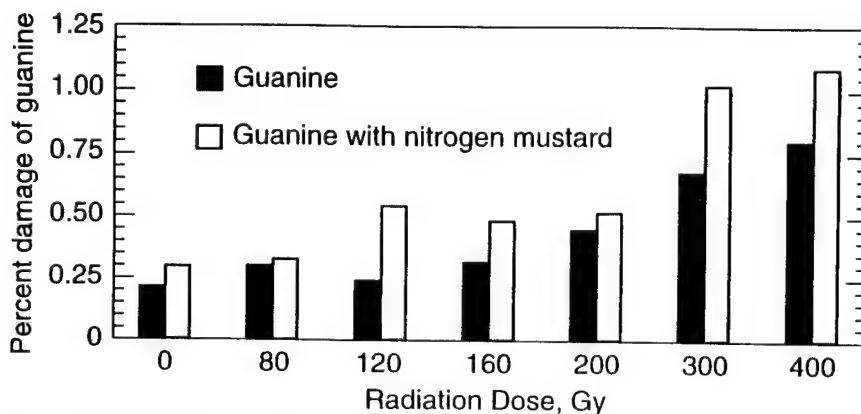

Fig. 5. Time course studies of product formation of guanine with mechlorethamine.

of the product formed as a function of radiation dose are shown in Figs. 6 and 7. Furthermore, product R from the irradiated samples was purified using HPLC, freeze-dried and transformed into its corresponding TMS derivative. The TMS derivative was analyzed using DIP/EI/MS. By comparing the mass spectral pattern with that reported for TMS derivative of 8-hydroxyguanine (Dizdaroglu, 1985; Fuciarelli et al, 1989), we determined chemical structure of product R to be 8-hydroxyguanine (R in Fig. 8).
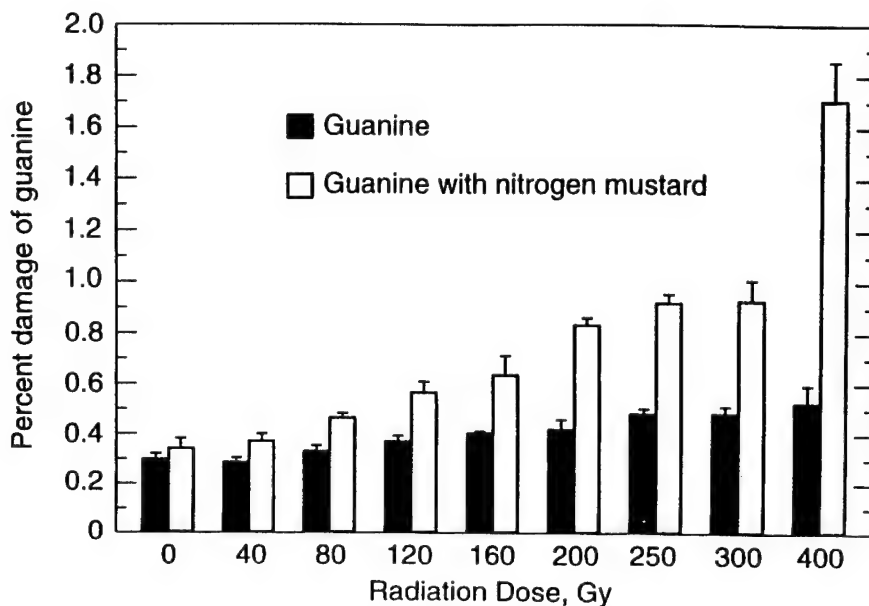
Fig. 6. The percentage of damaged guanine due to γ irradiation in the absence and presence of mechlorthamine at several doses.

Fig. 7. The percentage of damaged guanine due to fission neutron in the presence and absence of mechlorethamine at several doses.
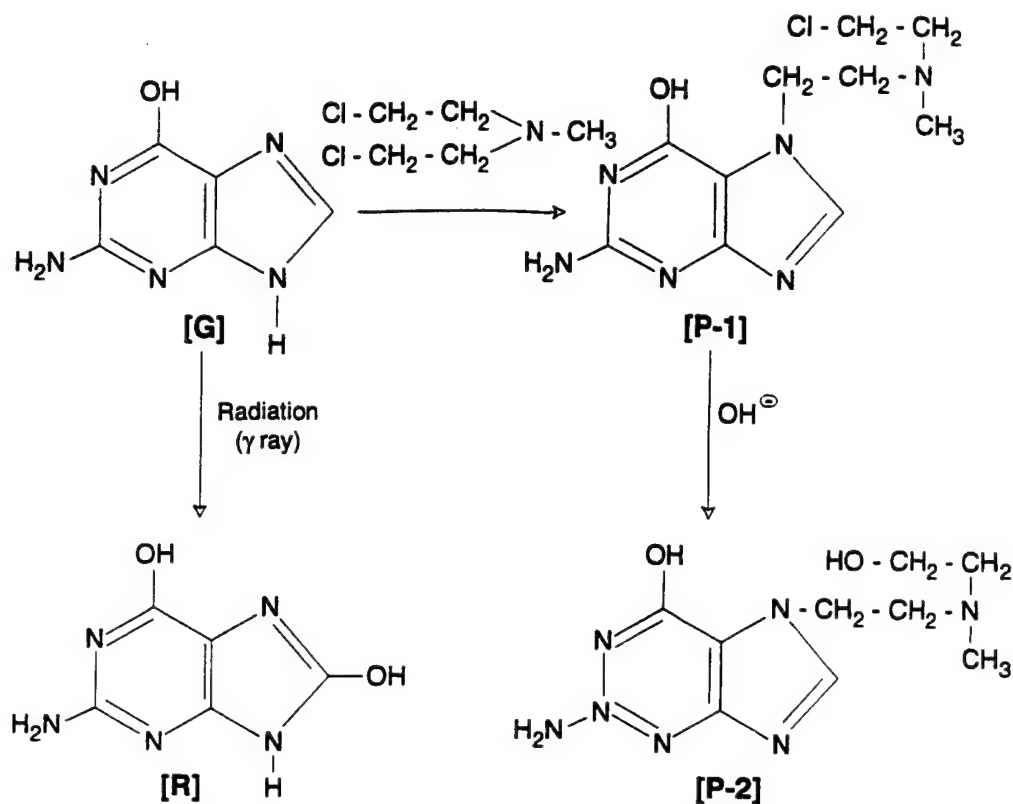
Fig. 8. Chemical structures and pathways of P-1, P-2, G, and R.

4. Discussion

To our knowledge, very few reports have been published adequately characterizing DNA damage produced by alkylating chemotherapeutic agents such as HN_2 in the presence of ionizing radiation despite the fact that both agents' primary effects are their interactions with DNA. To improve our perspectives of interactions at the DNA base level, we have determined the optimal conditions (pH, buffer, and time) governing HN_2 interaction with guanine in solutions. Our results suggest that only two monoadducts, P-1 and P-2 are produced. Both products were isolated, purified and characterized to be N-(2-chloroethyl)-N-[2-(7-guanyl)ethyl]methyl amine (P-1) and N-(2-hydroxyethyl)-N-[2-(7-guanyl)-ethyl]-methyl amine (P-2) using HPLC and mass spectrometry (for chemical structures see Fig. 8). Formation of these monoadducts can be explained by consideration of the scheme in Fig. 1. Kinetic mechanistic studies of Mattes (1992) are consistent with the observed adducts formation. Under our experimental conditions we did not detect formation of any diadduct from the guanine-HN_2 interaction. Interestingly, in cells, Larminant et al. (1993) have observed that mono-adduct to di-adduct formation ratio is approximately (95:5).

1139

At room temperature, the adduct formation was largest for pHs between 7.5 and 8.5, and declines if the pH was either raised or lowered. The relative percentage of product formed as determined from HPLC analysis suggests that only a small amount of guanine interacts with HN_2 even under optimal reaction conditions. Similarly, time course studies for interactions of guanine with HN_2 (1:1, m/m) examined at the optimal pH and time conditions showed no quantitative conversions of guanine to adduct formation. We interpret this as due to the relatively short stability of HN_2 in aqueous solution (Cummings et al 1993).

It is well known that the type of radiation can make a considerable qualitative and quantitative difference in the biological or chemical response produced even if equal amounts of energy are deposited. Ionization events from neutrons are clustered and therefore enhance recombination processes whereas γ rays produce rather diffused events in an aqueous medium. HPLC analysis of both sets of irradiation experiments showed only a single common radiation product (labeled R in Fig. 3). The radiation product was isolated, and its chemical structure was determined to be 8-hydroxy-guanine by mass spectral analysis. Product R was quantified from both irradiation sets of samples and results for γ and neutron irradiations are provided in Figs. 6 and 7) (Notes: (a), neutron irradiation data are preliminary and (b), Y-scale values are different in Figs. 6 and 7). As evidenced in the Figs. 6 and 7, HN_2 enhanced the radiation sensitivity of guanine in both the radiation types. Although different LET radiations produced identical radiation products, the quantity of the product formed with γ irradiation was significantly larger than that formed by neutrons. This enhancement is tentatively attributed to the higher ionization density of radicals formed by the neutrons that subsequently recombine resulting in fewer product molecule forming. Quantitative differences in the product formation have been previously reported in dilute aqueous solutions of dinucleoside monophosphates (Vaishnav and Swenberg, 1993) or plasmid DNA (Swenberg and Speicher, 1995).

Several hypotheses have been proposed for the radiation sensitivity enhancement mechanisms of target molecules in the presence of a radiosensitizer. In the present case, however, observed enhancement of radiation sensitivity of guanine can be well-explained by considering Adams'and Cook's hypothesis (Adams, 1969; Adams and Cook, 1969). In this model, the enhanced radiation sensitivity is attributed to difference in electron affinity between the target and the sensitizer: the direct or indirect effect of radiation results in charge separation within the target molecule followed by electron transfer from the negatively charged site to a more electron seeking sensitizer. If, therefore, a molecule of higher electron affinity is present, either as a complex or as a free molecule in the immediate environment of the ionized target molecule, electron transfer from the ionized target molecule to the sensitizer could occur, leaving the target molecule positively charged. This process is expected to compete with the charge recombination, thereby causing a self-"healing effect". Irreversible electron transfer to the sensitizer would then lower the probability of self-healing and favor the decay of the highly reactive positive target ion, which reacts with another neighboring neutral molecule, consequently transforming itself into a reactive free radical. Electron transfer from negatively charged radical-anion to the sensitizers has been demonstrated by pulse radiolysis (Greenstock et al., 1967). In the absence of known rate constants for electron transfer reactions between the target molecule and sensitizer, Adams' and Cook's hypothesis is consistent with nitrogen mustard-induced enhancement of radiation sensitivity of guanine.

Although the system studied here is a crude DNA model, the fundamental pathways involved in the interaction of nitrogen mustard, ionizing radiation, and DNA target guanine are expected to be similar to those in native DNA. In the absence of any repair processes, our data demonstrate that, under physiologically relevant conditions, nitrogen mustard forms covalent adducts with guanine, and in addition the mustard acts as a radiosensitizer, enhancing both high-and low-LET radiation sensitivity. The data presented here constitute another illustration of the importance of the microenvironment of DNA in altering its radiation sensitivity.

Acknowledgement

References

Adams, G. E., 1969, Molecular mechanisms of cellular radio-sensitization and protection. In: *Radiation Protection and Sensitization.* Edited by: H. L. Morson and M. Quintillani (Taylor and Francis Ltd., London), pp 1-12.

Adams, G. E. and Cooks, M. S., 1969, Electron-affinic sensitization. Structural basis for chemical radiosensitization in bacteria. *Int. J. Rad. Biol., 1,* 457-460.

Brarenblum, P. L., 1929, The modifying influence of dichloroethylsulfide on the induction of tumors in mice by tar, *J. Pathol. Bacteriol., 32,* 425-434.

Calabresi, P. and Parks, R. E., 1988, Antiproliferative agents and drugs used for immunosuppression, In: *The Pharmacological Basis of Therapeutics,* 5th edition, Edited by L. Goodman and A. Gilman, pp 1246-1257.

Cummings, J., Maclellan, A., Langdon, S. J., and Smyth, J. F., 1993, The long term stability of mechlor-ethamine hydrochloride (nitrogen mustard ointment measured by HPLC). *J. Pharm. and Pharmaco., 45,* 6-9.

Dizdaroglu, M., 1985, Applications of capillary gas chromatography-mass spectrometry to chemical characterization of radiation-induced base products in DNA: Implications for assassing DNA repair processes. *Anal. Biochem., 144,* 593-603.

Ehrenberg, L., 1961, Principles and methods of detection of chemical mutagenesis. In: *Chemical Mutagenesis, vol.2,* Edited by: A. Hollaeder (Plenum, New York) pp 212-284.

Farmer, P. B., 1994, Metabolism and reactions of alkylating agents. In: *Anticancer Drugs: Reactive Metabolism and Drug Interactions* (Pergamon Press, Oxford, U.K) pp 30-45.

Fuciarelli, A. F., Wegher, B. J., Gajewaski, E., Dizdaroglu, M., and Blakely, W. F., 1989, Quantitative measurement of radiation-induced base products in DNA using gas chromatography-mass spectrometry, *Rad. Res., 119,* 219-231.

Gilman, A. and Philips, F. S., 1946, The biological actions and therapeutic applications of the ß-chloroethylamines and sulfides, *Science, 103,* 409-415.

Gilman, A., 1963, Initial clinical trial of nitrogen mustard, *Am. J. Surg., 105,* 574-578.

Greenstock, C. L., Adams, G. E., Wilson, R. L., 1969, Electron transfer studies of nucleic acid derivatives in solution containing radiosensitizers. In: *Radiation Protection and Sensitization.* Edited by: H.L. Moroson and M. Quintiliani (Taylor and Francis, London) pp 65-69.

Gross, C. L., Waston, C. V., Petrali, J. and Papirmister, B., (1981), Effects of sulfur mustard on lycosomes from rat liver in vitro. *Toxicolo. Appl. Pharmacol., 61,* 147-151.

Larminant, F. and Zhen, W. and Bohr, V. A., 1993, Gene-specific DNA repair of interstrand cross-link induced by chemotherapeutic agents can be preferential, *J. of Biol. Chem., 268,* 2649-2654.

Lawley, P.D., and Martin, C. N., 1975, Molecular mechanisms in alkylation mutagenesis. Induced reversion of bactoriophage T4rII AP72 by ethyl methylsulfonate in relation to extent and mode of ethylation of purines in bacteriophage deoxyribonucleic acid, *Biochem. J., 145,* 85-90.

Ludlum, D. B., 1978, The alkylating agents and nitrosoureas. In: *Textbook of Cancer Chemotherapy.* Edited by: S. B. Brodsky, J. F. Khan and J. Conney (Grune and Straton, New York), pp 17-24.

Masta, A., Gray, P. J., and Phyllips, D. N., 1984, Molecular basis of nitrogen mustard effects on transcription processes: Role of depurination, *Nucl. Acid Res., 22,* 3880-3886.

Mattes, W. B, Hartley, J. A. and Kohn, K. W., 1986, DNA sequence selectivity of guanine-N-7 alkylation by nitrogen mustard, *Nucl. Acid Res., 14(7),* 2971-2987.

Mattes, W. B., 1992, Use of 8-^{3}H-guanine-labeled deoxyribo-nucleic acid to study alkylating agent reagent kinetics and stability. *Anal. Biochem., 206,* 161-167.

McCloskey, J. A., Lowson, A. M., Tsubyma, K., Krueger, P. M., and Stillwell, R. N., 1968, Mass Spectrometry of nucleic acid components. Trimethylsilyl derivatives of nucleosides and bases. *J. Am. Chem. Soc., 90,* 4182-4184.

McCloskey, J. A., 1974, Mass spectrometry. In: *Basic Principles in Nucleic Acid Chemistry, vol. 1.,* Edited by P.O.P. Ts'o (Academic Press, New York) pp 209-308.

McLafferty, F. W., 1980, Detailed mechanisms of ion fragmentations. In: *Interpretations of Mass Spectra, 3rd ed.* Edited by: N. J. T. Turro (Univ. Sci. Book, Mill Vally, CAL), pp 170-172.

Meier, H. L., Gross, C. L. and Papirmeister, B., 1987, 2,2'-Dichlorodidiethyl sulfide (sulfur mustard) decrease NAD$^+$ levels in human leucocytes, *Toxico. Lett., 39 (1),* 109-22.

Papirmeister, B., Feister, A. J., Robinson, S. I., and Ford, R.D., 1991, Medical defense against mustard gas: Toxic mechanisms and Pharmacological implications. *CRC Press,* Boca Raton, Florida.

Povirk, L. F., Shuker, D. E., 1994, DNA Damage and mutagenesis induced by nitrogen mustards, *Mut. Res, 318,* 205-226.

Roberts, J. J., Brent, T. P., and Crathorn, A. R., 1971, Evidence for the inactivation and repair of the mammalian DNA template after alkylation by mustard gas and half-mustard gas, *Eur. J. Cancer, 7,* 515-524.

Smith, W. J and Dunn, M. A., 1991, Medical defense against blistering chemical warfare agents, *Arch. Dermatol., 127,* 1207-1213.

Swenberg, C. E. and Speicher, J. M., 1995, Neutron and gamma-radiation sensitivity of plasmid DNA of varying superhelical density, *Rad. Res., 144,* 301-309.

Somani, S. M., 1993, Toxicokinetics and Toxicodynamics In: *Chemical Warfare Agents.* Edited by S.M. Somani (Academic Press, New York) pp. 13-56.

Tomaz, M. 1969, Extreme lability of the C-8 proton: A consequence of 7-methylation of guanine residue in model compounds in DNA and its analytical applications, *Biochim. et Biophy. Acta, 199,* 18-28.

Tomaz, M., 1970, Novel assy of 7-alkylation of guanine residues in DNA application to nitrogen mustard, triethylene-melamine and mitomycine C, *Biochim et Biophy. Acta, 213,* 288-

Vaishnav, Y. N., Holwitt, E., Swenberg, C. E. and Lee, H.-C and Kan, L.-S., 1991, Synthesis and characterization of stereoisomers of 5,6-dihydro-5,6-dihydroxy-thymidine, *J. Biomol. Struct. Dynam., 8,* 935-951.

Vaishnav, Y. N. and Swenberg, C. E., 1993, Radiolysis in aqueous solution of dinucleoside monophosphates by high-energy electrons and fission neutrons, *Rad. Res., 133,* 12-19.

DISTRIBUTION LIST

DEPARTMENT OF DEFENSE

ARMED FORCES RADIOBIOLOGY RESEARCH INSTITUTE
ATTN: PUBLICATIONS BRANCH
ATTN: LIBRARY

ARMY/AIR FORCE JOINT MEDICAL LIBRARY
ATTN: DASG-AAFJML

ASSISTANT TO THE SECRETARY OF DEFENSE
ATTN: AE
ATTN: HA(IA)

DEFENSE SPECIAL WEAPONS AGENCY
ATTN: TITL
ATTN: DDIR
ATTN: RAEM
ATTN: MID

DEFENSE TECHNICAL INFORMATION CENTER
ATTN: ACQUISITION
ATTN: ADMINISTRATOR

FIELD COMMAND DEFENSE SPECIAL WEAPONS AGENCY
ATTN: DASIAC
ATTN: FCIEO

INTERSERVICE NUCLEAR WEAPONS SCHOOL
ATTN: DIRECTOR

LAWRENCE LIVERMORE NATIONAL LABORATORY
ATTN: LIBRARY

UNDER SECRETARY OF DEFENSE (ACQUISITION)
ATTN: OUSD(A)/R&E

UNIFORMED SERVICES UNIVERSITY OF THE HEALTH SCIENCES
ATTN: LIBRARY

DEPARTMENT OF THE ARMY

HARRY DIAMOND LABORATORIES
ATTN: SLCSM-SE

OFFICE OF THE SURGEON GENERAL
ATTN: MEDDH-N

U.S. ARMY AEROMEDICAL RESEARCH LABORATORY
ATTN: SCIENCE SUPPORT CENTER

U.S. ARMY CHEMICAL RESEARCH, DEVELOPMENT, &
ENGINEERING CENTER
ATTN: SMCCR-RST

U.S. ARMY INSTITUTE OF SURGICAL RESEARCH
ATTN: COMMANDER

U.S. ARMY MEDICAL DEPARTMENT CENTER AND SCHOOL
ATTN: MCCS-FCM

U.S. ARMY MEDICAL RESEARCH AND MATERIEL COMMAND
ATTN: COMMANDER

U.S. ARMY MEDICAL RESEARCH INSTITUTE OF CHEMICAL
DEFENSE
ATTN: MCMR-UV-R

U.S. ARMY NUCLEAR AND CHEMICAL AGENCY
ATTN: MONA-NU

U.S. ARMY RESEARCH INSTITUTE OF ENVIRONMENTAL
MEDICINE
ATTN: DIRECTOR OF RESEARCH

U.S. ARMY RESEARCH LABORATORY
ATTN: DIRECTOR

WALTER REED ARMY INSTITUTE OF RESEARCH
ATTN: DIVISION OF EXPERIMENTAL THERAPEUTICS

DEPARTMENT OF THE NAVY

BUREAU OF MEDICINE & SURGERY
ATTN: CHIEF

NAVAL AEROSPACE MEDICAL RESEARCH LABORATORY
ATTN: COMMANDING OFFICER

NAVAL MEDICAL RESEARCH AND DEVELOPMENT COMMAND
ATTN: CODE 42

NAVAL MEDICAL RESEARCH INSTITUTE
ATTN: LIBRARY

NAVAL RESEARCH LABORATORY
ATTN: LIBRARY

OFFICE OF NAVAL RESEARCH
ATTN: BIOLOGICAL & BIOMEDICAL S&T

DEPARTMENT OF THE AIR FORCE

BROOKS AIR FORCE BASE
ATTN: AL/OEBZ
ATTN: OEHL/RZ
ATTN: USAFSAM/RZB

OFFICE OF AEROSPACE STUDIES
ATTN: OAS/XRS

OFFICE OF THE SURGEON GENERAL
ATTN: HQ AFMOA/SGPT
ATTN: HQ USAF/SGES

U.S. AIR FORCE ACADEMY
ATTN: HQ USAFA/DFBL

U.S. AIR FORCE OFFICE OF SCIENTIFIC RESEARCH
ATTN: DIRECTOR OF CHEMISTRY & LIFE SCIENCES

OTHER FEDERAL GOVERNMENT

ARGONNE NATIONAL LABORATORY
ATTN: ACQUISITIONS

BROOKHAVEN NATIONAL LABORATORY
ATTN: RESEARCH LIBRARY, REPORTS SECTION

CENTER FOR DEVICES AND RADIOLOGICAL HEALTH
ATTN: DIRECTOR

GOVERNMENT PRINTING OFFICE
ATTN: DEPOSITORY ADMINISTRATION BRANCH
ATTN: CONSIGNED BRANCH

LIBRARY OF CONGRESS
ATTN: UNIT X

LOS ALAMOS NATIONAL LABORATORY
ATTN: REPORT LIBRARY

NATIONAL AERONAUTICS AND SPACE ADMINISTRATION
ATTN: RADLAB

NATIONAL AERONAUTICS AND SPACE ADMINISTRATION
GODDARD SPACE FLIGHT CENTER
ATTN: LIBRARY

NATIONAL CANCER INSTITUTE
ATTN: RADIATION RESEARCH PROGRAM

NATIONAL DEFENSE UNIVERSITY
ATTN: LIBRARY TECHNICAL SERVICES

U.S. DEPARTMENT OF ENERGY
ATTN: LIBRARY

U.S. FOOD AND DRUG ADMINISTRATION
ATTN: WINCHESTER ENGINEERING AND
ANALYTICAL CENTER

U.S. NUCLEAR REGULATORY COMMISSION
ATTN: LIBRARY

RESEARCH AND OTHER ORGANIZATIONS

AUSTRALIAN DEFENCE FORCE
ATTN: SURGEON GENERAL

AUTRE, INC.
ATTN: PRESIDENT

BRITISH LIBRARY
ATTN: ACQUISITIONS UNIT

CENTRE DE RECHERCHES DU SERVICE DE SANTE DES ARMEES
ATTN: DIRECTOR

FEDERAL ARMED FORCES DEFENSE SCIENCE AGENCY FOR NBC
PROTECTION
ATTN: LIBRARY

FOA NBC DEFENCE
ATTN: LIBRARY

INHALATION TOXICOLOGY RESEARCH INSTITUTE
ATTN: LIBRARY

INSTITUTE OF NUCLEAR MEDICINE AND ALLIED SCIENCES
ATTN: DIRECTOR

INSTITUTE OF RADIOBIOLOGY, ARMED FORCES
MEDICAL ACADEMY
ATTN: DIRECTOR

OAK RIDGE ASSOCIATED UNIVERSITIES
ATTN: MEDICAL LIBRARY

RESEARCH CENTER OF SPACECRAFT RADIATION SAFETY
ATTN: DIRECTOR

RUTGERS UNIVERSITY
ATTN: LIBRARY OF SCIENCE AND MEDICINE

UNIVERSITY OF CALIFORNIA
ATTN: DIRECTOR, INSTITUTE OF TOXICOLOGY &
ENVIRONMENTAL HEALTH
ATTN: LIBRARY, LAWRENCE BERKELEY LABORATORY

UNIVERSITY OF CINCINNATI
ATTN: UNIVERSITY HOSPITAL, RADIOISOTOPE
LABORATORY

XAVIER UNIVERSITY OF LOUISIANA
ATTN: COLLEGE OF PHARMACY

REPORT DOCUMENTATION PAGE

Public reporting burden for this collection of information is estimated to average 1 hour per response, including the time for reviewing instructions, searching existing data sources, gathering and maintaining the data needed, and completing and reviewing the collection of information. Send comments regarding this burden estimate or any other aspect of this collection of information, including suggestions for reducing this burden, to Washington Headquarters Services, Directorate for Information Operations and Reports, 1215 Jefferson Davis Highway, Suite 1204, Arlington, VA 22202-4302, and to the Office of Management and Budget, Paperwork Reduction Project (0704-0188), Washington, DC 20503

1. AGENCY USE ONLY *(Leave blank)*	2. REPORT DATE August 1997	3. REPORT TYPE AND DATES COVERED Reprints

4. TITLE AND SUBTITLE AFRRI Reports, First - Second Quarters 1997	5. FUNDING NUMBERS NWED QAXM

6. AUTHOR(S)

7. PERFORMING ORGANIZATION NAME(S) AND ADDRESS(ES) Armed Forces Radiobiology Research Institute 8901 Wisconsin Avenue Bethesda, MD 20889-5603	8. PERFORMING ORGANIZATION REPORT NUMBER SR97-1 - SR97-10

9. SPONSORING/MONITORING AGENCY NAME(S) AND ADDRESS(ES) Uniformed Services University of the Health Sciences 4301 Jones Bridge Road Bethesda, MD 20814-4799	10. SPONSORING/MONITORING AGENCY REPORT NUMBER

11. SUPPLEMENTARY NOTES

12a. DISTRIBUTION/AVAILABILITY STATEMENT Approved for public release; distribution unlimited.	12b. DISTRIBUTION CODE

13. ABSTRACT *(Maximum 200 words)*

This volume contains AFRRI Scientific Reports SR97-1 through SR97-10 for January-June 1997.

14. SUBJECT TERMS	15. NUMBER OF PAGES 100
	16. PRICE CODE

17. SECURITY CLASSIFICATION OF REPORT UNCLASSIFIED	18. SECURITY CLASSIFICATION OF THIS PAGE UNCLASSIFIED	19. SECURITY CLASSIFICATION OF ABSTRACT UNCLASSIFIED	20. LIMITATION OF ABSTRACT UL

CLASSIFIED BY:

DECLASSIFY ON: